# AUTHIGENIC MINERALS IN VOLCANICLASTICS FROM AN EASTERN AFRICAN PALEOLAKE: A PROXY FOR PALEOENVIRONMENT

by

Kaitlyn M. Truss

A Thesis Submitted in

Partial Fulfillment of the

Requirements for the Degree of

Master of Science

in Geosciences

at

The University of Wisconsin-Milwaukee

May 2024

## ABSTRACT

AUTHIGENIC MINERALS IN VOLCANICLASTICS FROM AN EASTERN AFRICAN PALEOLAKE: A PROXY FOR PALEOENVIRONMENT

by

Kaitlyn M. Truss

The University of Wisconsin-Milwaukee, 2024
Under the Supervision of Dr. Lindsay J. McHenry

Olduvai Gorge exposes the stratigraphy of Paleolake Olduvai, an often saline-alkaline rift lake that records volcanism from the Ngorongoro Volcanic Highlands. In 2014, cores retrieved from the study area revealed new stratigraphy, including the lacustrine Naibor Soit Formation (Fm) and the volcaniclastic Ngorongoro Fm. In the Ngorongoro Fm part of the cores, mineralogy and geochemistry are the best paleoenvironmental proxies, since under saline-alkaline conditions, volcanic glass alters into specific authigenic minerals (e.g., zeolite, feldspar). This study employs X-Ray Diffraction, X-Ray Fluorescence, and Scanning Electron Microscopy to analyze authigenic mineralogy and geochemistry. The lower Ngorongoro Fm experienced the most alteration, with less preserved glass and more zeolites. The Upper Ngorongoro Fm experienced less alteration, preserving more glass and less zeolites. The uppermost units contained abundant glass and no alteration minerals, indicating very fresh conditions. Overall, there is a large-scale freshening trend throughout the duration of the Ngorongoro Fm.

## TABLE OF CONTENTS

## LIST OF FIGURES

## LIST OF TABLES

## LIST OF ABBREVIATIONS

| | |
|---|---|
| Fm | Formation |
| EARS | East African Rift System |
| NVH | Ngorongoro Volcanic Highlands |
| OGCP | Olduvai Gorge Coring Project |
| XRD | X-Ray Diffraction |
| SEM | Scanning Electron Microscopy |
| EDS | Energy Dispersive Spectrometry |
| XRF | X-Ray Fluorescence |
| ERV | East Rift Valley |
| CFCT | Coarse Feldspar Crystal Tuff |

## ACKNOWLEDGEMENTS

I would like to acknowledge several individuals and organizations that made the completion of this project possible.

First and foremost, I want to thank my advisor, Dr. Lindsay McHenry, for not only taking me on as a graduate student but allowing me to work on this project somewhat autonomously. I feel I have grown tremendously as a geologist and writer under your guidance and am very grateful for the support and opportunities you have given me.

I would also like to thank the OGCP Team (Ian G. Stanistreet, Harald Stollhofen, Lindsay McHenry, Jackson K. Njau, Kathy Schick, and Nicholas Toth) for allowing me to sample the cores and also for co-authoring my 2023 GSA abstract/talk. A special thank you is extended to Ian G. Stanistreet and Harald Stollhofen for creating the high-resolution core logs, referenced throughout this paper.

Additionally, I would like to acknowledge the Wisconsin Space Grant Consortium and the National Science Foundation for funding this research.

I owe many thanks to Gayantha R. L. Kodikara and Chase Glenister for assistance in the laboratory and for allowing many office visits to discuss new ideas.

I also owe a tremendous amount of gratitude to the UW-Milwaukee Department of Geosciences for the financial support during my time here. This aid helped me physically attend school, conduct laboratory research, and travel to present research.

Lastly, I would like to extend my love and gratitude to my family and friends. I would not be where I am today without the support and encouragement over the years. Thank you!

## I. INTRODUCTION

### Study Area

Paleolake Olduvai was a Pleistocene rift lake in the Olduvai basin, Tanzania, eastern Africa (Figure 1A). The Olduvai basin is a small subsidiary basin on the western flank of the eastern branch of the East African Rift System (EARS). In response to rifting, a large volcanic complex formed, filling the basin with volcaniclastic material from the southeast. Volcanic material and other detrital sediments were deposited in the basin, building a fluvial plain and delta on the western and northern basin margins and a pyroclastic fan complex on the eastern and southern basin margins (Ashley and Hay, 2002).

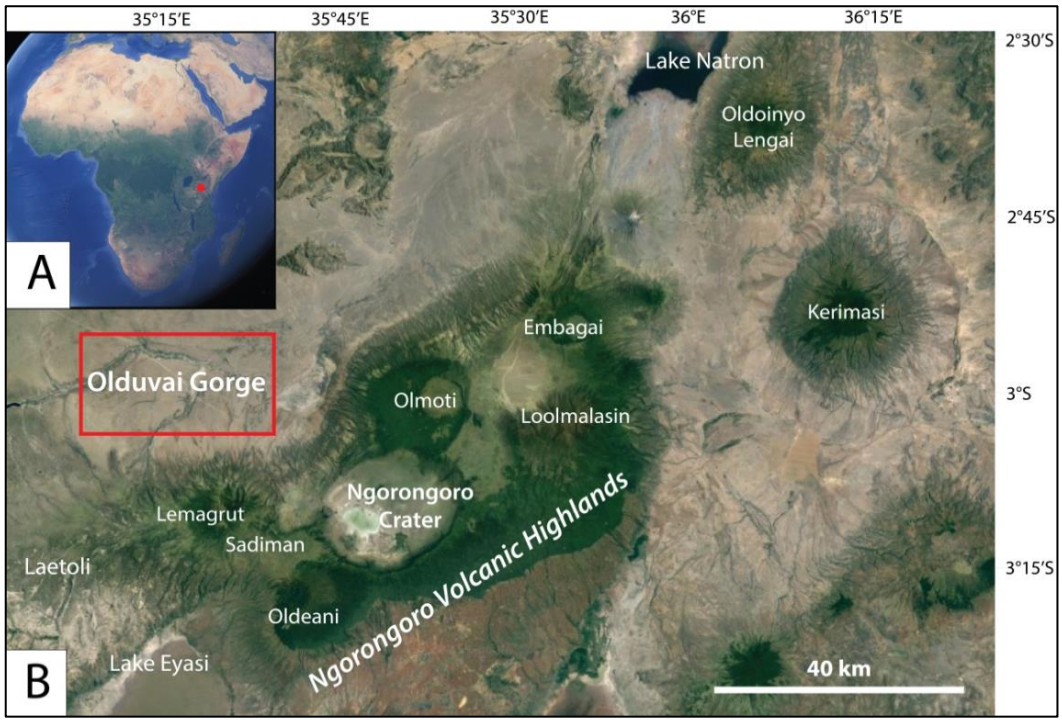


**Figure 1.** Location of Paleolake Olduvai. A: Inset map of Africa, red dot shows the location of our study area in Tanzania. B: Map showing the location of Olduvai Gorge (red rectangle) in relation to the Ngorongoro Volcanic Highlands and modern-day Lake Natron.

The paleolake stratigraphy is exposed by an erosional feature called Olduvai Gorge. Olduvai Gorge (Figure 1B) is an upper Pleistocene to Holocene fluvial incision that cuts into the Pleistocene lacustrine and volcanic deposits of the Olduvai basin (Hay, 1976). The gorge exposes a high-resolution stratigraphic record of the lake basin from center to margin and drains eastward from the Serengeti plains towards the Ngorongoro Volcanic Highlands (NVH) (Hay, 1976).

The beds exposed in the Olduvai outcrops (Figure 2) have been a target of study for over 100 years. Paleontological interest in the study area initiated in 1913, with excavations beginning in 1931 (Louis Leakey). Olduvai Gorge is well known for its abundance of well-preserved Pleistocene hominid and vertebrate fossils and stone artifacts (e.g. Leakey, 1971).

**Figure 2.** Image of an Olduvai Gorge outcrop. The exposed stratigraphy includes fluvial, lacustrine, and volcanic units. Also exposed is evidence for normal faulting, indicated by the displaced burnt orange unit (downthrown hanging wall).

The geologic setting responsible for the rocks observed in Olduvai Gorge has been intensively investigated and is reasonably well understood (e.g. Hay, 1976; Deino et al., 2021). The general stratigraphy of Olduvai Gorge (Figure 3) reveals a persistent hydrologically-closed paleolake, which was primarily saline and highly alkaline (McHenry et al., 2020a), reflecting an arid to semi-arid climate. Mg-rich clays, carbonates, and zeolites are preserved in these units, in addition to detrital and pyroclastic sediments (McHenry et al., 2020a). The oldest volcanic deposition observed in outcrop is from the Ngorongoro volcano, recorded in lower Bed I. Moving up through the stratigraphic column, the younger rock units record volcanic activity from younger volcanoes. The Olmoti volcano was active during the deposition of upper Bed I and younger volcanoes (e.g., Loolmalasin and Embagai) would have been active during the deposition of Beds II and Beds III (McHenry et al., 2020a, 2020b, Mollel and Swisher, 2012).

Valuable paleoclimatic information (e.g., changes in aridity) can also be obtained from Olduvai, as small subsidiary basins are highly responsive to climate change (Ashley and Hay, 2002). The Olduvai paleolake expanded and contracted over time in response to climate and tectonics, recording over 2 million years of changing lake conditions. The observed lake patterns associated with fluctuating climate include lake expansion during wet periods and lake contraction during dry periods (Sikes and Ashley, 2007). Evidence of these wet/dry periods are recorded by paleoclimatic indicators that are preserved predominantly within lake units. Such indicators include (but are not limited to) laminated lake clays, carbon and oxygen isotopes (Sikes and

Ashley, 2007), authigenic mineral assemblages (McHenry et al., 2020a), and bioindicators (e.g., phytolith, pollen, diatoms) (Rodriguez-Cintas at al., 2020).

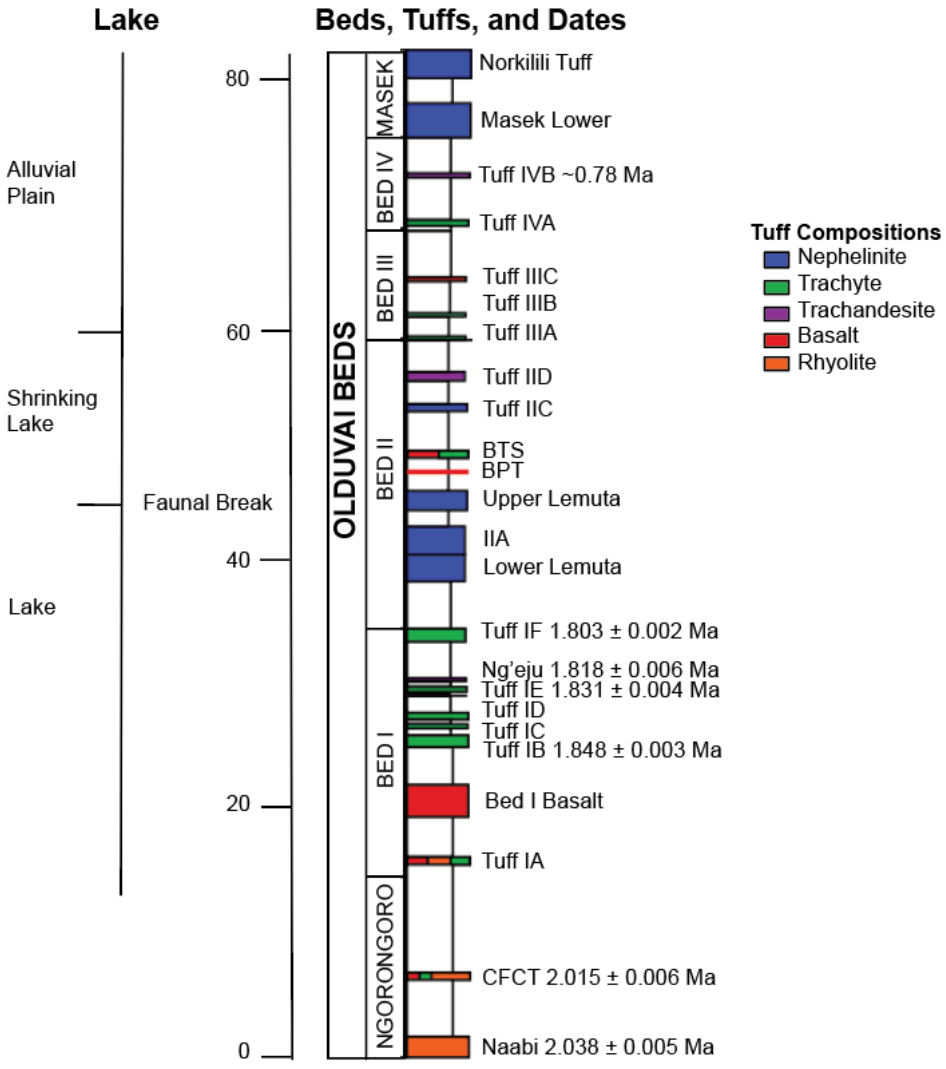


**Figure 3.** General stratigraphy of Olduvai Gorge, illustrated by a tephrostratigraphic framework defined by 'marker tuffs', which are labeled and color coded by rock type. Dates for individual tuffs from Deino, 2012. Figure from McHenry et al., 2020b.

New deep drilling by the Olduvai Gorge Coring Project (OGCP) in 2014 revealed deposits older than those observed in outcrop. These deposits include two major intervals of lacustrine-dominated deposition (the Naibor Soit Fm) that interfinger with two major expansions of the Ngorongoro volcaniclastic fan (Ngorongoro Fm) (Njau et al., 2021; Stanistreet et al., 2020b). While the lake intervals can be studied using traditional paleoclimate proxies, the conditions during the intervals dominated by the Ngorongoro volcanic fan are more challenging to interpret.

Although the Ngorongoro fan deposits are dominated by volcaniclastic material, intervals of fine-grained lacustrine sediments indicate that the lake was still present in the basin during volcanic deposition. McHenry et al. (2020a) examined the authigenic mineralogy of these lacustrine intervals to determine paleoclimatic conditions in the deeper lake-dominated parts of the cores. The observed assemblages indicate the early lake was highly saline-alkaline, transitioning to fresher conditions over time. Although this method was successful, the study was limited to lacustrine intervals, leaving large gaps in the paleoenvironmental record where lacustrine claystones were largely absent from the cores, which instead contained thick tephra and other volcaniclastic units. Valuable paleoenvironmental data may be available in these tephra-dominated intervals. Volcanic glass is preserved under fresher conditions and can alter into a variety of authigenic minerals under more saline-alkaline conditions.

The goal of this study was to examine the authigenic mineralogy and related geochemistry of tephra from the Ngorongoro Fm to assess the nature and degree of

alteration in units that have not yet been assessed for their paleoenvironmental record. The collected data can be compared to that of McHenry et al. (2020a), which documents changes in authigenic mineralogy for the fluviolacustrine intervals of the OGCP cores, and to that of the overlying Olduvai Beds. This will help identify any meaningful trends that can be used to interpret paleoenvironmental conditions during intervals of volcaniclastic fan deposition that can contribute towards understanding the paleoenvironmental record of the Olduvai basin.

Based on available data, we present two different hypotheses that will be tested in this study. First, we hypothesize that the authigenic mineralogy and associated geochemistry within the volcanic Ngorongoro Fm will fill gaps in the Olduvai paleoclimate record, reflecting an overall freshening trend consistent with that observed by McHenry et al. (2020a) for the more lacustrine deposits of the Naibor Soit Fm and lowermost Bed I. Second, we hypothesize that there will be an ‘insulation’ effect, with thinner tephra units and the exposed surfaces of thick volcanic units being subjected to a higher degree of alteration than the interiors of thicker units, which would be more insulated from the lake and ground water and therefore less altered.

To address these hypotheses, the primary objectives of this study were to 1) determine if thick tephra units deposited into a lake or lake-adjacent volcaniclastic fan-delta preserve evidence of alteration (e.g., authigenic minerals), 2) use the authigenic mineral assemblages to determine the degree of alteration associated with water-rock interactions in the Ngorongoro Fm, 3) compare bulk geochemical compositions of tuff

samples that display different degrees of alteration to identify any patterns in element mobility, 4) determine whether fluid interactions and associated alteration was limited to thinner volcanic units and exposed surfaces, or whether fluid was able to penetrate into the interior of thicker and potentially more insulated tephra and ignimbrites as well, and 5) assess if the overall tephra alteration in the Ngorongoro Formation reflects any large-scale transitions in paleoenvironmental conditions.

**Research Approach**

Understanding the long history (climate, lake levels, geochemistry) of Paleolake Olduvai requires understanding the authigenic mineral assemblages associated with varying degrees of alteration within the cores. Glass is typically absent from tuffs in Olduvai Beds I and II but is more often preserved in tuffs within the older Ngorongoro Formation (McHenry et al., 2020b). This study focuses on the mineralogy and geochemistry of altered volcaniclastic deposits from the Ngorongoro Fm.

The Ngorongoro tuffs have similar rhyolitic glass compositions to each other (McHenry et al., 2020b), so the starting composition for each sample interval should be similar. Additionally, sampling from cores allows us to meaningfully determine the distribution and abundance of alteration minerals with depth, since the cores are limited to a single position. Since we have a control on the starting composition, this fixed position can provide a depth record of the changing alteration environment over time.

Authigenic mineral assemblages can be identified using X-Ray Diffraction (XRD) and verified by Scanning Electron Microscopy (SEM) analysis. SEM allows us to observe mineral morphologies, which can help confirm mineral phases observed by XRD. SEM analysis also illustrates textural relationships of glass and minerals, which can then be used to assess the nature, timing, and degree of alteration caused by fluid interactions (e.g., depositional environment) associated with paleolake Olduvai.

This study compares the bulk composition of interior (more insulated) samples to exterior (less-insulted) samples of thicker volcanic and volcaniclastic units in contact with lake sediments. In principle, differences in composition could be attributed to primary magmatic differences, phenocryst content, or post-depositional element mobility tied to the alteration environment (McHenry, 2009). Because samples in this study should have similar starting compositions and phenocryst abundances, deviations in sample composition (measured by XRF) should reflect element mobility during alteration. Plotting XRF data for samples from the same units in an isocon diagram shows the extent of element mobility within a unit, reflecting possible insulation effects. This method can also help determine if the influence of paleolake fluids was limited to thinner volcanic units and exposed surfaces or if the fluids could permeate/alter thicker tephra and ignimbrite units as well.

Lastly, all data are synthesized and used to assess alteration patterns in the Ngorongoro Formation. These patterns are used to help determine the paleoclimatic

conditions during this formation period. Additionally, these findings can be compared to previous studies of paleolake Olduvai and even other east African paleoclimate studies to add to the overall climate record.

**Importance**

This project is relevant to multiple fields of study, including the mineralogy of altered volcanic deposits and the reconstruction of paleoenvironments based on authigenic minerals. Geochemical analyses of these cores, with a focus on the conditions of alteration, is paleoanthropologically important since Olduvai Gorge and nearby Laetoli are important early hominin sites (Hay, 1976). Understanding the geochemistry and mineralogy within the study area will help reconstruct the paleoenvironmental conditions in which these early hominins lived.

From a planetary geology perspective, this study is relevant to two Mars rover missions, Curiosity and Perseverance, which are both working to find chemical and mineral evidence of past habitable environments on Mars. Curiosity, on Mars since 2012, has analyzed many instances of altered igneous-derived rock and sediment in Gale crater (Rampe et al., 2020). Perseverance, active on Mars since 2021, has also analyzed igneous rock (basalt and olivine cumulate) in Jezero crater (Melsin et al., 2022). Both craters contain evidence of lacustrine intervals, and finding authigenic indicator minerals (e.g., zeolites) can help constrain the paleohydrochemical conditions and whether they represent past habitable environments.

The zeolite analcime has been identified by Curiosity in Gale crater (Rampe et al., 2020) and also by Perseverance in Jezero crater, which also detected the zeolite natrolite (Sarkar et al., 2024). Sarkar et al. (2024) suggests that the Na-zeolites found in Jezero could have been formed from low-temperature alteration of basaltic minerals by Na-rich fluids. Kodikara et al. (2023) and others have shown through modeling that zeolites are likely to have formed on Mars, as a result of the closed-system aqueous alteration of volcaniclastic materials of varied compositions. This work can help interpret the paleohydrochemistry of ancient Martian lakes, which is important when looking for potential habitable environments.

## II. BACKGROUND/LITERATURE REVIEW

### Geologic Setting

#### *Regional*

The East African Rift System (EARS) is a developing continental divergent boundary, separating the African plate into the Nubian plate (west) and the Somalian plate (east). The EARS consists of four major branches, cumulatively extending thousands of kilometers over eastern Africa. This study focuses on the northern Tanzanian portion of the Eastern Rift Valley (ERV), also referred to as the Gregory Rift (e.g., Olaka and Ebinger, 2023).

The ERV is comprised of the main Ethiopian rift (in modern-day Ethiopia), extending southward into the Kenyan rift valley (through Kenya, into Tanzania). The

early stages of rifting are characterized by doming and down-warping, where the mantle plume lifted the crust and caused normal faulting, crustal thinning, and associated isostatic adjustment. As the rift valley became more established, it developed a series of segmented rift basins, plateaus, inner rift systems, and large volcanic complexes (Trauth et al. 2005).

Rifting in the ERV began with an initial lava eruption in southwest Ethiopia. Ethiopian rift-volcanism (~45-33 Ma) was followed by rifting in northern Kenya (~33-25 Ma) and asynchronous rift volcanism (~15 and 8 Ma) (Trauth et al., 2007; Olaka and Ebinger, 2023). Lateral fault propagation with east-dipping normal faulting started in Ethiopia (20-14 Ma), followed by east-dipping normal faulting in northern Kenya (12-7 Ma) and southern Kenya (9-6 Ma). Full-graben morphology was generated ~5.5-3.7 Ma (Baker et al., 1988; Trauth et al., 2007).

The progressive rifting in east Africa led to the formation of large sedimentary basins surrounded by uplifted flanks (e.g., Olaka and Ebinger, 2023). Fluvio-lacustrine activity in east Africa started in the mid-Miocene, with the oldest lacustrine sequences in the southern Kenya and Tanzanian rift occurring during the early Pliocene (Trauth et al., 2007). By the Plio-Pleistocene, a series of small, partly alkaline lakes had formed in the eastern branch of the EARS. These lakes are typically less than 150 $km^2$ and shallow (less than 100m, often only a few meters deep). This study focuses on Paleolake Olduvai, which occupied a rift-basin that formed on the western flank of this southern extent of the Eastern Rift Valley in the early Pleistocene.

### *Local*

South of the Kenyan rift, the ERV further splits into two distinct rift valleys in northern Tanzania. The two rift valleys are separated by the Ngorongoro Volcanic Highlands (NVH), a volcanic complex comprised of several volcanoes that have remained active over the last 5 million years (Deino et al., 2012; Ashley et al., 2013). The modern-day NVH is over 3,000m high, which acts as an orographic barrier, trapping moist easterly winds from the Arabian Sea and creating a rain shadow to the west (Ashley et al., 2013). The rain shadow limited direct precipitation over the Olduvai basin, resulting in greater aridity to the west of the NVH. However, during periods of increased precipitation over the NVH, rainwater could still make it into the basin either from seasonal run-off, or from infiltrating into the relatively porous pyroclastic deposits in the highlands and migrating west towards the basin (Figure 4A).

The amount of water in paleolake Olduvai relied on these complex drainage patterns and was very sensitive, responding to changes in both volcano-tectonic activity and climate. These responses are recorded in the lake stratigraphy, with changes in lithology reflecting fluctuating lake level and associated geochemistry. Over time, the lake expanded during wet periods and contracted during dry periods. These wet/dry cycles appear to be consistent with regional climate patterns, paced by variations in precessional insolation, every ~23kyr (Trauth et al., 2007; Ashley et al., 2013; Stanistreet et al., 2020a; McHenry et al., 2020a).

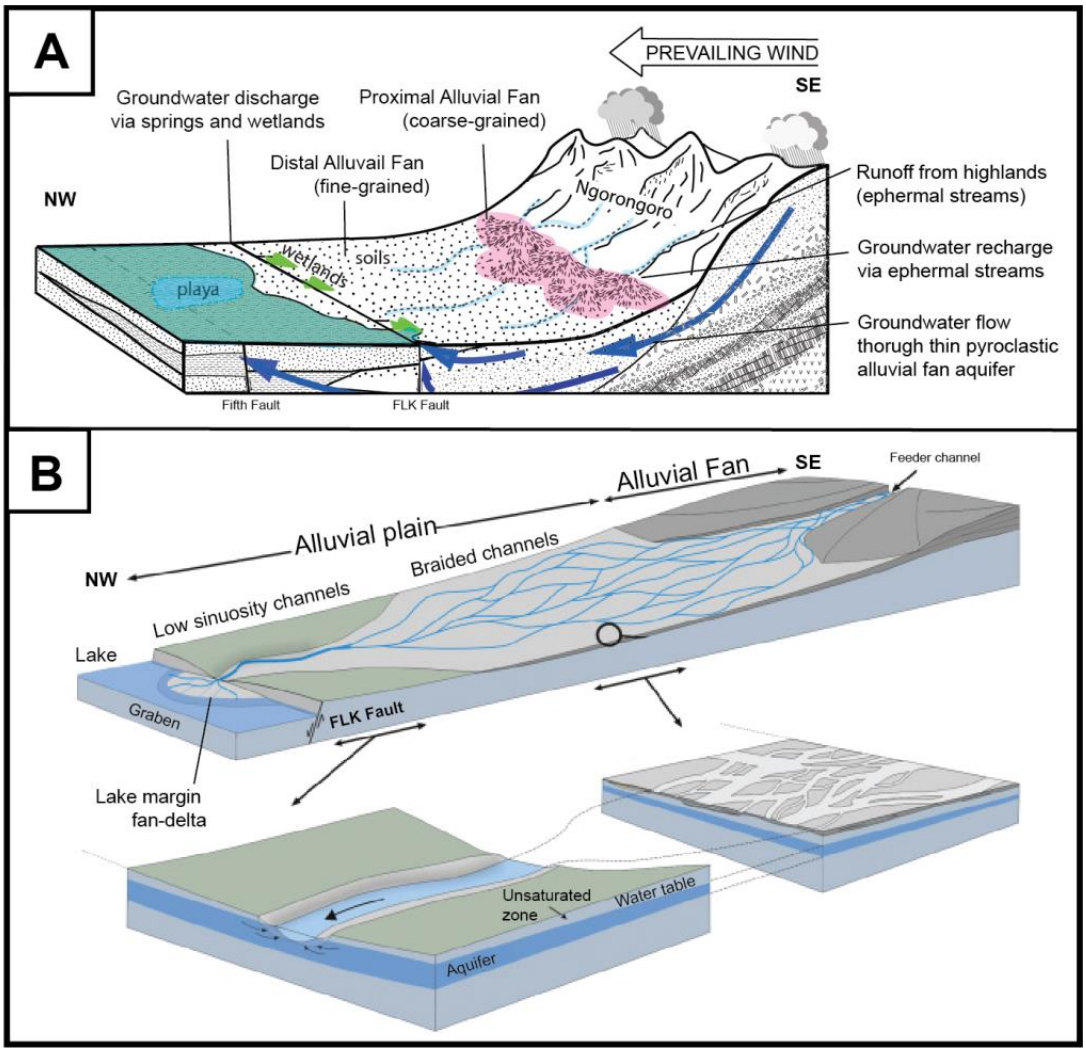


**Figure 4.** Olduvai drainage patterns. A) Rainfall over the highlands penetrated pyroclastic units, flowing subaerially into the basin. Groundwater was discharged via springs and wetlands along fault lines, maintaining wetlands and providing discharge that drained into paleolake Olduvai. Modified from Ashley et al., 2020. B) Surface discharge patterns from source to sink. In the alluvial plain, braided channels transitioned into low sinuosity channels, draining into the basin. Modified from Uribelarrea et al., 2017.

## Plio-Pleistocene East African Climate History

Several paleoenvironmental proxies are used to study the record of east African moisture levels, many of which are paced by precessional insolation. For example, the Baringo basin diatomites in the central Kenyan rift valley record rhythmic cycling of

major freshwater cycles consistent with ~23kyr Milankovitch precessional periodicity (Kingston et al., 2007). Other proxies that support precessional periodicity include drops in east Mediterranean marine dust abundance and increased formation of sapropelitic muds in the Eastern Mediterranean Basin, which rely on east African precipitation to provide freshwater discharge into the basin (Kingston et al., 2007, Ashley et al., 2013).

Some paleoenvironmental proxies reflecting African precipitation patterns (e.g. eolian dust preserved in marine cores and rhythmic stratification patterns in subtropical African lakes can also be associated with glacial/interglacial cycles linked to obliquity and eccentricity amplitudes. The coexistence of the main Milankovitch cycles (orbital precession ~23kyr, axial obliquity ~41kyr, and orbital eccentricity ~100-400kyr) suggests that climatic regimes in equatorial Africa are controlled by a complex interdependence of high and low-latitude orbital parameters (Lepre et al., 2007). Periods of aridification linked with long-term global cooling in east Africa occurred at 3.5-3.35, 2.5-2, and 1.8-1.6 Ma (Olaka and Ebinger, 2023). Periods characterized by the occurrence of large and deep lakes have been identified broadly in east Africa at 2.7-2.5, 1.9-1.7, and 1.1-0.9 Ma (Trauth et al., 2005).

The main driver for east African aridification (and associated climate variability) in the Plio/Pleistocene is thought to be the onset of Northern Hemisphere glaciation ~3.5-2.5 Ma. Kingston et al. (2007) suggest a low-latitude insolation threshold, above which the monsoonal system provides sufficient precipitation for lake formation in rift-basins.

The highest lake levels in east Africa seem to have occurred during interglacial periods, due to maximum low-latitude insolation during maximum precession (Trauth et al., 2021). Therefore, the lowest lake levels associated with high aridity were likely due to minimum low-latitude insolation during glacial periods.

Although orbital forcing plays a huge factor in east African climate variability, tectonic forcing may have a larger influence on observed wet/dry patterns. The extreme orographic relief resulting from uplift associated with the EARS had a major influence on climate on a continental scale, reorganizing atmospheric circulation and decreasing precipitation in east Africa (Olaka and Ebinger, 2023). Therefore, the environmental signals from east African rift-basins may be obscured locally and regionally by rain shadows, reflecting arid to semi-arid conditions, even during periods of orbitally-forced wet conditions at the regional level.

**Olduvai Basin**

The stratigraphy exposed by Olduvai Gorge records the complex history of the Olduvai basin. Based on Hay's (1976) interpretations, the basal layer of the basin fill is the Naabi Ignimbrite (~2.0 Ma), which is observed to disconformably overlie Precambrian metamorphic basement in the western basin. Hay (1976) divided the overlying Olduvai stratigraphy into a series of Beds (Figure 3), starting at its base with Bed I, followed by Beds II, III, and IV and finally the younger Beds (Masek, Ndutu, and Naisiusiu, deposited as the gorge was being eroded and infilled). The basin evolved

over time with progressive rifting, active volcanism, and changing hydrologic conditions. These factors caused subsidence, creating accommodation space for Paleolake Olduvai (when conditions were suitable to maintain lake level). The units observed in outcrop are the result of a variety of factors, including depositional environment and climate (e.g., wet vs. dry). Other factors that affected lithology include surface runoff, mass movement, and wind influence (Ashley and Hay, 2002).

Beds I and II are dominated by Paleolake Olduvai, which covered much of the basin at times of high lake level. During these intervals a fluvial plain and delta occupied the western and northern basin margins, a pyroclastic-alluvial fan complex occupied the eastern and southern basin margins, and a small freshwater wetland developed on the southeastern margin (Ashley and Hay, 2002). This lake expanded and contracted over time, leaving interfingered lacustrine and lake margin deposits. The lake and associated environments changed due to basin evolution and climate. In middle to upper Bed II and later, a fluvial facies developed and with increased aridity an eolian facies developed. The resulting lithologies observed in the Olduvai Beds primarily include lacustrine claystones, fallout deposits (tuffs), reworked tephra (tuffaceous claystones), carbonates, and siliciclastic and volcaniclastic sandstone, siltstone, and conglomerates.

The lateral variation in lithofacies coupled with erosion and rift-related faulting complicate stratigraphic correlation in the field (Ashley and Hay, 2002). Because of this, the volcanic units (tuffs) exposed in outcrop have been the focus of several studies.

With each pulse, volcanics blanketed the area, with thicker deposits (including flows) in the eastern gorge closer to their source. Some of these deposits are well-preserved, continuous across the basin, can be dated, and have a unique geochemical signature/ fingerprint (e.g., McHenry et al., 2020b). For this reason, these volcanic deposits are termed ‘marker tuffs’ and are used to correlate units across the entire basin and to constrain the timing of eruptive events and related depositional events preserved in the surrounding units. Hay (1976) established a basin-wide tephrostratigraphic framework based on detailed field mapping of these marker tuffs. Later work improved and corrected these correlations using mineral chemistry, $^{40}Ar/^{39}Ar$ dating, and paleomagnetic studies (e.g. McHenry 2005; Deino 2012). An updated tephrostratigraphic column (depicting marker tuffs with ages) is presented in Figure 3.

The position (and depth) of the drainage sump for the basin changed over time due to tectonic, accommodation, sediment supply, and volcanic factors. Hay (1976) interpreted these changes as a northward then eastward progression of the depocenter, eventually leading to the modern drainage sump at Olbalbal. Figure 5 illustrates the aerial extent of each phase of Paleolake Olduvai, based on Hay’s (1976) paleogeographic reconstruction of the lake during the time these formations were deposited.

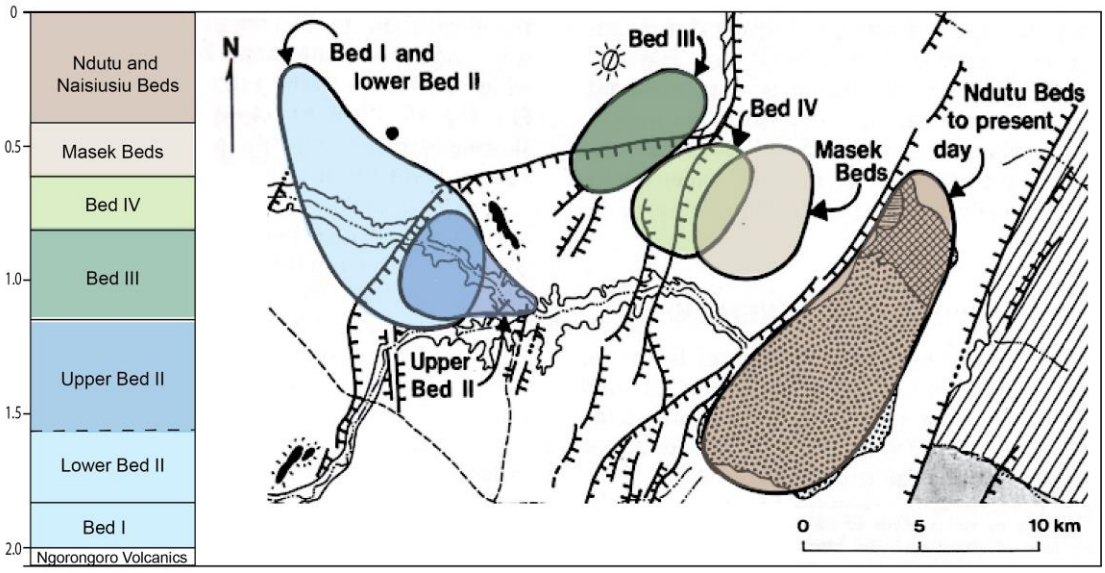


**Figure 5.** Map showing the inferred location of the drainage sump (depocenter) for different formations in the Olduvai Basin, based on outcrop interpretations from Hay (1976). A large, perennial lake occupied the basin during Bed I and lower Bed II deposition, following the culminating eruptions of the Ngorongoro volcano. Widespread faulting constrained the lake to a downthrown graben in upper Bed II. The drainage sump shifted northward for Bed III, then progressively shifted SE with the drainage sump toward the present day Olbalbal Swamp (dark brown).

### *Climatic Clues in Outcrop*

While lithology alone can provide useful information regarding depositional environment and climate (e.g., a waxy green claystone that indicates lake expansion during wet periods), more specific information regarding lake chemistry can be deduced from other physical characteristics like unit color. Many of the claystone and tuffs preserved in Olduvai contain a substantial amount of authigenic minerals (Hay, 1976). Authigenic minerals (e.g., clays and zeolites) form in situ and when preserved, provide information about a fluid's geochemical parameters (e.g., alkalinity, pH, salinity) at the

time of formation. The authigenic mineral assemblages preserved in Olduvai are associated with varying degrees of saline-alkaline fluid alteration.

In outcrop, tuffaceous units that contain less authigenic minerals have had less interaction with saline-alkaline fluids and appear white/pale grey to light olive green. The tuffaceous units that contain more authigenic minerals (especially zeolites) have had more interaction with saline-alkaline fluids and appear yellow to orange. Therefore, a white/pale grey to light olive green tuff may indicate the unit is less altered and a yellow to orange tuff may indicate the unit is more altered. An example of an altered yellow tuff (Tuff IF) in outcrop is given in Figure6.

**Figure 6.** Yellow zeolitization of Tuff IF in Olduvai Gorge outcrop. Photo by Lindsay McHenry.

**Olduvai Gorge Coring Project**

In 2014, The Olduvai Gorge Coring Project (OGCP) recovered four long sediment cores (1A, 2A, 3A, and 3B) from three different positions within the expected depocenter of Paleolake Olduvai (Figure 7a). Drilling into the depocenter was intended to retrieve cores of maximum thickness from all major Olduvai geological formations, aiming to obtain a paleoenvironmental and paleoclimatic dataset as complete and continuous as possible (Stanistreet et al., 2020b). Drilling decisions were informed by Hay's (1976) interpretations. Based on outcrop exposures, the Pleistocene deposits (above metamorphic bedrock) were anticipated to be 100-150 m thick, however none of the cores, including the deepest core (2A, 245 m long), reached bedrock.

The cores drilled totaled 611.72 m, with 575.48 m recovered (94.08% recovery rate) (Njau et al., 2021). The cores revealed new stratigraphy that was not observed in outcrop, including a long record of the volcanic history of the Ngorongoro volcano (Figure 8). Borehole 1A is the shortest core, ending before the Ngorongoro units. Borehole 2A records the volcanic history of a fan-delta from the Ngorongoro volcano and older lake intervals. Borehole 3A contains some of the Ngorongoro fan-delta but is not as deep as 2A, and Borehole 3B was drilled at the same site at an angle to obtain paleomagnetic data. Based on the more complete stratigraphic record provided by the cores, a new map showing the full aerial extent of Paleolake Olduvai (during Bed I maximum flooding) and the confined lake depocenter (during upper Bed II deposition) was created to reflect updated interpretations (Figure 7b).

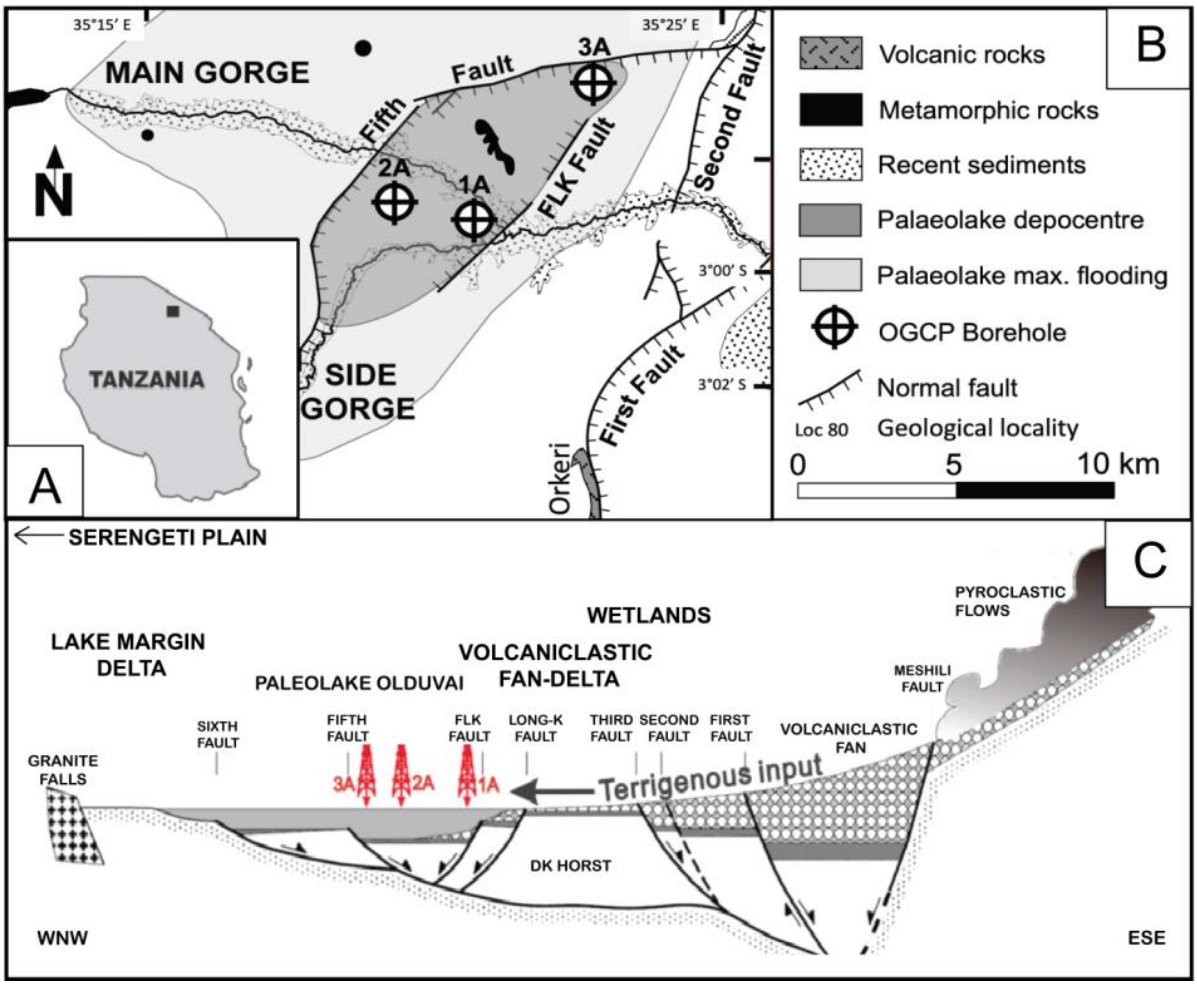


**Figure 7.** Position of OGCP 2014 boreholes. A. Inset map showing position of study area within Tanzania. B. Map showing position of boreholes, with lake extent (based on Beds I and II) updated to reflect post-drilling interpretation of lake extent and depocenter. C. Position of boreholes in cross section, near the Fifth Fault, based on of Tuff IE time (~1.81Ma) in Bed I stratigraphy. Modified from Stanistreet et al., 2020b.

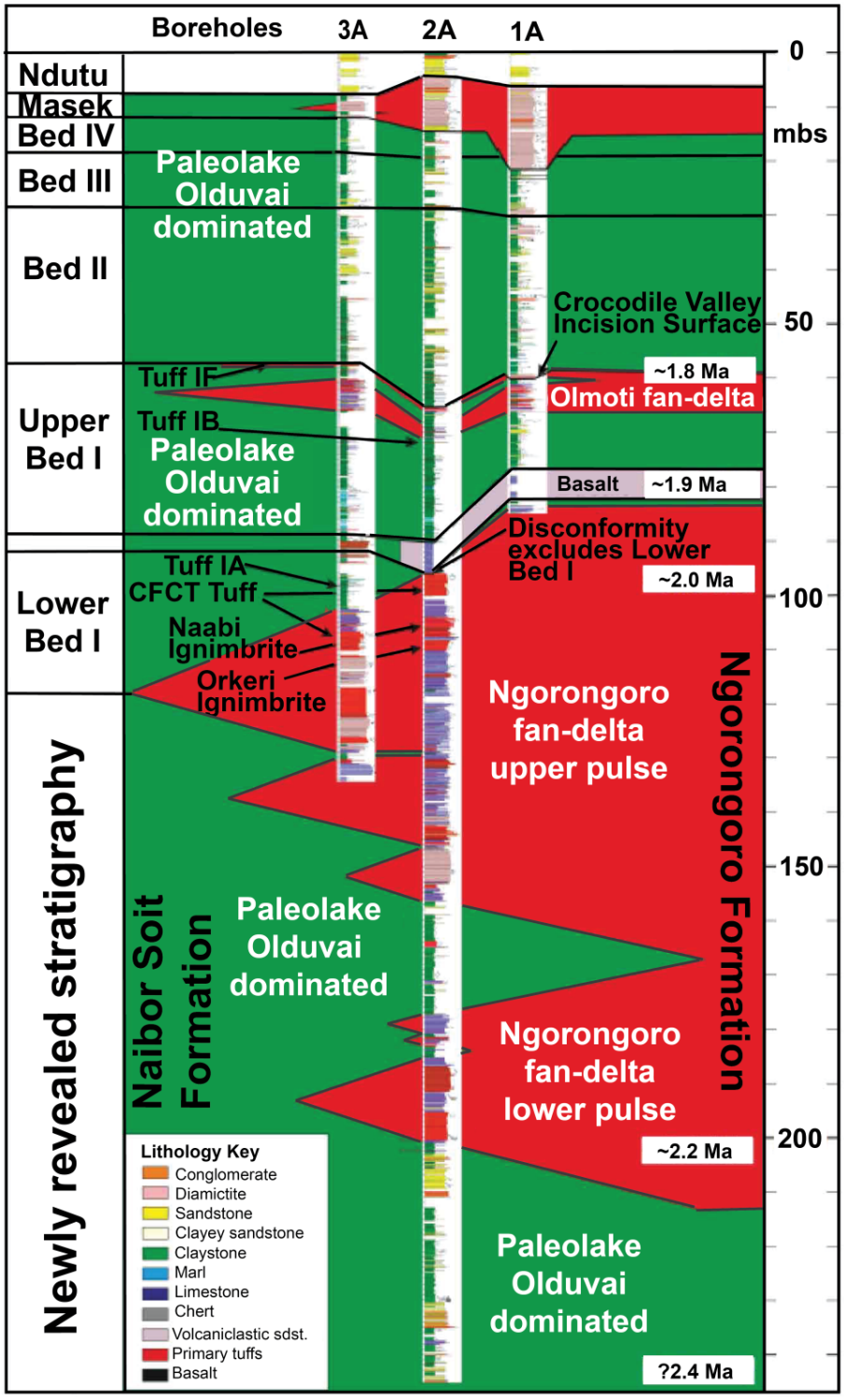


**Figure 8.** Stratigraphic column of OGCP 2014 cores (Modified from Stanistreet et al., 2020b).

The OGCP cores have been studied extensively using a variety of different proxies, with a focus on stratigraphy (trying to tie their records to outcrop exposures) and paleoclimate/ paleoenvironment reconstruction. These cores are accompanied by detailed core logs (Stanistreet et al., 2020b) to guide sampling. Previous and current paleoenvironment studies of these cores have focused mainly on the lake sediment intervals, but these cores also contain thick sections of volcanic deposits. The paleolake deposits interfinger with volcanic ashes, ignimbrites (centimeters to meters thick each), and sandstones derived from the reworking of these materials after deposition. These deposits contain a record of the volcanic history of the neighboring Ngorongoro Volcanic Highlands (NVH), which contributed pulses of volcanic materials into the Olduvai paleolake basin over most of its 2-million-year history (e.g. McHenry et al., 2020b). While these volcanic intervals have been used to constrain core ages (Deino et al., 2021) and their general tephra composition (McHenry et al., 2020b), they have not yet been assessed for their potential paleoenvironmental record.

**Ngorongoro Formation**

While the Ngorongoro Volcanic Highlands (NVH) include many volcanoes (Figure 1B), the volcanic pulses recorded in the Ngorongoro Formation (FM) are likely derived solely from Ngorongoro volcano, as this was the only known nearby active eruptive center at the time and also the only known source of rhyolites in the NVH (Mollel et al., 2008). Mollel et al. (2012) date basaltic to rhyolitic ignimbrites from Ngorongoro's crater walls to 2.3-2.0 Ma. Younger tuffs from the cores (from Olduvai Bed I) likely originated

from Olmoti volcano, as the oldest known Olmoti-derived tuffs are dated at 1.80 ±0.01 Ma (McHenry et al., 2008).

The Ngorongoro volcano is the largest volcano in the NVH. Eruptions and subsequent mass wasting and erosion distributed pyroclastic, volcaniclastic, and detrital material into the lake basin, over a 240 kyr duration (Mollel et al., 2008). At Olduvai, the deposits of volcanic origin are separated by interfingering lacustrine sediments, which indicate that the tuffs are from multiple eruptive events separated in time rather than from a single event (McHenry et al., 2020b).

The volcanic materials exposed in the lower part of Olduvai Gorge, considered to have erupted from Ngorongoro Volcano (Hay, 1976), were previously assigned to Olduvai Bed I (along with the overlying deposits). After the OGCP 2014 cores revealed additional units from the long volcanic history of the Ngorongoro volcano, all volcanic and volcaniclastic products interpreted as deposited by the Ngorongoro volcano were reassigned to the newly-defined Ngorongoro Fm. The formation, defined in Stanistreet et al., 2020b, is only recorded to its full (known) extent in core 2A, and only the uppermost units are exposed in outcrop. It is a pile of volcanic and volcano-sedimentary/ volcaniclastic deposits topped by the Coarse Feldspar Crystal Tuff (CFCT) and the Naabi Ignimbrite.

The Naabi and CFCT are recognized in outcrop in the western part of Olduvai Gorge and along the 1st Fault (Figure 7, McHenry et al., 2008). The Naabi Ignimbrite is

the oldest stratigraphic unit exposed in the western part of Olduvai Gorge (Deino et al., 2012; McHenry et al., 2020b), unconformably overlying metamorphic Archean basement rocks of the Tanzania Craton and Neoproterozoic basement of the pan-African Mozambique belt (Hay, 1976, Deino et al., 2021).

$^{40}Ar/^{39}Ar$ dating by Deino et al. (2012) and Deino et al. (2021) better constrained the ages of these ignimbrites (CFCT 2.0027 Ma ± 0.0057, Naabi 2.0330 Ma ± 0.0013). Age constraints, different glass and mineral compositions, and stratigraphic separation (McHenry et al., 2008; McHenry et al., 2020b) indicate these units are from two separate eruptions. However, both may be related to the development of the Ngorongoro caldera (Hay 1976).

Leading up to the caldera collapse, volcanics from the Ngorongoro volcano were deposited into Paleolake Olduvai during two major pulses. In between these two pulses, the lake had a major phase of transgression, depositing a lacustrine intertongue unit, part of the lacustrine Naibor Soit Formation defined by Stanistreet et al., 2020b. Therefore, the fans developed by deposition into the lake should be referred to as fan-deltas (Stanistreet et al., 2020b). The fan-deltas consist of volcaniclastic sand and scattered gravel clasts of lava, tuff, pumice, feldspar, and some obsidian, scoriae, and clay grains. The sandstones are interbedded with volcanic conglomerates 20 to 70 cm thick with clasts of lava (some vesicular), tuff, pumice, occasional obsidian, clay, and feldspar. Also present are 5 cm to 250 cm thick volcanic diamictite (mudflow) units, with a clast composition like that of the volcanic conglomerates.

The uppermost boundary of the upper Ngorongoro Fm (second pulse) is the interface between reworked units of the CFCT and the overlying thick claystone interval, where the lake dominated. This is a known diachronous boundary in the cores and in outcrop**.** Volcanic units in the Ngorongoro Fm include primary volcanic fine ash, coarse ash, lapilli ash, and ash lapilli tuffs, in units 5 cm to 200 cm thick. The tuffs are pumice-rich or crystal-rich, also containing lithic fragments in variable mixes (Stanistreet et al., 2020b). Additionally, the tuffs are mainly rhyolitic, with varying compositions of glass, anorthoclase to sanidine feldspar, small amounts of augite, quartz, and titanomagnetite and/or ilmenite. Other minerals are rare and limited to the capping ignimbrites (e.g., aenigmatite in the Naabi and hornblende in the CFCT, respectively) (McHenry et al., 2020b). Although thick volcanic units dominated, thin layers of lacustrine sediments still persisted and floated pumice is common, indicating the lake or related fluvial networks was still present at this time.

**Naibor Soit Formation**

The fluvio-lacustrine dominated upper Naibor Soit Formation (Fm) directly underlies the base of the upper Ngorongoro Fm in the cores. The upper Naibor Soit Fm is dominated by claystone, with thin layers of sandstone associated with turbidity currents. Segments of thicker sandstones, diamictites, and tuff units represent periods of low lake levels/prograding fan delta into the lake depocenter (Stanistreet et al., 2020b). The upper Naibor Soit Fm also contains short intervals of (thin) volcanic layers. The base of the upper Naibor Soit Fm directly overlies the lower Ngorongoro Fm (lower

pulse). The lower Ngorongoro Fm has similar characteristics to the upper Ngorongoro Fm (though it is not as thick) and directly overlies the lower Naibor Soit Fm.

The lower Naibor Soit Fm is considerably different from the upper Naibor Soit Fm. The claystone facies associated with the lake depocenter still persist, but this time with more evidence of a fluvial-propagated pro-delta sequence (prograding sand packages) from the southwest (Stanistreet et al., 2020b). Another major difference is the lack of volcanic layers, which shows that this depositional interval likely pre-dates activity at Ngorongoro. This formation contains small molluscan, plant, and fragments of animal fossils, indicating there were once much fresher conditions pre-Ngorongoro.

**Mineralogy/Geochemistry/Depositional Environments**

Because important biologically-derived paleoclimate indicators (e.g., phytoliths, diatoms, pollen) may not be present/preserved under extreme (saline-alkaline) conditions (Deocampo et al., 2009, 2018), mineralogy and geochemistry may be the only meaningful paleoenvironmental proxies available in the Ngorongoro Fm. These minerals are very sensitive to shifts in lake water chemistry, so preserved mineral proxies (e.g., zeolites, feldspars, clays) can record changes in lakes caused by both paleoclimatic conditions and tectonics.

Volcanic glass reacts to form zeolites by a dissolution-precipitation process (Hay and Sheppard, 2001). When in contact with fluid (e.g., water), glass becomes hydrated and then experiences ion exchange between ions in the water and in the glass structure

(Li et al., 2021). Soluble cations ($Na^+$, $K^+$, $Ca^{2+}$) are rapidly leached from the glass and dissolve into the fluid, leaving vacancies in the glass. This leaching occurs simultaneously with hydrolysis (Li et al., 2021). During hydrolysis, water molecules break into $H^+$ and $OH^-$ ions. The $H^+$ ions fill the vacancies left in the glass and the $OH^-$ ions stay in solution, increasing pH (Frankel et al., 2018). In addition to increasing pH, this process increases alkalinity of the solution, which in turn accelerates the rate of glass dissolution (Chipera and Apps, 2001).

Alkalinity and pH are also dependent on the volume of water in the system. Lower lake levels (during dry periods) have a higher concentration of cations while higher lake levels (during wet periods) have a higher volume of freshwater that dilutes the concentration. In arid climates, alkaline lakes that experience extensive evaporation concentrate salts until becoming saline-alkaline. In extreme cases, highly alkaline interstitial brines can form (Langella et al., 2001).

Slightly different mineral assemblages will form from varying intensities of saline-alkaline conditions, as changes in ionic concentration of the lake water will result in compositionally different minerals. Therefore, the observed mineral assemblages correlate with lake water chemistry. In more extreme, saline-alkaline conditions (pH>9), authigenic minerals (i.e., zeolites) will dominate. Under fresher conditions, there are fewer mobile ions to concentrate into authigenic minerals (although Al-rich clays may dominate). As a result, the observed authigenic mineral assemblages can provide

information about diagenetic conditions and their associated geochemical parameters (pH, salinity, temperature, and starting compositions).

The volcanics observed in Olduvai outcrops above the Ngorongoro Formation (in Bed I) are silica-undersaturated trachytes derived from the Olmoti volcano. Based on findings from McHenry et al. (2020a), there are several lake clay intervals that contain authigenic mineral assemblages consistent with more saline-alkaline fluids. While the weathering of trachyte can contribute to the alkalinity of fluids within a basin (regardless of the starting alkalinity of the fluid), the trachytic materials from the Olmoti volcano (in upper Bed I) were determined to have been deposited into an already saline-alkaline lake.

The authigenic mineral assemblages observed in the trachytic units of Olduvai Bed I are the result of in-situ alteration of volcanic glass in a semi-arid, closed basin under saline-alkaline conditions (pH ≥9). Normally mobile, the cations that are leached from trachytic material ($Ca^{2+}$, $Na^{+}$, $K^{+}$) can remain within the closed system and be incorporated into zeolites and other alteration products (Hay and Sheppard, 2001; McHenry, 2009). Elements that are incompatible with zeolite structures (e.g., Ti, Mg, and Fe) are instead concentrated into authigenic clay minerals (McHenry, 2009, 2010).

The observed assemblages vary with changing lake conditions, depending on how saline and/or alkaline the fluid is at the time. Volcanic glass is typically preserved in ‘fresher’ (less saline-alkaline) conditions, but may undergo partial dissolution with the

local precipitation of certain alteration minerals that can form under moderately alkaline conditions (e.g., clays and the zeolite mineral erionite) in pore spaces of pumice. When glass dissolves under fresher, moderately alkaline conditions, the zeolite mineral clinoptilolite can precipitate with high Si activity and the zeolite mineral chabazite can precipitate with a high $Ca^{2+}$ concentration. Further glass dissolution can result in a high $K^{+}$ concentration, which under more alkaline conditions can help form the higher-alteration zeolite mineral phillipsite. With increased alteration, high $K^{+}$ coupled with high salinity will form the zeolite analcime (McHenry et al., 2020a, 2023). Under extreme conditions, earlier-formed zeolites can be replaced by authigenic feldspar. This process is illustrated in Figure 9. Authigenic clay and zeolite names and formulas are listed in Tables 1 and 2.

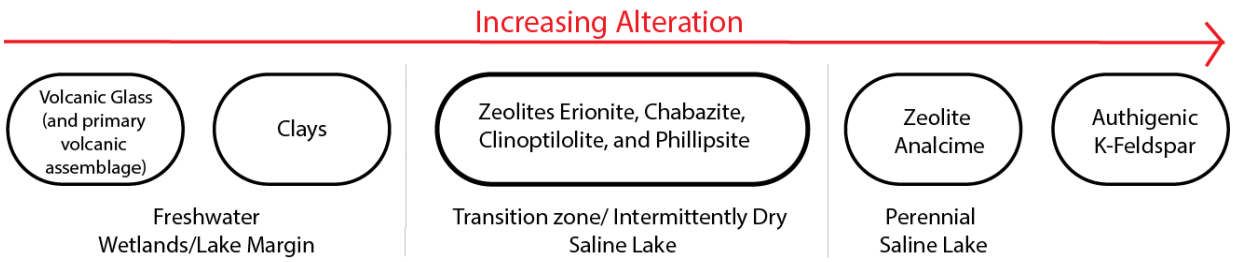


**Figure 9.** Authigenic minerals in Olduvai. Conceptual flowchart showing alteration associated with depositional environment.

**Table 1**

Clay minerals present in Olduvai Gorge, with formulas and environment they form in.

| Clay Mineral | General Formula | Adsorbed or absorbed cations | Environment |
|---|---|---|---|
| Kaolinite | $Al_2Si_2O_5(OH)_4$ | | Less alkaline, fresh water lake |
| Montmorillonite | $(Na,Ca)_{0.33}(Al, Mg)_2(Si_4O_{10})(OH)_2 \cdot nH_2O$ | Hydrated exchangeable cations | Low salinity |
| Illite | $(K,H)Al_2(Si,Al)_4O_{10}(OH)_2XH_2O$ | K | High salinity |

From McHenry et al., 2023

**Table 2**

Zeolite minerals present in Olduvai Gorge with formulas and environment they form in.

| Mineral Series | Example Formula | DEC* | Environment |
|---|---|---|---|
| Analcime | $Na(AlSi_2O_6) \cdot H_2O$ | Na, Minor K | High salinity ($Na^+ > K^+$) |
| Chabazite | $Ca_2[Al_4Si_8O_{24}] \cdot 13H_2O$ | Ca, Na, K | Less alkaline, high $Ca^{2+}$ |
| Clinoptilolite | $Na_6(Si_{30}Al_6)O_{72} \cdot 20H_2O$ | Na, K, Ca | High Si activity |
| Erionite | $K_{10}[Si_{26}Al_{10}O_{72}] \cdot 30H_2O$ | K, Na, Ca | Glass alteration |
| Phillipsite | $K_6(Si_{10}Al_6)O_{32} \cdot 12H_2O$ | K, Na, Ca | High $K^+$ |

*DEC= Dominant extraframework cations.
From McHenry et al., 2023

Hay (1970) applied methods that Sheppard and Gude (1968) used to study Paleolake Tecopa (California) to characterize different alteration profiles identified in Olduvai Gorge. He found that the paleolake margin contained zeolites but was also the most likely environment in which to find original (less altered) glass, likely because of freshwater flux at the margins. The central lake deposits were similar to the Sheppard and Gude (1968) findings for Tecopa, with potassium feldspar, phillipsite, and no glass.

The alluvial deposits ranged from completely zeolitized towards the lake center to unaltered closer to the lake margins. The variation in authigenic mineral assemblages between different alteration profiles can be illustrated as ‘alteration zones’ in aerial view. Figure 10 depicts the depositional environments associated with these alteration zones, based on Hay’s (1976) interpretations.

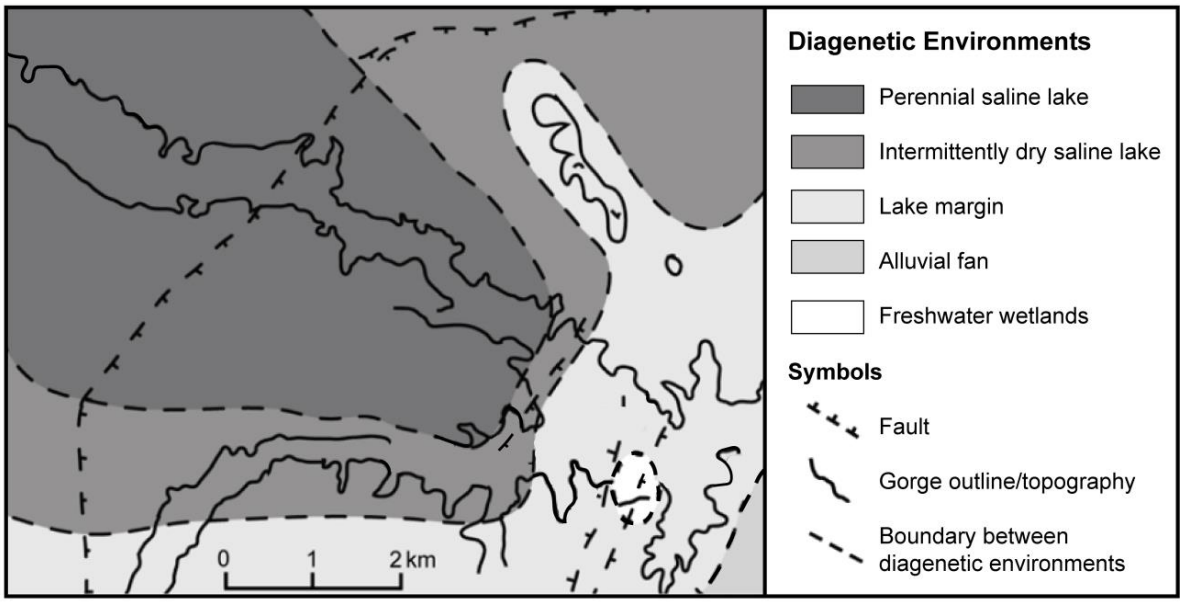


**Figure 10.** Map of a portion of Paleolake Olduvai, showing the location of different depositional environments for Upper Bed II, based on outcrop studies (e.g., sedimentology and authigenic mineralogy). The most altered mineral assemblages are found in the perennial saline lake and the least altered are along the fresher, flooded lake margin. Paleogeography and paleoenvironmental reconstruction after Hay (1976) and Ashley and Hay (2002). Modified from McHenry (2010).

The alteration zone concept still applies to the study area, but the OGCP studies have better constrained the position and extent of the paleolake. Figure 11 depicts the aerial extent of Paleolake Olduvai during maximum flooding (in Bed I), based on OGCP core data. All three boreholes were sited in the lake depocenter, constrained between

the 5th and FLK faults. The figure also leaves out the position of the “intermittently dry saline lake”, as this position would change over time with lake level, tectonics, and sediment input. Using this map, the alteration profiles are classified into three different lithofacies: a fresh-glass facies, a K-feldspar facies, and a zeolite facies.

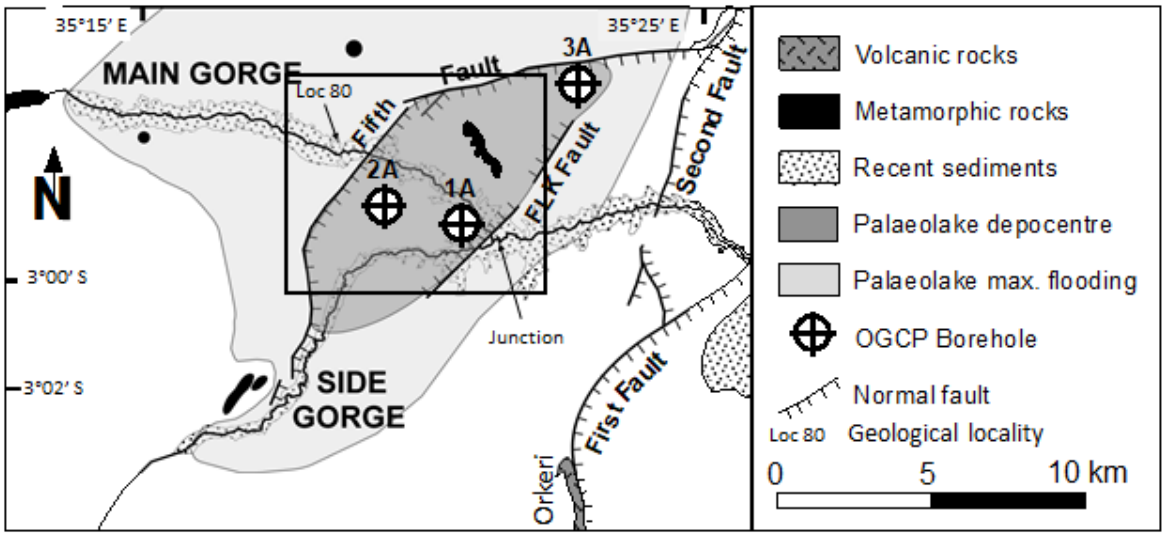


**Figure 11.** Map of Paleolake Olduvai depicting the lake depocenter, maximum extent of flooding, and the position of the OGCP 2014 boreholes. Based on OGCP core interpretations of Bed I. The black box represents the map area shown in Figure 12. From McHenry et al., 2020b.

A fresh-glass facies is found along the distal lake margin, above the water table and farther from the lake depocenter. The lake margin is associated with fresher conditions resulting in less altered assemblages, preserving the original volcanic assemblage (e.g., anorthoclase), large amounts of vitreous tuff (glass) and minor amounts of zeolites and authigenic clays. A K-feldspar facies is found in the lake depocenter. The depocenter is associated with perennial saline lake conditions resulting in highly altered assemblages, with large amounts of clay minerals, zeolites (phillipsite and analcime), and even authigenic feldspars (K-feldspar or albite). Lastly, a zeolite

facies is found in the proximal lake margin (transition zone between the perennial lake and distal lake margin). The transition zone is associated with intermittently dry saline lake conditions resulting in less altered mineral assemblages, still containing clay minerals and zeolites (chabazite, erionite, clinoptilolite), but also preserving relict glass.

Although these alteration profiles were determined based on alteration assemblages associated with younger Olmoti-derived trachyte (altered under saline-alkaline conditions), they can inform our understanding of altered tephra from older units within the same paleobasin, including Ngorongoro-derived rhyolites. Rhyolitic glass and saline-alkaline pore water provides the material needed to form zeolites and subsequent K-feldspar (Sheppard and Gude, 1969). Similar alteration patterns can be used to compare the assemblages from known depositional environments and determine how lake conditions might have changed over time.

Because vertical boreholes are at a fixed position, changes in authigenic mineral assemblages throughout the core should reflect changes in climatic conditions over time. However, the lake's level and position was subject to change based on other factors like tectonics and sediment input over time. These factors changed the position, extent, and type of depositional environment in the basin. For example, Figure 12 shows the position of Paleolake Olduvai after a northern progradation of the Ngorongoro-sourced volcanic fan pushed the lake into a new position (Stollhofen et al., 2021). The shoreline position varied based on changes in lake level and fan

progradation/retreat. This was immediately followed by a wet phase that transitioned into the Bed I lake.

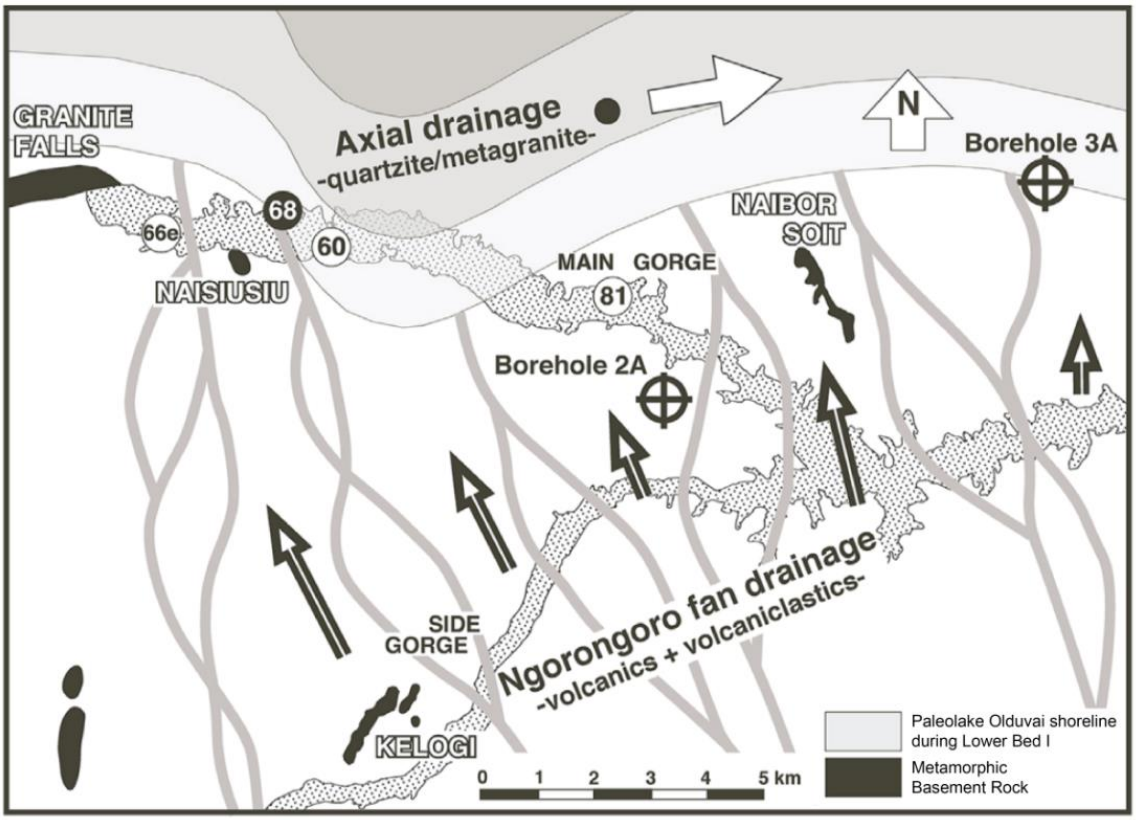


**Figure 12.** Map depicting the position of Paleolake Olduvai after being displaced by the Ngorongoro volcaniclastic fan (between CFCT and Bed I). Interpretation based on data from Trench 168 (highlighted locality 68). The lake returned immediately after CFCT emplacement at 2.015 ± 1.006 Ma, evidenced by the transition from a debris-flow dominated fan to a lacustrine fan-delta toe, clays indicating a low-energy shoreline over the fan and surrounding grasslands, and preserved freshwater fauna. From Stollhofen et al., 2021.

Understanding how outside factors change both lithology and mineral assemblage is important when interpreting climate change from these units. For this reason, a more accurate determination of the degree of alteration can be made by comparing mineral assemblages of samples from the same depositional environment (indicated by lithologies). Differences in mineral assemblages from samples of the same

depositional environment can then be used to determine if there are changes in climatic conditions.

Prior to the recovery of the OGCP cores in 2014, mineralogical studies focused on identifying changes in climatic conditions were limited to the Olduvai beds exposed in outcrop (and in trenches). Studying these cores, McHenry et al. (2020a) used authigenic mineralogy to determine paleoclimatic conditions from different lithologies (a combination of tuff, coarser grained volcaniclastic claystone, sandstone, conglomerate, and diamictites) in the older Ngorongoro and Naibor Soit Formations.

Based on the mineral assemblages of the lacustrine intervals in the cores, McHenry et al. (2020a) found that the lower Naibor Soit Fm represented an early saline-alkaline lake with the dominant zeolites transitioning from analcime (indicating extremely saline-alkaline conditions) to phillipsite and chabazite (indicating less, but still highly saline-alkaline conditions). A major environmental change occurred in the lower Ngorongoro pulse, with the dominant zeolite transitioning to erionite and chabazite (indicating lower alkalinity). The Upper Naibor Soit Fm indicates a fresher lake than that of the lower Naibor Soit Fm, with erionite and chabazite as the dominant zeolites. The Upper Ngorongoro Fm consists of rhyolitic glass and minor erionite and chabazite. Lastly, a lack of zeolites in the units between the Upper Ngorongoro Fm and the Bed I basalts indicate particularly freshwater conditions at the position of Core 3A, the only core that preserves this interval.

While McHenry et al. (2020a) successfully used authigenic mineral assemblages to reconstruct paleoclimatic conditions, the study mainly focused on fine-grained lacustrine intervals, with few samples from the Upper Ngorongoro Fm in core 2A. This study will focus on the mineralogy of the entire Ngorongoro Fm (upper in cores 2A and 3A, lower in core 2A) and will limit sampling to tuffaceous units (including diamicites) to better understand the extent of alteration in the volcanic units of the Ngorongoro Fm.

Based on zeolite studies by Hay and Shepard (2001), we can make assumptions regarding paleoclimatic controls in our study area. First, data from other studies (e.g., Hay, 1976; Stanistreet et al., 2020a) reflect a hydrologically closed, saline-alkaline rift-lake environment in an arid to semi-arid climate. Second, this part of the cores is at or less than 200 meters deep, which suggests that alteration occurred at or near ambient pressure and temperature. Third, there are no hot, welded tuffs in this part of the cores that could have caused geothermal/hydrothermal alteration.

## III. METHODS

### Sampling

Selected intervals of the OGCP cores (Figure 13), stored at the Continental Drilling Core (CSD) Facility at the University of Minnesota- Twin Cities (in Minneapolis, MN) were sampled in June 2022 for analyses at the University of Wisconsin-Milwaukee (UWM). Intervals of interest, with a focus on contacts between volcanic deposits (ash/tuff/ignimbrites) from the Ngorongoro Fm and lake sediments, were chosen using the detailed core logs (e.g., Stanistreet et al., (2020b)) and in-person observations. Only cores 2A and 3A were analyzed since they contain deposits of Ngorongoro Formation volcaniclastics.


**Figure 13.** Photo of core 2A-60Y-1 being sampled at the CSD Facility.

Rhyolitic units of the Ngorongoro Formation were targeted for sampling in this study. While there are a few trachytic and basaltic outliers in the cores, these intervals were avoided. Sampling focused on pumice, lapilli, and ash since the aims of this study were to examine the alteration of volcanic glass. Thirty-one new samples were collected for this study (Tables 3 and 4). Lake sediments from this interval have already been analyzed by XRD and published (McHenry et al., 2020a), so no lake claystone intervals were sampled. Lithologies listed in these tables are based on Stanistreet et al. (2020b), and indicate whether the sampled unit was primary (e.g., airfall tuffs, pyroclastic flows) or reworked (e.g. debris flows, float pumice). Intervals labeled as “diamictites” likely reflect lahar deposition.

The OGCP samples collected for analysis were chosen based on varying proximity to lacustrine sediments (using detailed core logs, e.g., Stanistreet et. al., (2020b). These interfaces allow us to assess how the composition of selected intervals of ash deposits were influenced by fluids related to the saline-alkaline lake. An example core segment (3A-49Y-1) is shown in Figure 14. This diagram shows the position of each sample within the core segment (relative to finer-grained lake sediments), the lithology (from Stanistreet et al., 2020b), and a picture of each sample. More examples are shown in Appendix A.

Because unit thickness varies, the following classification system specifies the degree of stratigraphic separation (insulation) from the lacustrine sediments (differences in rock type will be taken into consideration during later analyses): “Proximal” indicates

the sample was either directly touching or very close to lake sediment (in some cases directly in the lake sediments, e.g. pumice float). “Intermediate” indicates the sample was towards the middle of a unit and away from lake sediments, but the unit may be thinner than other units analyzed in this study or may be surrounded by lake sediments (rather than further insulated by other volcanic units). Lastly, “Separated” implies that the sample is from a very thick volcanic unit (relative to other unit thicknesses), far from lake sediments and perhaps further insulated by other volcanic intervals.

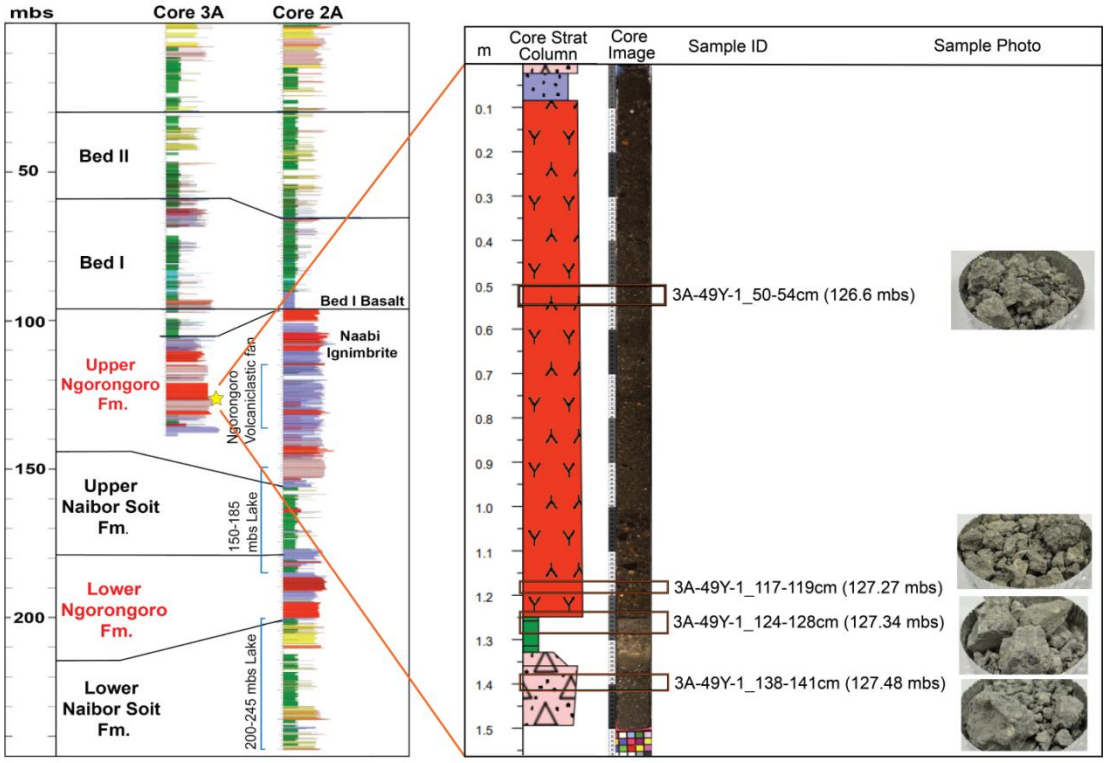


**Figure 14.** Core 3A-49Y-1, showing location of samples in the core and the variation in stratigraphic separation from a lake clay. Sample 3A-49Y-1_124-128 is a waterlogged float pumice that is touching the lake clay and is therefore labeled as “proximal” indicating little to no stratigraphic separation (thus no insulation) from a lake clay interval. Sample 3A-49Y-1_50-54cm is an ash lapilli tuff sampled from the middle of the unit. Because the term “separated” is reserved for well-insulated samples (in meters thick units of tephra), this sample is labeled as “intermediate” indicating there is stratigraphic separation (and potential insulation) from a lake interval, but it is not classified as stratigraphically far from the lake clay unit.

**Table 3**

Sample ID, lithology, depth, and stratigraphic proximity to lake clays in core 2A. Lithologies based on Stanistreet et al., 2020b.

| Unit | Sample ID | Lithology | MBS | Proximity to Lake Clay |
|---|---|---|---|---|
| Ngorongoro Fm (Upper Pulse) | | | | |
| | 2A-47Y-2_10-12cm | Debris Flow Pumice | 117.95 | Proximal |
| | 2A-47Y-2_25-32cm | Debris Flow Pumice | 118.1 | Proximal |
| | 2A-47Y-2_79-83cm | Debris Flow Pumice | 118.64 | Intermediate |
| | 2A-50Y-2_134-137cm | Airfall Tuff Pumice fallout | 128.84 | Proximal |
| | 2A-51Y-1_32-35cm | Float pumice | 129.32 | Proximal |
| | 2A-51Y-1_40-42cm | Pumice wash | 129.4 | Proximal |
| | 2A-54Y-1_80-81cm | Waterlogged pumice | 138.8 | Proximal |
| | 2A-60Y-1_59.5-62cm | Airfall tuff | 153.595 | Proximal |
| | 2A-63Y-2_45-48cm | Airfall tuff | 163.946 | Proximal |
| | 2A-63Y-2_114-117cm | Airfall tuff | 164.636 | Intermediate |
| Ngorongoro Fm (Lower Pulse) | | | | |
| | 2A-69Y-2_34-37cm | Ash lapilli tuff | 181.801 | Intermediate |
| | 2A-70Y-1_4-6cm | Stacked fine Airfall ash | 183.04 | Proximal |
| | 2A-70Y-1_32-34cm | Stacked fine Airfall ash | 183.32 | Proximal |
| | 2A-70Y-2_109-112cm | Volcaniclastic sandy debris flow | 184.1 | Proximal |
| | 2A-72Y-1_136-142cm | Ash lapilli tuff | 190.36 | Separated |
| | 2A-72Y-2_64-67cm | Pyroclastic flow pumice | 191.095 | Separated |
| | 2A-72Y-2_99-102cm | Lapilli ash tuff | 191.445 | Intermediate |
| | 2A-74Y-3_25-34cm | Lapilli ash tuff | 196.765 | Separated |
| | 2A-74Y-3_109-117cm | Pyroclastic flow | 197.605 | Separated |

**Table 4**

Sample ID, lithology, depth, and stratigraphic proximity to lake clays in core 3A.

| Unit | Sample | Lithology | MBS | Proximity to Lake Clay |
|---|---|---|---|---|
| *Ngorongoro Fm (Upper Pulse)* | | | | |
| | 3A-41Y-1_40-42cm | Pumice in coarse ash | 105.5 | Proximal |
| | 3A-41Y-1_58-60cm | Lapilli ash tuff | 105.68 | Proximal |
| | 3A-41Y-1_82-84cm | Fine laminated ash | 105.92 | Proximal |
| | 3A-41Y-2_24-26cm | Float pumice in lapilli ash tuff | 106.841 | Proximal |
| | 3A-41Y-2_109-112cm | Ash lapilli tuff, pyroclastic flow, obsidian clasts | 107.691 | Separated |
| | 3A-45Y-2_10-12cm | Weathered pumice in diamictite | 115.575 | Proximal |
| | 3A-49Y-1_50-54cm | Ash lapilli tuff | 126.6 | Intermediate |
| | 3A-49Y-1_117-119cm | Ash lapilli tuff | 127.27 | Proximal |
| | 3A-49Y-1_124-128cm | Waterlogged float pumice | 127.34 | Proximal |
| | 3A-49Y-1_138-141cm | Diamictite with pumice | 127.48 | Proximal |
| | 3A-50Y-1_36-39cm | Waterlogged floating pumice | 129.46 | Proximal |
| | 3A-50Y2_41-43cm | Waterlogged pumice float | 130.91 | Proximal |

The collected samples were transported back to the University of Wisconsin-Milwaukee, where they were unpackaged and left to air dry for a few days. Upon drying, the samples were organized by core, in order of their relative position within the core (Figure 15). Sample color and observed glass/minerals were used to postulate the expected degree of alteration for each sample, based on Hay's (1976) observations. White/pale grey to light olive green samples were expected to be less altered (e.g., more glass, less authigenic minerals) and yellow to orange samples were expected to be more altered (e.g., less glass, more authigenic minerals). Brown samples may be associated with the formation of a paleosol, therefore the color may not reflect saline-alkaline alteration.

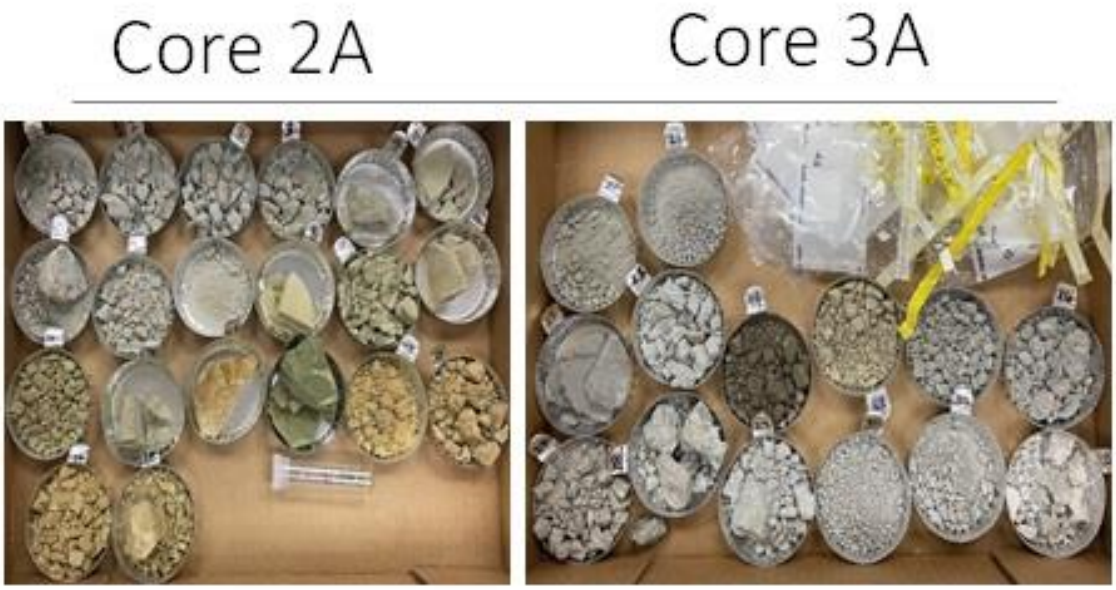


**Figure 15.** Dried OGCP 2014 core samples. Samples are organized from left to right (continuing onto the next row) by increasing depth in each core. The first 11 trays in core 2A and all samples in core 3A are from the Upper Ngorongoro Fm. The remaining core 2A samples are from the Lower Ngorongoro Fm.

**Sample Preparation and X-Ray Diffraction**

Samples were prepared for X-Ray Diffraction (XRD) analysis to determine the mineral assemblage of each unit sampled. Pumice/lapilli were separated from the bulk sample (to limit the effects of detrital contamination) by hand using a picking tool. ~3 g of lapilli from each sample were powdered to approximately 45 microns. Bulk samples were used when lapilli could not be extracted or from finer ash units that did not contain lapilli. Powdered samples were mounted into a cavity sample holder and analyzed using a Bruker D8 Focus XRD system (Cu Ka radiation, 4 s per 0.01° 2θ, 2°–60° range, Sol-X energy dispersive detector) (McHenry, 2009). Patterns were analyzed using the *DIFFRAC.EVA* software (ICDD PDF-2 mineral database) to determine mineral assemblages for each sample.

## Loss on Ignition

The analyzed XRD powder was recovered, dried overnight in a 105°C drying oven, and then prepared for Loss on Ignition (LOI) analysis. Approximately 0.5 g of each dried sample was weighed into a weighed crucible and placed into a muffle furnace at 1050˚C for 15 minutes and then cooled in a desiccator. The cooled crucibles were weighed again post-ignition and the measurements were used to calculate LOI.

## X-Ray Fluorescence

Powdered samples were analyzed for major and minor element compositions using X-ray Fluorescence (XRF) Spectrometry. A dried split of each powder was used. Approximately 1 g of ammonium nitrate, 10.000 g of Claisse 50:50 LiT:LiM flux with an integrated LiB non-wetting agent and 1.000 grams of sample were combined in a weighing dish and poured into a crucible. Each sample was fused and cast into a mould in a Claisse M4 fluxer, using a ~20-minute routine.

Each bead was analyzed using a Bruker AXS, Inc. Pioneer S4 WD-XRF instrument, using a calibration curve based on eleven USGS standards. Instrument precision was determined by alternately running standards and measuring the variability between analyses (McHenry, 2009). The beads were analyzed for eighteen major, minor, and some trace elements (Byers et al., 2016).

**Scanning Electron Microscopy**

Sample selection for SEM analysis was strongly dependent on what was available after other lab analyses. Many samples were from specific, thin intervals in the core, which limited sample size. Pumice and lapilli were picked out of these small samples to powder for XRD and XRF analyses, leaving a small amount of material for SEM analysis. Additionally, friable samples could not be used as they would crumble into powders, which affected sample preparation and also destroyed the textural relationships desired from this analysis. Finer-grained (ash fall) samples were also avoided for the reasons above. After determining what could be analyzed (e.g., pumice, lapilli), samples were selected for SEM analysis based on their XRD patterns. The purpose of this was to choose samples that would represent different degrees of alteration and provide enough representation of each mineral assemblage identified by XRD.

After samples were selected, a colloidal graphite and epoxy mixture was prepared (one part colloidal graphite to two parts epoxy) to mount pumice samples. A dab of the epoxy mixture was carefully placed onto a 15mm aluminum pin, followed by embedding a piece of pumice and curing for a minimum of 24 hours under vacuum. After the epoxy cured, the top half of each sample was broken off to expose a fresh surface to analyze. The samples were outgassed for an additional 24 hours, then carbon coated before scanning.

The samples were examined using a Hitachi S-4800 scanning electron microscope to observe the crystal shapes and textural relationships between the authigenic minerals. Secondary electrons (SE) were used to observe the 3D crystal morphologies.

Samples identified as ‘altered’ by their XRD patterns were examined first to observe the morphologies of the known minerals. After each mineral’s morphology was observed, more samples were examined to help identify minerals or confirm the mineral assemblages identified in XRD.

***Energy Dispersive Spectrometry (EDS)***

Select samples were examined using a Bruker Quantax ESPIRIT EDS system, installed in the Hitachi S-4800 scanning electron microscope. Electrons from the primary electron beam will excite fluorescence within the sample, generating characteristic X-rays for the elements with which it interacts with. The elemental makeup for a particular point on an observed mineral. The characteristic X-rays are displayed as a spectra that the viewer can use to aid in identification of mineral phases present in the sample.

# IV. RESULTS

## X-Ray Diffraction

Because authigenic minerals form from the dissolution of amorphous volcanic glass, the degree of alteration can be determined by the observed ratio of amorphous vs. crystalline material in the XRD pattern. In crystalline samples, incident X-rays are diffracted at specific angles by the crystal lattice, resulting in defined peaks in an XRD pattern, which are used to identify minerals. If a specimen is amorphous (lacks long-range crystallographic order), there will be no defined crystal peaks. Instead, there will be a broad amorphous ‘hump’ in the XRD pattern. Samples that contain both rock and amorphous material produce diffraction patterns with both crystalline and amorphous patterns (Rowe and Brewer, 2018). A relatively unaltered vitreous sample will mainly be glass, thus having a large amorphous hump and possibly very low-intensity crystalline peaks (often specific to volcanic phenocrysts), if present at all. A moderately-altered sample will have less glass and more authigenic minerals, which will look like a less intense hump and more crystalline peaks. Lastly, a very-altered sample will have no glass, and more authigenic minerals with high-intensity peaks (Figure 16). All XRD plots presented include both the original ray X-ray count data (upper pattern) and the processed pattern below, which has been smoothed and background subtracted and used for pattern matching.

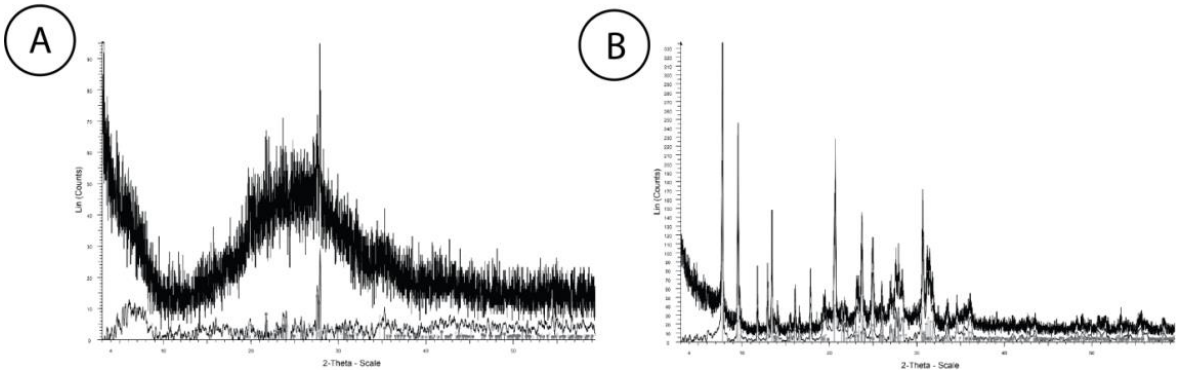


**Figure 16.** Examples of XRD patterns displaying degree of alteration. In each graph, the upper pattern is the raw counts and the lower pattern is the smoothed and background-subtracted pattern. A) A relatively 'unaltered' XRD pattern displaying a characteristic amorphous hump. B) An 'altered' XRD pattern displaying more crystalline peaks and lacking an amorphous hump.

XRD patterns from the analyzed Ngorongoro Fm samples range from relatively unaltered to moderately altered. Figure 17 shows representative XRD patterns displaying this range of alteration. All XRD patterns contain minerals relating to the primary volcanic assemblage (anorthoclase and occasional quartz) and some smectitic clay (matched as "montmorillonite"). Relatively unaltered samples also display the characteristic amorphous 'hump' corresponding to volcanic glass. With increased alteration, the slightly altered samples still contain the characteristic amorphous 'hump', but it is less intense than in the unaltered samples. XRD patterns for these samples also contain small to moderately intense peaks associated with 'low-alteration' zeolites (erionite and chabazite). Lastly, the moderately altered samples lack an amorphous glass hump and have higher intensity peaks for the same low-alteration zeolites (erionite and chabazite). 'Higher alteration' zeolites (clinoptilolite and phillipsite) were only present in a few samples. No 'high alteration' minerals (zeolite analcime and

authigenic feldspars) were observed within the Ngorongoro FM samples. The mineral assemblage for each sample is reported in Tables 5 and 6, with the corresponding XRD patterns in Appendix B.

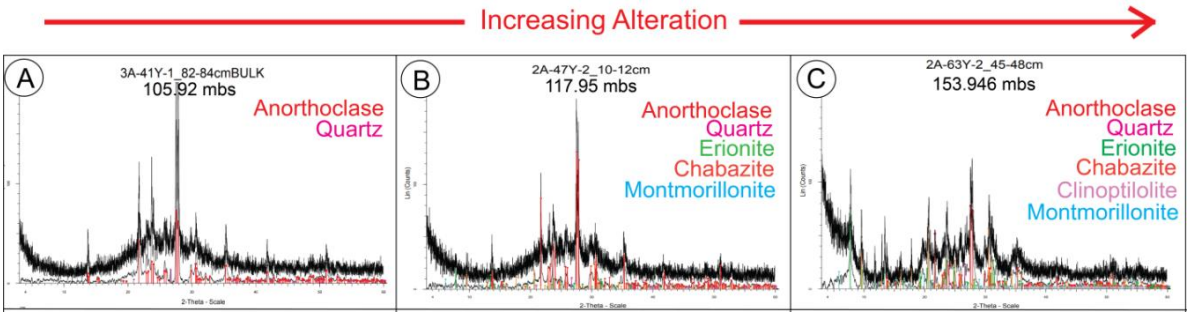


**Figure 17.** Representative XRD patterns showing the variation in alteration. A) 'Relatively Unaltered', maintains original mineral assemblage (primary volcanic minerals), more glass (amorphous hump), may have minimal clay and zeolite. B) 'Slightly Altered', maintains original mineral assemblage, glassy amorphous hump, some clay, some zeolites (chabazite, erionite). C) 'Moderately altered', maintains original mineral assemblage, may still have some amorphous glass, but amorphous hump is much smaller/missing, with more clay and zeolites (sharper and more intense peaks), erionite, chabazite, clinoptilolite and phillipsite may be present. Note abundant clay (montmorillonite).

**Table 5**

Mineral assemblage for each sample in core 2A.

| Unit | Sample ID | mbs | Am | Ac | Q | Er | Ch | Ca | Ph | Cl | Sm |
|---|---|---|---|---|---|---|---|---|---|---|---|
| *Ngorongoro Fm (Upper Pulse)* | | | | | | | | | | | |
| | 2A-47Y-2_10-12cm | 117.95 | *XXX* | *XXX* | *X* | *X* | *X* | - | - | - | *X* |
| | 2A-47Y-2_25-32cm | 118.10 | *XXX* | *XX* | *X* | *X* | *X* | - | - | - | *X* |
| | 2A-47Y-2_79-83cm | 118.64 | XXX | XX | X | X | X | XX | - | - | X |
| | 2A-50Y-2_134-137cm | 128.84 | XXX | XX | X | X | XX | X | X | - | X |
| | 2A-51Y-1_32-35cm | 129.32 | XXX | XX | X | X | X | X | - | - | X |
| | 2A-51Y-1_40-42cm | 129.40 | XXX | XX | X | X | X | XX | - | - | X |
| | 2A-54Y-1_80-81cm | 138.80 | XXX | XX | - | XX | XX | - | - | - | X |
| | 2A-60Y-1_59.5-62cm | 153.60 | X | XX | - | XXX | XXX | - | - | - | X |
| | 2A-63Y-2_45-48cm | 163.95 | X | XX | XX | XX | XX | - | - | X | X |
| | 2A-63Y-2_114-117cm | 164.64 | X | XXX | XX | XX | XXX | - | - | X | X |
| *Ngorongoro Fm (Lower Pulse)* | | | | | | | | | | | |
| | 2A-69Y-2_34-37cm | 181.80 | X | XXX | - | XXX | XX | - | - | - | - |
| | 2A-70Y-1_4-6cm | 183.04 | XXX | XXX | - | XX | XX | - | - | - | - |
| | 2A-70Y-1_32-34cm | 183.32 | X | XXX | - | XXX | XXX | - | - | - | - |
| | 2A-70Y-2_109-112cm | 184.10 | X | XXX | XX | XXX | XXX | - | XX | XX | X |
| | 2A-72Y-1_136-142cm | 190.36 | XX | XXX | - | XXX | XX | - | - | - | - |
| | 2A-72Y-2_64-67cm | 191.10 | XX | XXX | - | XXX | XX | - | - | - | - |
| | 2A-72Y-2_99-102cm | 191.45 | XX | XXX | X | XXX | XX | - | - | - | - |
| | 2A-74Y-3_25-34cm | 196.77 | XXX | XXX | - | XX | XXX | - | - | - | - |
| | 2A-74Y-3_109-117cm | 197.61 | XXX | XX | - | XX | XX | - | X | - | X |

XXX = Major. XX = Minor. X = Trace. – = absent
Am: Amorphous, Ac: anorthoclase, Q: quartz, Er: erionite, Ch: chabazite, Ca: calcite, Ph: phillipsite, Cl: clinoptilolite, Sm: smectite (montmorillonite)

**Table 6**

Mineral assemblage for each sample in core 3A.

| Unit | Sample ID | mbs | Am | Ac | Q | Er | Ch | Ca | Ph | Cl | Sm |
|---|---|---|---|---|---|---|---|---|---|---|---|
| *Ngorongoro* | *Fm (Upper Pulse)* | | | | | | | | | | |
| | 3A-41Y-1_40-42cm | 105.50 | XXX | XXX | X | - | - | - | - | - | - |
| | 3A-41Y-1_58-60cm | 105.68 | XXX | XXX | X | - | - | - | - | - | - |
| | 3A-41Y-1_82-84cm | 105.92 | XXX | XXX | X | - | - | - | - | - | - |
| | 3A-41Y-2_24-26cm | 106.84 | XXX | XX | X | - | - | - | - | - | XX |
| | 3A-41Y-2_109-112cm | 107.69 | XXX | X | X | - | - | - | - | - | XX |
| | 3A-45Y-2_10-12cm | 115.58 | XXX | X | X | - | - | - | - | - | XX |
| | 3A-49Y-1_50-54cm | 126.60 | XXX | XX | X | X | X | - | - | X | XX |
| | 3A-49Y-1_117-119cm | 127.27 | XXX | XX | X | X | - | - | - | - | XX |
| | 3A-49Y-1_124-128cm | 127.34 | XXX | XX | X | X | - | - | - | - | X |
| | 3A-49Y-1_138-141cm | 127.48 | XXX | XX | X | X | - | - | - | - | XX |
| | 3A-50Y-1_36-39cm | 129.46 | XXX | X | X | X | - | - | - | - | XX |
| | 3A-50Y2_41-43cm | 130.91 | XXX | XX | - | X | - | - | - | - | X |

XXX = Major. XX = Minor. X = Trace. – = absent
Am: Amorphous, Ac: anorthoclase, Q: quartz, Er: erionite, Ch: chabazite, Ca: calcite, Ph: phillipsite, Cl: clinoptilolite, Sm: smectite (montmorillonite)

## Scanning Electron Microscopy

Figure 18 includes representative morphologies for the volcanic glass and minerals observed with SEM. Anorthoclase is a part of the primary volcanic assemblage and displayed euhedral to subhedral prismatic crystals, depending on the orientation viewed (it appeared more subhedral when surrounded by glass). While anorthoclase was identified in every XRD pattern, it was most apparent in 'relatively unaltered' samples, probably due to the absence of clays and zeolites that would cover/mask it in more altered samples. Erionite grows in long, euhedral hexagonal prisms and appeared to be the same size (~50um across) regardless of degree of alteration. Erionite was observed as singular needles, bundles of needles, and occasionally as disordered fibrous masses. Chabazite grows in euhedral to subhedral rhombohedral to pseudocubic crystals, much smaller than erionite (typically ~5um across). While singular chabazite crystals were observed, it was more common to see clusters of it. When observed, clinoptilolite was platy. Lastly, a smectite mineral (likely montmorillonite given the XRD patterns and context from previous research, e.g., McHenry et al., 2023) was observed in most samples. This mineral coated glass and primary minerals with a wavy texture. This was not always apparent and often not observed except under high magnification. More examples of each mineral can be found in Appendix C.

Minerals observed in SEM that did not have morphologies consistent with the minerals identified using XRD were examined with EDS to determine elemental compositions. These minerals were then identified as secondary or accessory minerals associated with rhyolitic rocks. Examples of these minerals can be found in Appendix D.

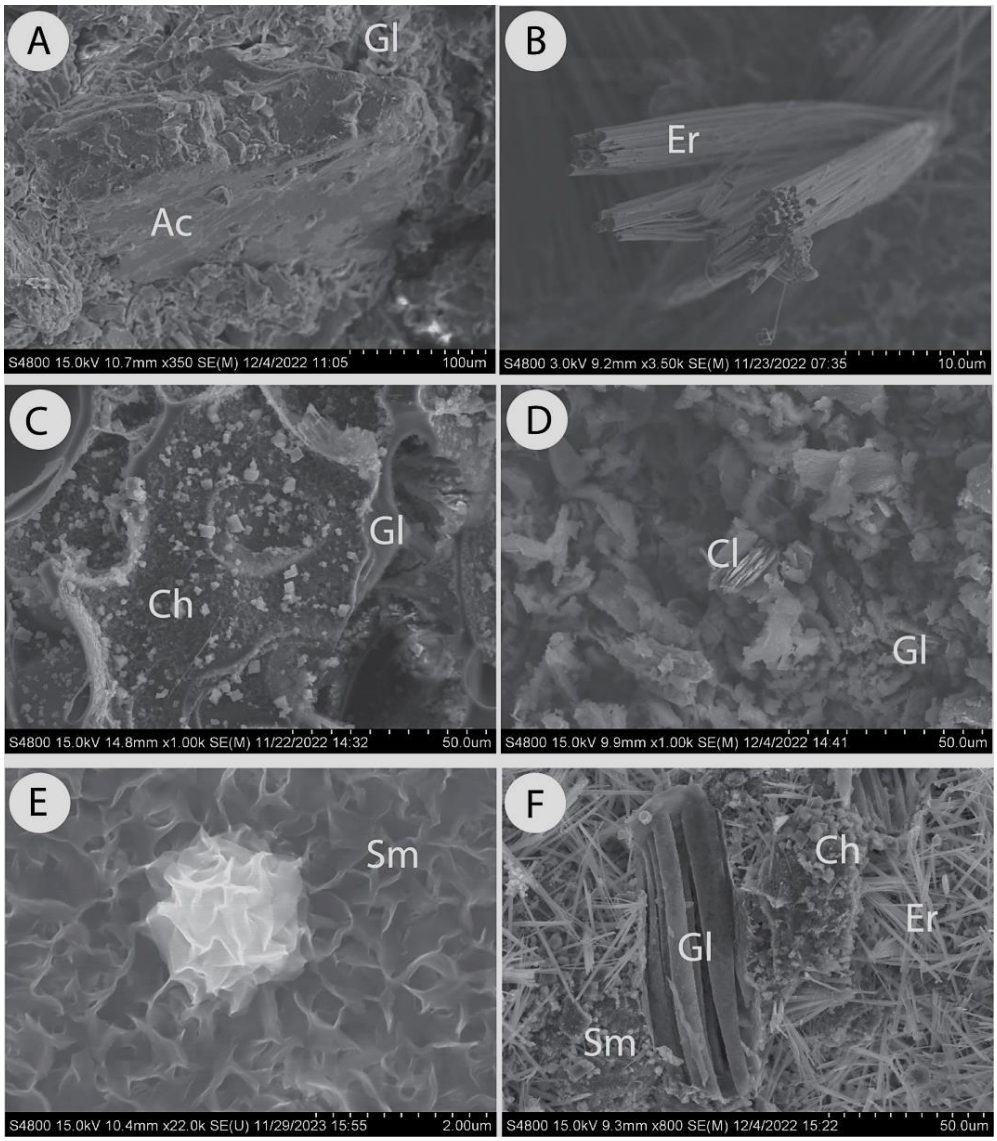


**Figure 18.** SE Images of fresh pumice surfaces. A) Sample 3A-50Y-1_36-39cm, a 'relatively unaltered' sample as indicated by XRD. Euhedral to subhedral anorthoclase (Ac) phenocryst surrounded by shards of volcanic glass (Gl). B) Sample 2A-51Y_32-35cm, a 'moderately altered' sample as indicated by XRD. Small, euhedral erionite (Er) crystals, displaying a fibrous habit. C) Sample 2A-51Y_32-35cm. Small, euhedral chabazite (Ch) crystals displaying rhombohedral habit growing directly on glass (Gl) surface of the pumice. D) Sample 2A-63Y-2_45-48cm, a 'moderately altered' sample as indicated by XRD. Platy clinoptilolite (Cl) surrounded by shards of volcanic glass (Gl) and possibly clay. E) Sample 3A-49Y-1_50-54cm, a 'relatively unaltered' sample as indicated by XRD. Wavy smectite (Sm) mineral, likely montmorillonite either nucleating or growing on top of another mineral. F) Sample 2A-47Y-2_10-12cm, a 'moderately altered' sample, indicated by XRD. Smectite (Sm) appears to be the first mineral to form, coating the volcanic glass (Gl) in the bottom left corner. Fibrous erionite (Er) blades form next, followed by chabazite (Ch) rhombuses.

X-Ray Fluorescence

Major element compositions for core 2A samples are given in Tables 7 and 8. Major element compositions for core 3A samples are given in Table 9. Minor element compositions for all samples are given in Appendix E.

**Table 7**

Major element compositions for samples from the Upper Pulse of the Ngorongoro

| Sample | mbs | SiO2 | TiO2 | Al2O3 | Fe2O3 | Mn | MgO | CaO | Na2O | K2O | P2O5 | Sum | LOI |
|---|---|---|---|---|---|---|---|---|---|---|---|---|---|
| 47Y-2_10-12cm | 117.95 | 63.90 | 0.70 | 12.81 | 6.61 | 0.23 | 0.58 | 0.92 | 4.90 | 4.00 | 0.06 | 99.75 | 4.83 |
| 47Y-2_25-32cm | 118.10 | 62.94 | 0.64 | 12.68 | 6.48 | 0.26 | 0.60 | 1.45 | 4.90 | 3.96 | 0.05 | 99.85 | 5.70 |
| 47Y-2_79-83cm | 118.64 | 60.20 | 0.54 | 11.69 | 6.24 | 0.23 | 0.62 | 4.03 | 4.47 | 3.88 | 0.05 | 99.63 | 7.47 |
| 50Y-2_134-137cm | 128.84 | 64.59 | 0.49 | 12.61 | 6.01 | 0.19 | 0.29 | 0.58 | 4.60 | 3.95 | 0.04 | 99.91 | 6.38 |
| 51Y-1_32-35cm | 129.32 | 63.84 | 0.51 | 13.04 | 5.37 | 0.19 | 0.31 | 1.04 | 4.75 | 4.19 | 0.05 | 99.31 | 5.84 |
| 51Y-1_40-42cm | 129.40 | 62.90 | 0.42 | 12.85 | 4.69 | 0.21 | 0.26 | 2.47 | 4.71 | 4.21 | 0.04 | 99.91 | 6.96 |
| 54Y-1_80-81cm | 138.80 | 62.65 | 0.59 | 13.79 | 5.65 | 0.17 | 0.44 | 0.68 | 4.97 | 3.84 | 0.08 | 99.37 | 6.33 |
| 60Y-1_59.5-62cm | 153.60 | 61.04 | 0.79 | 14.09 | 4.86 | 0.05 | 0.69 | 0.38 | 5.59 | 3.46 | 0.08 | 99.16 | 7.89 |
| 63Y-2_45-48cm | 163.95 | 58.61 | 0.88 | 13.97 | 7.96 | 0.07 | 0.94 | 0.52 | 5.42 | 3.57 | 0.14 | 98.86 | 6.59 |
| 63Y-2_114-117cm | 164.64 | 58.51 | 1.05 | 14.47 | 6.45 | 0.09 | 0.66 | 1.33 | 6.61 | 2.62 | 0.15 | 98.85 | 6.60 |

**Table 8**

Major element compositions for samples from the Lower Pulse of the Ngorongoro

| Sample | mbs | SiO2 | TiO2 | Al2O3 | Fe2O3 | Mn | MgO | CaO | Na2O | K2O | P2O5 | Sum | LOI |
|---|---|---|---|---|---|---|---|---|---|---|---|---|---|
| 69Y-2_34-37cm | 181.80 | 61.29 | 0.54 | 14.66 | 6.34 | 0.12 | 0.42 | 0.43 | 5.84 | 3.94 | 0.06 | 99.36 | 5.49 |
| 70Y-1_4-6cm | 183.04 | 63.98 | 0.45 | 13.13 | 5.92 | 0.17 | ND | 0.52 | 5.36 | 3.06 | 0.03 | 98.98 | 5.90 |
| 70Y-1_32-34cm | 183.32 | 62.60 | 0.28 | 13.69 | 4.88 | 0.16 | ND | 0.24 | 6.11 | 3.44 | 0.03 | 99.29 | 7.45 |
| 72Y-1_136-142cm | 184.10 | 60.24 | 0.55 | 13.51 | 6.51 | 0.18 | 0.31 | 1.04 | 5.84 | 3.49 | 0.07 | 97.95 | 6.03 |
| 72Y-2_64-67cm | 190.36 | 60.50 | 0.54 | 13.58 | 6.25 | 0.17 | 0.30 | 1.04 | 5.78 | 3.63 | 0.07 | 98.27 | 6.19 |
| 72Y-2_99-102cm | 191.10 | 60.09 | 0.58 | 13.25 | 6.62 | 0.19 | 0.36 | 1.23 | 5.82 | 3.53 | 0.08 | 98.11 | 6.13 |
| 74Y-3_25-34cm | 196.77 | 63.59 | 0.58 | 12.90 | 6.02 | 0.18 | 0.43 | 0.80 | 6.02 | 3.58 | 0.06 | 98.70 | 4.37 |
| 74Y-3_109-117cm | 197.61 | 62.74 | 0.65 | 12.23 | 6.96 | 0.18 | 0.62 | 0.65 | 5.44 | 3.94 | 0.06 | 98.56 | 4.93 |

**Table 9**

Major element compositions for core 3A samples.

| Sample | mbs | SiO2 | TiO2 | Al2O3 | Fe2O3 | Mn | MgO | CaO | Na2O | K2O | P2O5 | Sum | LOI |
|---|---|---|---|---|---|---|---|---|---|---|---|---|---|
| 41Y-1_40-42cm | 105.50 | 65.74 | 0.45 | 12.76 | 5.02 | 0.14 | 0.55 | 0.53 | 4.55 | 4.28 | 0.03 | 98.85 | 4.59 |
| 41Y-1_58-60cm | 105.68 | 65.88 | 0.44 | 12.98 | 4.53 | 0.13 | 0.59 | 0.66 | 4.80 | 4.25 | 0.03 | 98.68 | 4.16 |
| 41Y-1_82-84cm | 105.92 | 65.62 | 0.40 | 13.34 | 4.32 | 0.12 | 0.25 | 0.55 | 5.20 | 4.40 | 0.04 | 98.29 | 3.82 |
| 41Y-2_24-26cm | 106.84 | 63.44 | 0.57 | 12.67 | 5.88 | 0.14 | 1.53 | 0.91 | 3.90 | 3.59 | 0.05 | 98.70 | 5.80 |
| 41Y-2_109-112cm | 107.70 | 58.67 | 1.56 | 12.02 | 9.17 | 0.24 | 1.61 | 1.95 | 4.27 | 3.28 | 0.39 | 98.02 | 4.63 |
| 45Y-2_10-12cm | 115.58 | 62.12 | 0.65 | 12.43 | 7.13 | 0.22 | 0.96 | 0.54 | 3.51 | 3.45 | 0.06 | 97.76 | 6.49 |
| 49Y-1_50-54cm | 126.60 | 62.61 | 0.55 | 13.72 | 5.68 | 0.16 | 0.90 | 0.72 | 4.29 | 3.91 | 0.06 | 98.07 | 5.28 |
| 49Y-1_117-119cm | 127.27 | 62.69 | 0.55 | 13.63 | 5.62 | 0.15 | 0.90 | 0.66 | 4.30 | 3.92 | 0.05 | 97.95 | 5.27 |
| 49Y-1_124-128cm | 127.34 | 63.99 | 0.43 | 12.76 | 5.37 | 0.15 | 0.51 | 0.57 | 4.07 | 4.32 | 0.04 | 97.86 | 5.44 |
| 49Y-1_138-141cm | 127.48 | 63.79 | 0.46 | 13.34 | 5.35 | 0.15 | 0.74 | 0.58 | 4.01 | 4.11 | 0.04 | 99.05 | 6.30 |
| 50Y-1_36-39cm | 129.46 | 62.47 | 0.53 | 14.12 | 5.26 | 0.15 | 0.94 | 0.74 | 3.91 | 3.81 | 0.06 | 98.47 | 6.18 |
| 50Y-2_41-43cm | 130.91 | 62.25 | 0.58 | 13.62 | 5.50 | 0.25 | 0.47 | 0.89 | 4.13 | 4.37 | 0.08 | 98.04 | 5.70 |

## V. DISCUSSION

### X-Ray Diffraction

Every sample in core 2A and 3A contained anorthoclase and most samples contained quartz. These minerals are a part of the primary volcanic assemblage for these rhyolitic units. Lack of quartz in a few samples is likely due to a slight difference in composition (e.g., more trachytic material) or lower abundance of phenocrysts compared to glass.

Volcanic glass was present to some degree in all samples in cores 2A and 3A, even in more zeolitized samples. When present, the dominant clay mineral was a smectite (matched to montmorillonite), as indicated by a broad peak at ~6º 2-theta. The most abundant zeolite, erionite, was found in all samples from core 2A and half of the samples from core 3A. Erionite likely precipitated straight from pore fluids interacting with rhyolitic glass and not necessarily as a result of saline-alkaline fluids tied to the lake. The combination of montmorillonite and erionite indicates that low-level alteration occurred in a fresher environment with lower salinity compared to the overlying Olduvai Beds.

The second most abundant zeolite in these samples is chabazite, which forms under slightly more alkaline conditions. SEM images for some samples clearly show chabazite growing on erionite, and every instance of chabazite in these samples occurs with erionite, indicating that erionite started forming first and chabazite started forming second. This would have occurred as $SiO_2$ was removed from the system and more

$Ca^{2+}$ was added. A few samples from core 2A contained both chabazite and calcite. In this instance, calcite likely formed from additional $Ca^{2+}$ (and associated alkalinity) after erionite and chabazite had already removed some of the ions from the system.

Clinoptilolite occurred in a few samples from core 2A and one sample from core 3A. Clinoptilolite occurs when $SiO_2$ activity is higher. It occurs with other zeolites in these samples, probably because the formation of zeolites is associated with more glass dissolution, which makes $SiO_2$ more mobile. There are a few instances of phillipsite in samples from core 2A. Phillipsite occurs with higher $K^+$ concentrations. Phillipsite occurrence correlates with less intense anorthoclase peaks in these samples. It is also more prominent in samples near thicker lacustrine units, indicating it can form from higher alkalinity provided by concentrated lake water.

Mineral assemblages appear to agree with the expected degree of alteration, determined by observed sample colors (Figure 15). Less altered tuff samples (e.g., more glass, less authigenic minerals) tend to be white/pale grey and more altered tuff samples (e.g., less glass, more authigenic minerals) tend to be yellow to orange, although fine-grained ash tuffs may be a lighter buff color.

Some samples may have had a more complicated history, and the overall sample color may not represent the degree of alteration. In these cases, only clast color must be considered. For example, sample 3A-41Y-2_109-112cm is dark brown, a color that reflects weathering into a paleosol horizon rather than the degree of alteration with

saline-alkaline fluids. However, the pumice clasts in this sample were white, and contained no zeolites, reflecting less alteration/fresher conditions. Another example, sample 2A-72Y-1_136-142cm is green, a color that should reflect less alteration (e.g., Hay (1976)). However, when the pumice clasts were broken open, they were a buff color and contained zeolites, indicating a higher degree of alteration.

**Scanning Electron Microscopy**

Minerals must be present at the 1- 5% abundance level to be reliably detected in XRD powder patterns, depending on the mineral. Some relatively unaltered samples contained some alteration minerals that were likely under the detection limit of XRD, which could therefore not be confirmed using this technique. Luckily, SEM could be used to double-check XRD pattern matching, especially to determine the presence or absence of zeolite phases. Figure 19 shows a small (40um across) crystal of erionite that was found in an otherwise “unaltered” sample. A review of the XRD pattern after the observation of erionite using SEM led to its identification in the XRD pattern, where it would otherwise have been overlooked. This indicates that the sample is not completely unaltered and thus we refer to it as ‘relatively unaltered’. This could potentially indicate the conditions at the time this sample interacted with the lake were sufficiently saline-alkaline to start producing zeolites. Alternatively, the presence of erionite in this sample could just indicate that some pore fluid interacted with the surface of this glass, locally altering a portion of the glass and forming a miniscule amount of erionite.

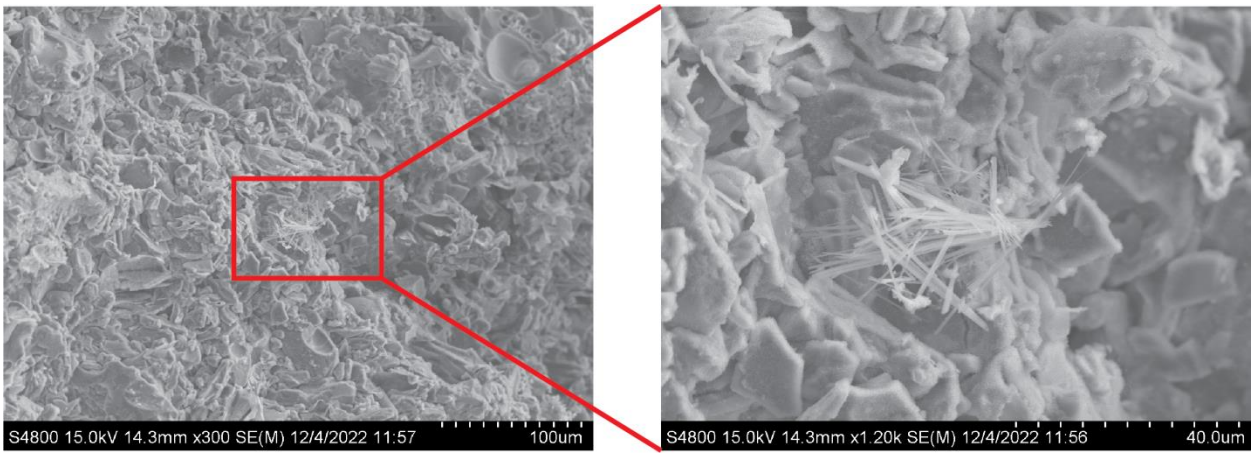


**Figure 19.** A ‘relatively unaltered’ glassy sample with a small cluster of fibrous erionite needles.

SEM was also useful for determining what clays were present in samples. No clay separations or special treatments were performed for this study, making clay identification from a broad XRD peak tricky. When a sample was viewed in SEM, the clay texture became apparent and helped accurately identify clays. All observed clays had a wavy texture (Figure 19E), which is characteristic of smectitic clays like montmorillonite.

Additionally, SEM provided insight into the order of authigenic mineral formation. Order of formation can be helpful when interpreting how the fluid chemistry may have evolved. For example, clay is observed as a thin coating in fresher samples. Slightly altered samples will start to form the zeolites erionite and chabazite on exposed surfaces, with large erionites growing out of the clay surfaces, followed by smaller clusters of chabazite growing on both the clay surface and the erionite surface. This order of formation indicates that clays formed from less saline fluid and coated the

existing volcanic glass and minerals. Then, the fluid further interacted with the glass and forming erionite. Then, when enough $Ca^{2+}$ was leached from the glass, chabazite formed.

**Piecing together: XRD and SEM**

After conducting XRD and SEM analyses, the representative images from each set of results can be combined to better visualize volcanic alteration in the Ngorongoro Fm (Figure 20). All XRD patterns contain minerals from the primary volcanic assemblage (anorthoclase and occasional quartz). Unaltered samples have a very prominent amorphous hump in XRD, which correlated with a predominantly glassy texture in SEM. This glassy hump lessened in intensity with increased alteration (slightly altered samples have a less intense hump, moderately-altered samples have little to no hump). In SEM, this is observed as a decrease in the glass to authigenic mineral ratio. The most common zeolites observed in both XRD and SEM were chabazite and erionite, but a few samples also contained zeolites clinoptilolite and/or phillipsite. Additionally, most samples contained clays, including illite and/or smectite (montmorillonite). Illite and smectite were identified using characteristic broad peaks at 9º 2θ (illite) and 6º 2θ (smectite).

Authigenic minerals associated with high degrees of alteration (the zeolite mineral analcime and K-feldspar) were not observed in any samples from the Ngorongoro Fm. Because these minerals are expected in the lake depocenter if conditions are sufficiently saline-alkaline, this indicates that the lake was not as saline-

alkaline during the alteration of the Ngorongoro Formation as it was during the alteration of the overlying Olduvai Beds, where these authigenic phases are common.

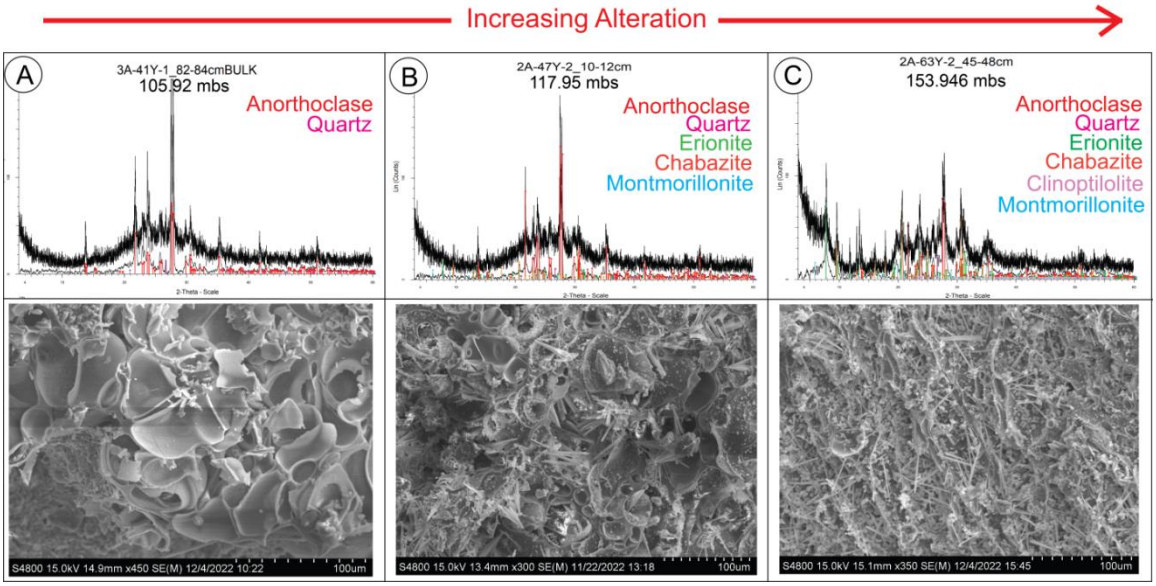


**Figure 20.** SEM images compared to representative XRD patterns, showing variations in the degree of alteration. A) Pumice vesicles are preserved. Only glass and primary volcanic assemblage, no zeolites present. B) Pumice vesicles are still present, but now have zeolites growing in them. C) Pumice vesicles are still present, but with more zeolites growing in them.

## X-Ray Fluorescence

A series of isocon diagrams were plotted using major element data (Tables 7, 8, and 9) and minor element data (Appendix E) from XRF analysis. Isocon plots are typically used to determine volume loss during weathering, but when calculated without density, can still be used to show relative enrichment and depletion of mobile elements relative to samples exposed to fresher conditions (e.g., McHenry, 2010). Plotting two samples of the same unit with varying proximity to a lake interval (e.g., stratigraphically close and stratigraphically separated from lake clays in the core) should help determine

if volcanic units were highly altered throughout, largely unaltered throughout, or whether alteration was more intense in direct contact with the lake interface.

In a closed basin system, most mobile elements are conserved through redistribution within the system. As glass is hydrated, alkaline cations ($Na^{2+}$, $Ca^{2+}$, $K^{+}$) are leached and begin to concentrate into authigenic minerals like zeolites (e.g., McHenry, 2010). Immobile elements are used to plot 1:1 isocon lines. Elemental concentrations are typically adjusted using a multiplier (e.g., $TiO_2$*15 or $SiO_2$/10) so the values can fit within the plot area. Elements falling above the isocon line are enriched and elements that fall below the line are depleted compared to the less altered sample, which is plotted on the x-axis. Representative isocon plots showing the compositional difference between interior and lake clay adjacent units of core 3A-49Y-1 are presented in Figure 21.

Figure 21a plots two lapilli ash tuff samples from the same volcanic unit. A sample that is stratigraphically close to a lake interval (3A-49Y-1_117-119cm) is plotted against a sample that is stratigraphically separated from the same lake interval (3A-49Y-1_50-54cm). Most elements plot close to the isocon line, indicating there was little to no difference in how the samples experienced leaching or enrichment of major elements, regardless of the degree of stratigraphic separation from the lake interface. The fact that they both have identical LOI values (5.27% and 5.28%) suggests that both have been altered to a similar degree and that neither is completely fresh.

Figure 21b plots a waterlogged pumice sample (3A-49Y-1_124-128cm) against the same stratigraphically separated lapilli ash sample (3A-49Y-1_50-54cm) from the first example. Because the waterlogged pumice is also a part of the same volcanic unit as the first example, it should have the same original composition as the stratigraphically close sample used previously. Therefore, differences in Figs. 21a and b should reflect variation in the degree of alteration that occurred in the interior of thick volcanic units versus the alteration that occurred in samples in direct contact with the lake.

The Figure 21b isocon is overall very similar to the Figure 21a plot. Most major elements plot close to the line except for $Mg^{2+}$ (which is depleted). During tephra alteration $Mg^{2+}$ depletion occurs with the formation of zeolites, whereas $Mg^{2+}$ enrichment occurs with the formation of clays (e.g., McHenry, 2010). Both lapilli ash tuff samples appear to have a similar amount of clay based on their XRD patterns, while the waterlogged pumice appears to have less clay (Table 6), consistent with the observed $Mg^{2+}$ depletion in the Figure 21b isocon plot.

In addition to $Mg^{2+}$ depletion, minor elements $Ba^{2+}$ and $Sr^{2+}$ are also depleted. $Ba^{2+}$ typically tracks $K^{+}$ and both are generally concentrated in the most altered samples (e.g., in the zeolite phillipsite). However in the Figure 21b isocon diagram, $Ba^{2+}$ is depleted while $K_2O$ is enriched. This could be attributed to the small sample size available from the core, which may not be representative of the entire unit. For example, minor and trace elements may be concentrated in accessory minerals in the rhyolite

(e.g., zircon, apatite, titanite) which may not be evenly distributed between different small samples of the same unit. A much larger sample volume would thus be required to determine this, beyond what is available from cores.

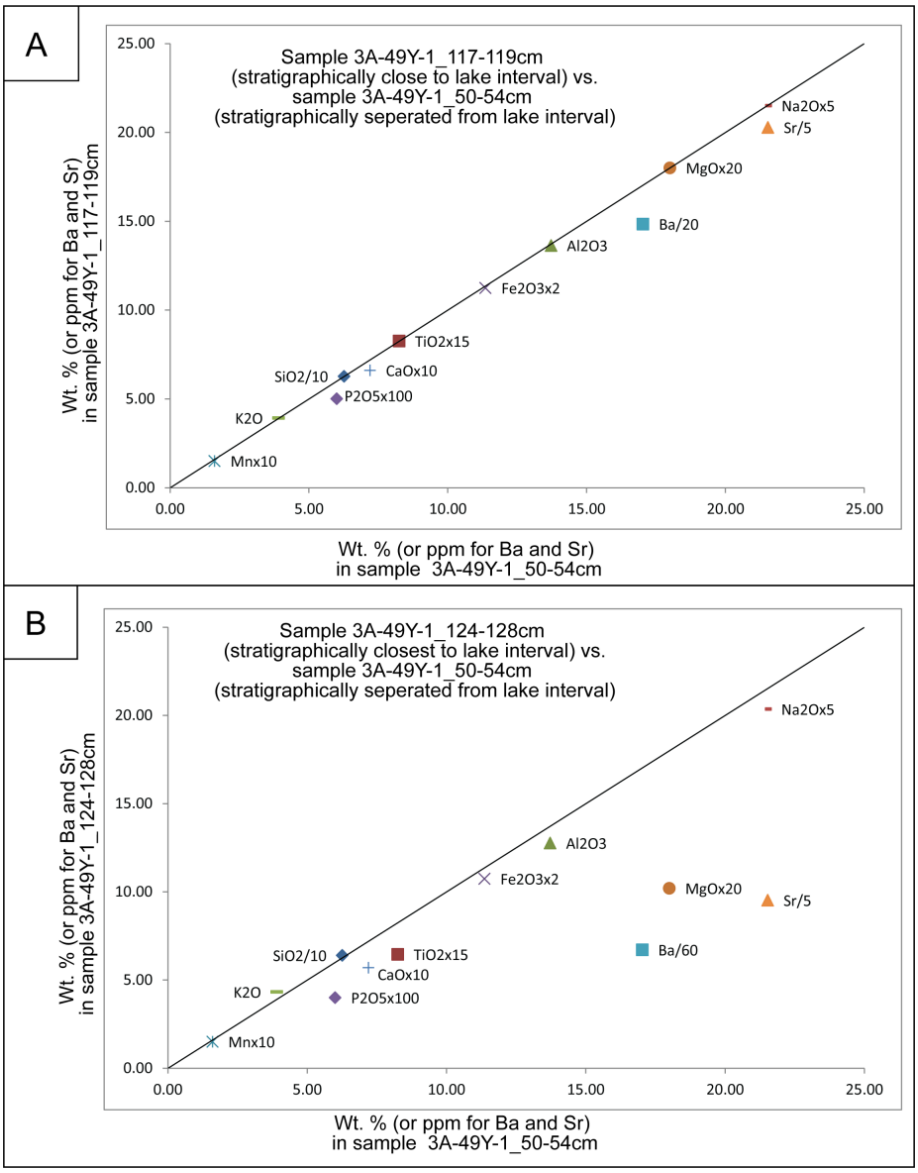


**Figure 21.** Isocon diagrams plotting major elements (and minor elements Ba2+ and Sr2+), with corrections shown on element labels. A: A lake-proximal sample plotted against a more stratigraphically separated sample. B: A lake-proximal sample (closest/touching lake) plotted against the same stratigraphically separated sample.

The depletion of both $Ba^{2+}$ and $Sr^{2+}$ in the Figure 21b isocon diagram suggests that the waterlogged pumice sample experienced more leaching of these elements and is thus more altered than the sample that is stratigraphically separated from the lake interface. However, the respective mineral assemblages suggest the opposite is true. This inconsistency is likely due to the nature of closed-basin alteration, where mobile elements are redistributed into authigenic minerals rather than being removed from the system. It is possible that both samples experienced the same amount of leaching, but for one sample the leached cations were locally redistributed in new alteration phases while in the other these cations were able to migrate further. This suggests that the isocon diagrams may not be showing the true degree of alteration, as they would for an open system (e.g., McHenry (2010)).

This interpretation is supported by relatively consistent LOI values (Tables 7,8, and 9). Devitrified glass, smectitic clays, and zeolites all contain water and can thus all exhibit elevated LOIs, even though some reflect a higher degree of overall alteration or interaction with more saline-alkaline fluids (e.g., McHenry, 2009).

While the lapilli ash tuff sample that was stratigraphically separated from the lake interval (3A-49Y-1_50-54cm) for this part of Core 3A was expected to be the most insulated from the effects of the lake, it appears to be the most altered sample, based on its mineral assemblage. Surprisingly, the sample that appears least altered (based on XRD and Isocon diagrams) is the waterlogged pumice sample that was in direct contact with lake fluids. To fully explain this, several factors need to be considered.

Paleolake Olduvai was less saline-alkaline at the time of Upper Ngorongoro Fm deposition compared to the underlying Naibor Soit Formation of the Lower Ngorongoro Formation (e.g., McHenry et al., 2020a). The waterlogged pumice sample was likely deposited and started to experience some alteration in this fresher (only somewhat saline-alkaline) lake or perhaps in a fluvial environment before being buried by the prograding Ngorongoro volcaniclastic fan-delta. The prograding fan-delta likely displaced the lake as described by Stollhofen et al. (2021) as shown in Figure 12. This thick lapilli ash tuff unit may have lacked direct exposure to the lake, but would still have been in contact with groundwater (e.g., Figure 4A). The thick lapilli ash tuff unit appears to be similarly altered throughout, indicating that its thickness did not insulate it from saline-alkaline fluids. The water occupying the fan's pore space likely reacted with the surrounding material and produced the observed low-alteration zeolites.

The presence of glass in these samples indicates the reaction did not go to completion, meaning the amount of time the sample was exposed to saline-alkaline fluids was limited (Hay and Kyser, 2001; McHenry et al., 2020a). While there was no difference in bulk composition between the two lapilli ash tuff samples, they did have slightly different mineral assemblages. Samples 3A-49Y-1_117-119cm and 3A-49Y-1_124-128cm have the same assemblage of anorthoclase, quartz, erionite, and montmorillonite. The zeolite erionite suggests alteration occurred with less alkaline (fresher) fluids compared to samples that contain other zeolites. Sample 3A-49Y-1_50-54cm has a similar assemblage, but with two additional zeolites (chabazite and clinoptilolite) that suggest alteration occurred with slightly more alkaline pore water.

Sample 2A-47Y-2_79-83cm contains calcite while the others do not, resulting in expected apparent CaO depletion in samples compared against it (Figure 22). Otherwise, both isocon diagrams plot elements fairly close to the isocon line, indicating little to no change in bulk composition between samples.

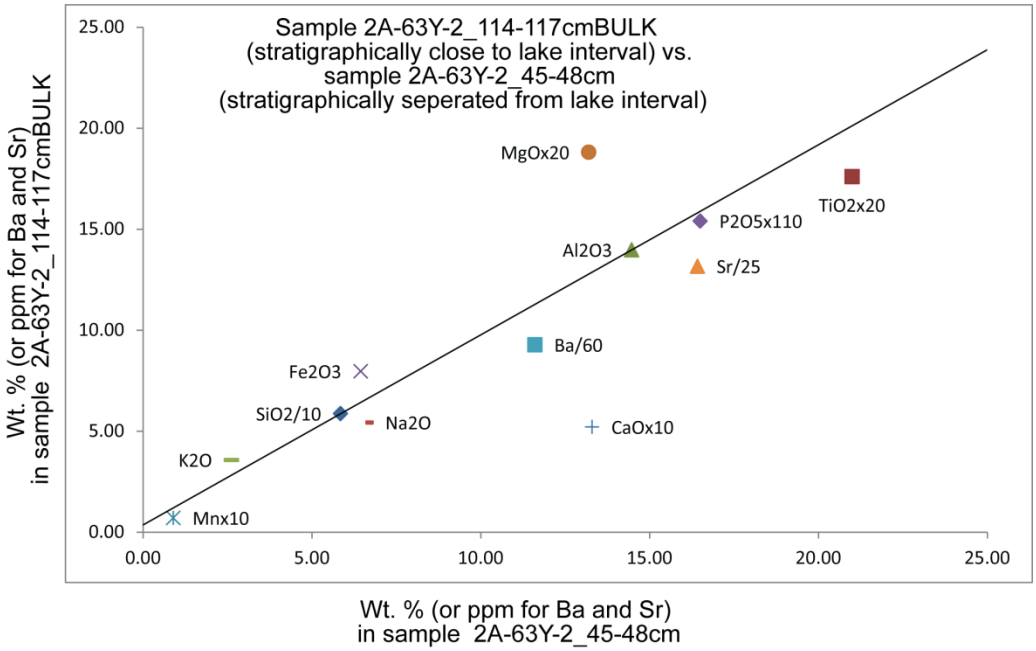


**Figure 22.** Isocon diagram for samples from core 2A-63Y-2, plotting all major elements (and minor elements Ba2+ and Sr2+). A sample that is stratigraphically closest to a lake interval (2A-63Y-2_114-117cm) is plotted against a samples that is stratigraphically separated from the same lake interval (2A-63Y-2_45-48cm). Most major elements plot fairly close to the isocon line, indicating little to no change between the samples.

Overall, all Isocon diagrams (see Appendix F) show little to no difference in bulk composition, indicating there is no insulation effect in any of the thick tephra units (regardless of stratigraphic proximity to a lake clay interval). While the degree of alteration is fairly consistent for each pair of samples, slight variations in mobile element concentrations (e.g., Mg, Ba, Sr, and Ca) were occasionally observed. This could be

attributed to the amount of time a sample is exposed to saline-alkaline fluids, or how open the system was with regard to the removal of leached components.

**Overall Trends**

The samples used in this study were collected from the 2014 OGCP long sediment cores. The cores reveal stratigraphy not exposed in outcrop, including volcaniclastic units of the Ngorongoro Fm and lacustrine units of the Naibor Soit Fm. Core 2A is the most stratigraphically complete core, recording both prograding pulses of the Ngorongoro volcaniclastic fan-delta, while Core 3A only records the upper pulse of the Ngorongoro fan-delta. McHenry et al. (2020a) used authigenic mineralogy of lacustrine intervals to reconstruct paleoclimatic conditions in the Ngorongoro and Naibor Soit Fms, but this approach had not yet been applied to the tephra-dominated units of the Ngorongoro Fm. The goal of this study was to identify authigenic mineral assemblages of tephra from the Ngorongoro Fm and to assess any geochemical trends throughout the formation. Data is compared to that of McHenry et al. (2020a) for the interfingering Naibor Soit Fm and to that of the overlying Olduvai Beds to help constrain the geochemical conditions present at the time of alteration, which can in turn be used to reconstruct paleoenvironmental conditions.

Based on XRD data, all samples contained (to at least some degree) volcanic glass and primary volcanic minerals (anorthoclase and occasional quartz). Samples from the Upper Ngorongoro Fm in core 3A appeared to be fresher than those in core

2A, indicated by more preserved glass and less authigenic minerals. Samples from the Lower Ngorongoro Fm (only in core 2A) appeared to have a higher degree of alteration, indicated by less preserved glass and more authigenic minerals. The degree of alteration appeared to correlate with color (Figure 15). The ‘fresher’ samples with more glass and less authigenic minerals appeared to be white to grey. More altered samples (containing more zeolites) were buff to yellow in color.

Every sample in the Lower Ngorongoro Fm in core 2A contained erionite and chabazite, with little glass preserved. Phillipsite, clinoptilolite, and montmorillonite were only present in a couple of samples in this part of the core. Every sample in the Upper Ngorongoro Fm in core 2A contained erionite, chabazite, montmorillonite, and relict glass. A few samples also contained calcite and rare phillipsite and clinoptilolite in a couple of samples. The upper portion of core 3A (above 106 mbs) did not contain any authigenic minerals, just glass and primary volcanic minerals. Below 106 mbs in Core 3A, all samples contained montmorillonite. Below 126 mbs, all samples also contained erionite. Only one sample (126.6 mbs) contained erionite, chabazite, and clinoptilolite.

Element mobility was determined using isocon diagrams, plotting a sample that is stratigraphically close to a lake interval (potentially not as insulated from lake effects) against a stratigraphically separated sample (potentially more insulted from lake effects). Because most samples only displayed a low degree of alteration, there was little difference in bulk composition between samples. Additionally, it was difficult to

determine if there were any meaningful patterns of element mobility, as authigenic minerals concentrate mobile elements in a closed system. This interpretation is supported by relatively consistent LOI values between samples within the same unit/interval, indicating a similar level of hydration and similar amount of hydrated minerals (e.g., dioctahedral clays and zeolites) within the samples. These findings are akin to those in McHenry (2009; 2010) for the overlying Olduvai Beds.

Unit thickness may still have an influence on alteration, but this has more to do with the type of unit and associated depositional environment. For example, the authigenic mineral assemblage of thinner units of airfall ash deposited directly into the lake would reflect lake conditions. In contrast, a thick tephra unit (reflecting fan progradation) would push the lake away and the resulting assemblage would reflect local alteration as an effect of pore water present in the fan (rather than lake conditions).

Based on XRD results, the highest degree of alteration does seem to occur in samples of fine ash (Table 5 and 6). This could be because the ash provided a greater amount of surface area with which the fluids could interact, or because it was deposited directly into a saline-alkaline lake environment. The thicker tephra units reflect a different depositional environment (e.g., volcaniclastic fan), with alteration limited to pore water chemistry and groundwater interactions rather than the lake. Because of this, the lake level and type/amount of volcanic material being deposited must be taken

into consideration when interpreting environmental conditions from authigenic mineral assemblages.

Overall, the authigenic mineral assemblages identified in the Ngorongoro Fm reflect fresher, less saline-alkaline environments than the overlying Olduvai Beds (above lower Bed I). The change in authigenic assemblage from the lower and upper pulse of the Ngorongoro Fm reflects overall lake freshening, in agreement with McHenry et al. (2020a) (Figure 23). This agreement indicates that both lacustrine and fan-delta deposits can provide meaningful paleoenvironmental data. Therefore, tephra alteration can be used to fill in gaps in the paleoenvironmental record obtained from other published work.

In the Lower Naibor Soit Fm, the primary zeolite transitions from analcime to phillipsite and chabazite. The Lower Ngorongoro Fm interrupted lake deposition, primarily containing zeolites erionite and chabazite (with more glass preserved in the upper portion of this formation). When lake deposition resumed, the primary zeolites of the Upper Naibor Soit Fm were also erionite and chabazite. The Upper pulse of the Ngorongoro Fm again interrupted lake deposition at the position of the cores and contains the zeolites erionite and chabazite. The same pulse within Core 3A exhibited less alteration (less abundant zeolites, better preservation of volcanic glass), indicating fresher conditions at the position of this core within the basin.

Short-term changes in moisture in the Olduvai basin are attributed to monsoon-driven seasonal flooding. If long-term precessional cycles are present in the deeper part of the cores, they are obscured by tectonics and volcanics. However, one preserved wet period occurs during the transition between the Upper Ngorongoro Fm and Olduvai Bed I, indicated by fresh glass (with no alteration minerals) present within lacustrine sediments in core 3A at the base of Bed I (McHenry et al., 2020a). Correlative units are not found in core 2A due to an unconformable surface.

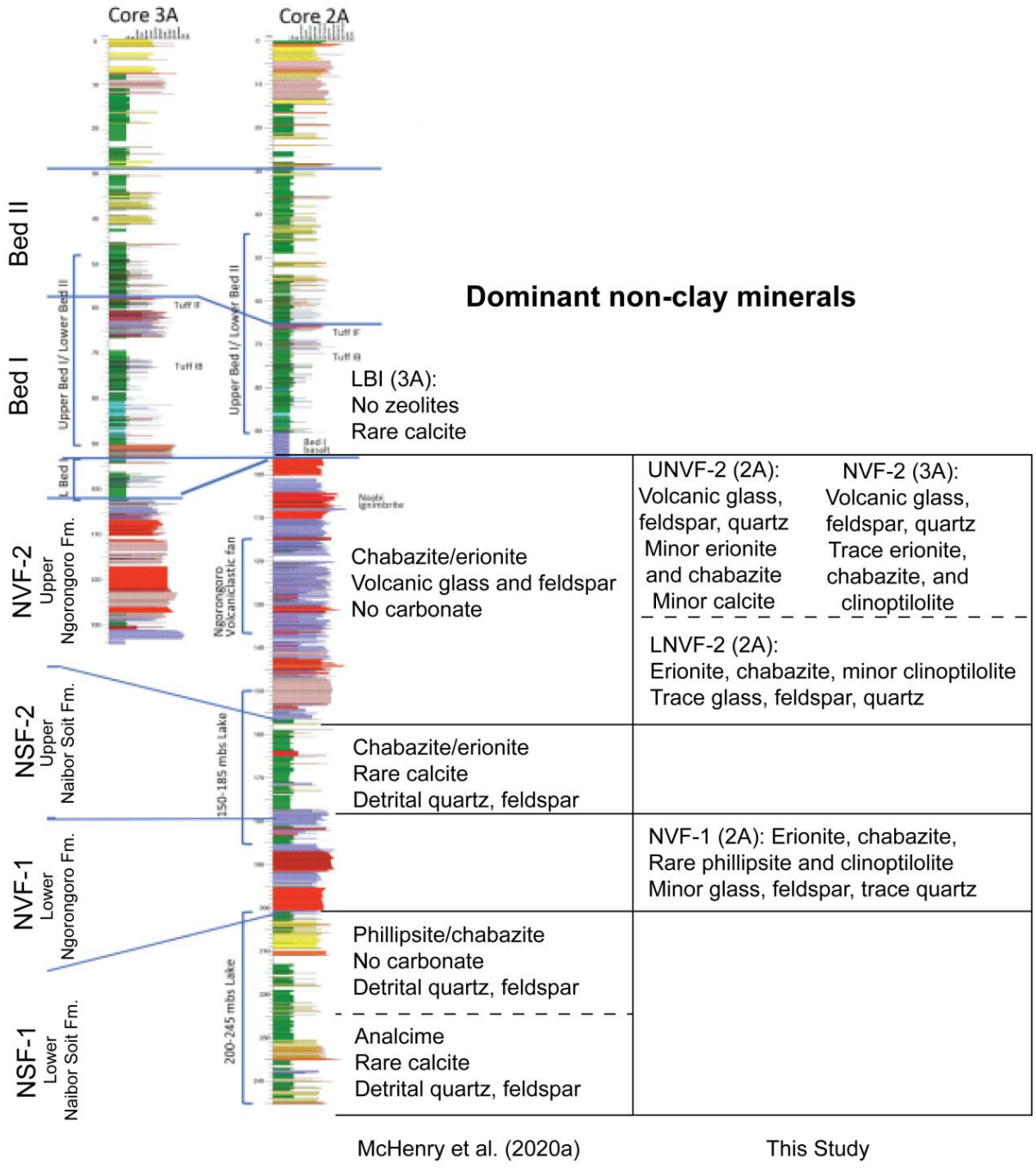


**Figure 23.** Dominant non-clay minerals for each major stratigraphic interval, listed next to stratigraphic columns for cores 2A and 3A. Minerals listed in the left column are from McHenry et a. (2020a). Minerals listed in the right column are from this study. See legend for Figure 8. Figure modified from McHenry et al. (2020a).

## VI. CONCLUSIONS

This study investigated the alteration of volcanic glass deposited into a closed-basin lake to determine paleoenvironmental conditions (e.g., water level, salinity, alkalinity, aridity, and pH). This study concludes that:

1. The thick tephra deposits in the Ngorongoro Fm preserve authigenic minerals that indicate that these units experienced alteration.
2. While the Lower Ngorongoro Fm appears to be slightly more altered than the Upper Ngorongoro Fm, the authigenic mineral assemblages of altered tephra from the entire formation reflect lower degrees of alteration (relict glass, low-alteration zeolites, and montmorillonite) than the overlying Olduvai Beds (above lower Bed I), which rarely preserve volcanic glass and often contain zeolites reflecting more advanced saline-alkaline alteration (phillipsite, analcime) and authigenic K-feldspar.
3. Little to no change in bulk geochemical composition (reflecting little to no element mobility) was observed within altered tuffs. This is attributed to the observed low degrees of alteration and/or the local redistribution of mobile elements within the closed-system environment.
4. Thicker volcanic units appeared to be uniformly altered throughout, with no notable difference in authigenic assemblage or bulk elemental composition between samples from their surfaces (exposed to saline-alkaline lake waters) and their interiors. The thickness of these units does not appear to provide a significant insulating effect from the influence of saline-alkaline fluids. The

variation in degree of alteration within these units appears to correlate with changes in depositional environment rather than unit thickness.

Large-scale differences in tephra alteration patterns throughout the Ngorongoro Fm suggest a general trend of freshening upwards, in agreement with other proxies that reveal an overall freshening of the lake between the saline-alkaline conditions of the Lower Naibor Soit Fm and the much fresher conditions at the top of the Ngorongoro Fm in Core 3A. Because this overall freshening trend is reflected in both the lacustrine and tephra units, the paleoenvironmental conditions deduced from this study can be used to fill gaps in the paleoenvironmental record of the Olduvai basin. This is in agreement with our first hypothesis.

The degree of alteration was not notably different in samples of the same volcanic deposit, regardless of the location of the interval within the unit. This is also the case when comparing thin volcanic units to thicker volcanic units. This indicates there is no ‘insulation’ effect existing within the Ngorongoro Fm, which is in disagreement with our second hypothesis. Individual volcanic units appear to be evenly altered throughout, suggesting that alteration (and the associated formation of zeolites) reflects groundwater interactions and not just direct contact with lake waters.

## REFERENCES CITED


Ashley, G.M., Hay, R.L., 2002. Sedimentation patterns in a Plio–Pleistocene volcaniclastic rift-margin basin, Olduvai Gorge, Tanzania. In: Ashley, G.M., Renaut, R.W. (Eds.), Sedimentation in Continental Rifts: SEPM Special Publication, vol. 73, pp. 107–122.

Ashley, G.M., Bunn, H.T., Delaney, J.S., Barbobi, D., Dominguez-Rodrigo, M., Mabulla, A.Z.P., Gurtov, A.N., Baluyot, R., Beverly, E.J., and Baquedano, E., 2013. Paleoclimatic and paleoenvironmental framework of FLK North archeological site, Olduvai Gorge, Tanzania. Quaternary International, pp. 1-12. http://dx.doi.org/10.1016/j.quaint.2013.08.052.

Ashley, G.M., de Wet, C.B., Houser, L.M., Delaney, J.S., 2020. Widespread freshwater carbonate in the Olduvai Basin, a precursor to a major eruption in the East African Rift System. The Depositional Record. 6:331–351. https://doi.org/10.1002/dep2.105.

Azzarà, B., Boschian, G., Brochu, C.A., Delfino, M., Dawid, A., Iurino, D.A., Kimambo, J.S., Manzi, G., Masao F.T., Menconero, S., Njau, J.K. & Cherin, M., 2021. A new cranium of Crocodylus anthropophagus from Olduvai Gorge, northern Tanzania. Research in Paleontology and Stratigraphy, vol. 127(2): 275-295. https://doi.org/10.13130/2039-4942/15771.

Baker, B.H., Mitchell, J.G., Williams, A.J., 1988. Stratigraphy, geochronology and volcano-tectonic evolution of the Kedong-Navasha-Kinangop region, Gregory Rift Valley, Kenya. Journal of the Geological Society, v. 145 (1), pp. 107-116. https://doi.org/10.1144/gsjgs.145.1.0107**.**

Byers, H.L., McHenry, L.J. and Grundl, T.J., 2016. Forty-Nine Major and Trace Element Concentrations Measured in Soil Reference Materials NIST SRM 2586, 2587, 2709a, 2710a and 2711a Using ICP-MS and Wavelength Dispersive-XRF. Geostandards and geoanalytical research, 40(3), pp.433-445.

Chipera, S.J., and Apps, J.A., 2001. Geochemical stability of natural zeolites. Geol. Soc. Am. Bull. DOI: 10.2138/rmg.2001.45.3

Cochemé, J.J., Lassauvagerie, A.C., Gonzalez-Sandoval, J., Perez-Segura, E. and Munch, P., 1996. Characterization and potential economic interest of authigenic zeolites in continental sediments from NW Mexico. Mineral Deposita 31, 482-491.

Deino, A.L., 2012. 40Ar/39Ar dating of Bed I, Olduvai Gorge, Tanzania, and the chronology of early Pleistocene climate change. J. Hum. Evol. 63, 251–273.

Deino, A.L., et al., 2021. Chronostratigraphy and age modeling of Pleistocene drill cores from the Olduvai Basin, Tanzania (Olduvai Gorge Coring Project). Palaeogeography, Palaeoclimatology, Palaeoecology, 571, p. 109990.

Deocampo, D.M., et al., 2018. Paleoclimate records from authigenic clays and zeolites: examples from the Pleistocene Olduvai Gorge, Tanzania, and Pliocene Chemeron Formation, Baringo Basin, Kenya. Geological Society of Americal *Abstracts with Programs*. Vol. 50, No. 6. Doi: 10.1130/abs/2018AM-322944.

Deocampo, D.M., Cuadros, J., Wing-Dudek, T., Olives, J., and Amouric, M., 2009. Saline lake diagenesis as revealed by coupled mineralogy and geochemistry of multiple ultrafine clay phases: Pliocene Olduvai Gorge, Tanzania. American Journal of Science, Vol. 309, Issue 9, pp. 834-868.

Frankel, G.S., Vienna, J.D., Lian, J., Scully, J.R., Gin, S., Ryan, J.V., Wang, J., Kim, S.H., Windl, W., Du, J., 2018. A comparative review of the aqueous corrosion of glasses, crystalline ceramics, and metals. Npj Material Degradation 2:15.

Hay, R.L., 1970. Silicate reactions in three lithofacies of a semi-arid basin, Olduvai Gorge, Tanzania. Min. Soc. Amer., Spec. Pap. 3, 237-255.

Hay, R.L., 1976. Geology of the Olduvai Gorge: a study of sedimentation in a semiarid basin. London, Berkeley, Los Angeles: University of California Press, 1976. 220 pp.

Hay, R.L., Kyser, T.K., 2001. Chemical sedimentology and paleoenvironmental history of Lake Olduvai, a Pliocene lake in northern Tanzania. Geol. Soc. Am. Bull., 113, 1505–1521.

Hay, R.L., Sheppard, R.A., 2001. Occurrence of Zeolites in Sedimentary Rocks: An Overview. *Reviews in Mineralogy and Geochemistry* 2001;; 45 (1): 217–234. doi: https://doi.org/10.2138/rmg.2001.45.6

Kingston, J.D., Deino, A.L., Edgar, R.K., and Hill, A., 2007. Astronomically forced climate change in the Kenyan Rift Valley 2.7-2.55 Ma: implications for the evolution of early hominin ecosystems. Journal of Human Evolution, 35, pp. 487-503.

Kodikara, G.R.L., McHenry, L.J., and van der Meer, F.D., 2023. Spectral mapping of zeolite bearing paleolake deposits at Lake Tecopa, California and its implications for mapping zeolites on Mars. Geosystems and Geoenvironment, v 2. https://doi.org/10.1016/j.geogeo.2022.100119.

Langella, A., Cappelletti, P., and de'Gennaro, R., 2001. Zeolites in closed hydrologic systems. Geol. Soc. Am. Bull. DOI: 10.2138/rmg.2001.45.7.

Leakey, M.D., 1971. Olduvai Gorge: Excavations in Beds I and II; 1960- 1963: Cambridge, U.K., Cambridge University Press. 309 p.

Lepre, C.J., Quinn, R.L., Joordens, J.C.A., Swisher III, C.C., and Feibel, C.S., 2007. Plio-Pleistocene facies environments from the KBS Member Koobi Fora Formation: implications for climate controls on the development of lake-margin hominin habitats in the northeast Turkana Basin (northwest Kenya). Journal of Human Evolution, 53, pp. 504-514.

Li, X., Jiang, L., Liu, J., Wang, M., Li, J., and Yan, Y., 2021. Insight into the interaction between water and ion-exchanged aluminosilicate glass by nanoindentation. Materials (Basel), 14(11): 2959. doi: 10.3390/ma14112959.

McHenry, L.J., 2005. Phenocryst composition as a tool for correlating fresh and altered tephra, Bed I, Olduvai Gorge, Tanzania. Stratigraphy 2(2):101-115. https://doi.org /10.29041/strat.02.2.01

McHenry, L.J., 2009. Element mobility during zeolitic and argillic alteration of volcanic ash in a closed-basin lacustrine environment: Case study Olduvai Gorge, Tanzania. Chemical Geology, 265(3-4), pp.540-552.

McHenry, L.J., 2010. Element Distribution Between Coexisting Authigenic Mineral Phases in Argillic and Zeolitic Althered Tephra, Olduvai Gorge, Tanzania. Clays and Clay Minerals, Vol. 58, No. 5, pp.627–643.

McHenry, L.J., Foerster, V., and Gebregiorgis, D., 2023.Paleolakes of eastern Africa: zeolites, clay minerals, and climate. Elements, Vol. 19, pp. 96-103.

McHenry, L.J., Kodikara, G.R., Stanistreet, I.G., Stollhofen, H., Njau, J.K., Schick, K. and Toth, N., 2020a. Lake conditions and detrital sources of Paleolake Olduvai, Tanzania, reconstructed using X-ray Diffraction analysis of cores. Palaeogeography, Palaeoclimatology, Palaeoecology, 556, p.109855.

McHenry, L.J., Mollel, G.F., Swisher III, C.C., 2008. Compositional and textural correlations between Olduvai Gorge Bed I tephra and volcanic sources in the Ngorongoro Volcanic Highlands, Tanzania. Quaternary International, v. 178, issue 1. doi:10.1016/j.quaint.2007.01.004.

McHenry, L.J., Stanistreet, I.G., Stollhofen, H., Njau, J.K., Toth, N. and Schick, K., 2020b. Tuff fingerprinting and correlations between OGCP cores and outcrops for Pre-Bed I and Beds I/II at Olduvai Gorge, Tanzania. Palaeogeography, Palaeoclimatology, Palaeoecology, 548, p.109630.

Meslin, P.Y., et al., 2022. Evidence for perchlorate and sulfate salts in Jezero crater, Mars, From SuperCam observations. In 53rd Annual Lunar and Planetary Science Conference, 2694.

Mollel, G.F., Swisher III, C.C., 2012. The Ngorongoro Volcanic Highland and its relationships to volcanic deposits at Olduvai Gorge and East African Rift volcanism. Journal of Human Evolution, 63: 274-283.

Mollel, G.F., Swisher III, C.C., Feigenson, M.D., Carr, M.J., 2008. Geochemical evolution of Ngorongoro Caldera, Tanzania: implications for crust-magma interaction. Earth Planet. Sci. Lett. 271, 337–347. https://doi.org/10.1016/j.epsl.2008.04.014.

Njau, J.K., Toth, N., Schick, K., Stanistreet, I.G., McHenry, L.J., and Stollhofen, H., 2021. The Olduvai Gorge Coring Project: Drilling high resolution palaeoclimatic and apaeoenvironmental archives to constrain hominin evolution. Palaeogeography, Palaeoclimatology, Palaeoecology. V. 561. https://doi.org/10.1016/j.palaeo.2020.110059

Olaka, L., and Ebinger, C.J., 2023. Tectonic and Paleoclimatic Setting for Hominin Evolution in Eastern Africa. Elements, Vol. 19, pp. 82-87.

Rodríguez-Cintas, A., et al., 2020. Palaeovegetation changes recorded in Palaeolake Olduvai OGCP Core 2A (2.09–2.12 Ma) Naibor Soit Formation Olduvai Gorge, Tanzania. Palaeogeography, Palaeoclimatology, Palaeoecology, Volume 557, 109928. https://doi.org/10.1016/j.palaeo.2020.109928.

Rampe, E.B., 2020. Mineralogy and geochemistry of sedimentary rocks and eolian sediments in Gale crater, Mars: A review after six Earth years of exploration with Curiosity. Geochemistry. https://doi.org/10.1016/j.chemer.2020.125605.

Rowe, M.C., and Brewer, B.J., 2018. AMORPH: A statistical program for characterizing amorphous materials by X-ray diffraction. Computers and Geosciences, Vol. 120, pp. 21-31.

Sarkar, S., Ghosh, S., Mukherjee, A., Bose, N., and Ray, D., 2024. Detection of natrolite on Mars using Perseverance rover data. In 55th Annual Lunar and Planetary Science Conference, 1053.

Sheppard, R.A., and Gude, A.J. III., and Munson, E.L., 1965. Chemical composition of diagenetic zeolites from tuffaceous rocks of the Mojave Desert and vicinity, California. American Mineralogist 50, 244-249.

Sheppard, R.A. and Gude, A.J. III., 1968. Distribution and genesis of authigenic silicate minerals in tuffs of Pleistocene Lake Tecopa, Inyo County, California. U.S. Geol. Surv., Prof. Paper 597, 38 pp.

Sheppard, R.A. and Gude, A.J. III., 1973. Zeolites and associated authigenic silicate minerals in tuffaceous rocks of the Big Sandy Formation, Mohave County, Arizona. U. S. Geological Survey, Professional Paper 830, 36 pp. .

Sikes, N.E., and Ashley, G.M., 2007. Stable isotopes of pedogenic carbonates as indicators of paleoecology in the Plio-Pleistocene (upper Bed I), western margin of the Olduvai Bain, Tanzania. Journal of Human Evolution, 53, pp. 574-594.

Stanistreet, I.G., Doyle, C., Hughs, T., Rushworth, E.D., Stollhofen, H., Toth, N., Schick, K., and Njau, J.K., 2020a. Changing depocentre environments of Palaeolake Olduvai and carbonates as marker horizons for hiatuses and lake-level extremes. Palaeogeography, Palaeoclimatology, Palaeoecology, 560, p. 110032.

Stanistreet, I.G., Stollhofen, H., Deino, A.L., McHenry, L.J., Toth, N.P., Schick, K.D. and Njau, J.K., 2020b. New Olduvai Basin stratigraphy and stratigraphic concepts revealed by OGCP cores into the Palaeolake Olduvai depocentre, Tanzania. Palaeogeography, Palaeoclimatology, Palaeoecology, 554, p.109751.

Staples, L.W. and Gard, J.A., 1959. The fibrous zeolite erionite: its occurrence, unit cell, and structure. Mineralogical Magazine 32, 261-281.

Trauth, M.H., Asrat, A., Berner, N., Bibi, F., Foerster, V., Grove, M., Kaboth-Bahr, S., Maslin, M.A., Mudelsee, M., Schabitz, F., 2021. Northern Hemisphere Glaciation, African climate and human evolution. Quaternary Science Reviews, 268, 107095. https://doi.org/10.1016/j.quascirev.2021.107095

Trauth, M.H., Maslin, M.A., Deino., A.L., Strecker, M.R., 2005. Late Cenozoic moisture history of East Africa. Science, v. 309, issue 5743, pp. 2051-2053. https://doi.org/10.1126/science.1112964.

Trauth, M.H., Maslin, M.A., Deino., A.L., Strecker, M.R., Bergner, A.G.N., and Dühnforth, M., 2007. High- and low-latitude forcing of Plio-Pleistocene East African climate and human evolution. Journal of Human Evolution, 53, pp. 475-486.

Uribelarrea, D., et al., 2017. A reconstruction of the paleolandscape during the earliest Acheulian of FLK West: The co-existence of Oldowan and Acheulian industries during lowermost Bed II (Olduvai Gorge, Tanzania). Palaeogeography, Palaeoclimatology, http://dx.doi.org/10.1016/j.palaeo.2017.04.014.

**Appendix A: Detailed Core Log with Sample Images.**
*Sedimentological interpretations after Stanistreet et al., 2020b.*

## 2A-47Y-2

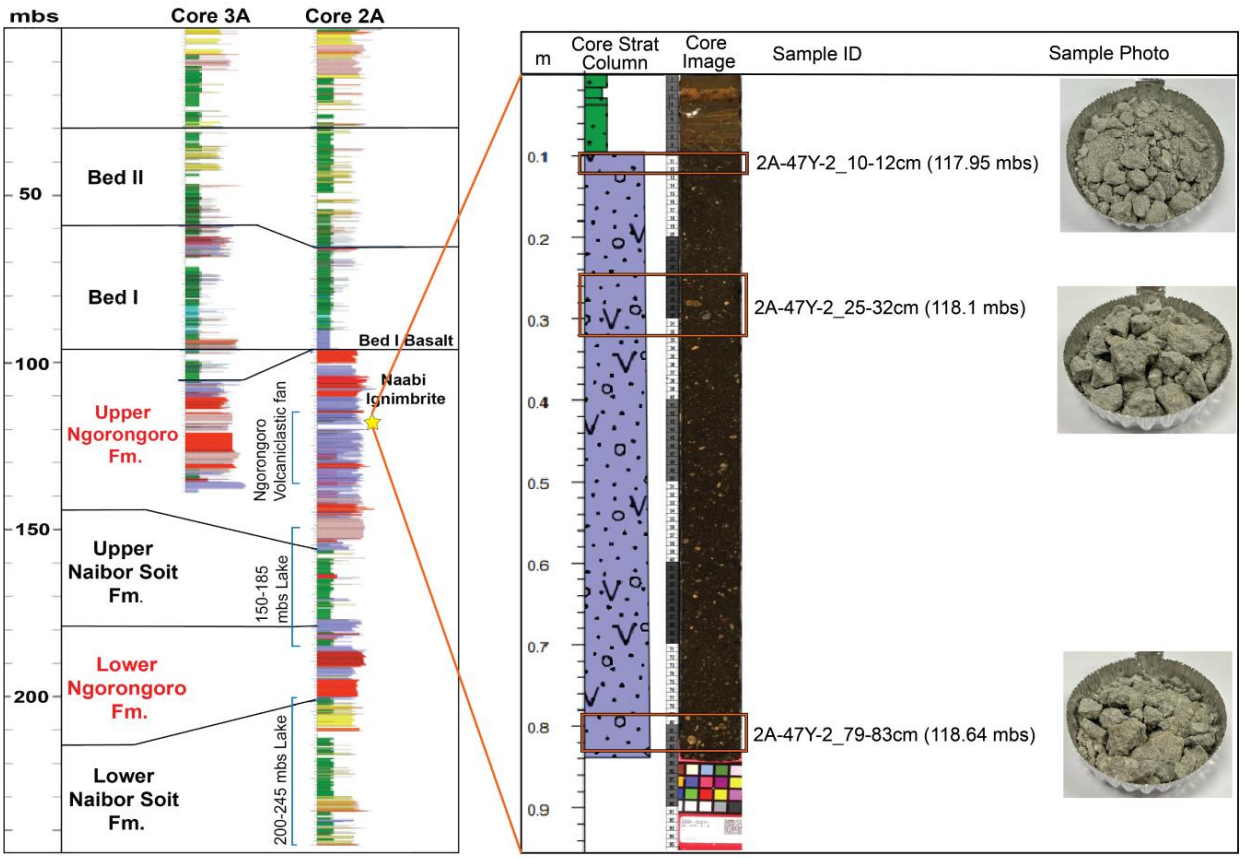


**Figure 24.** Core 2A-47Y-2. The sampled unit (purple) is a thick volcaniclastic debris flow composed of poorly sorted gravel with pumice clasts scattered throughout (very few feldspar and obsidian clasts are also present but should not affect data since only pumice is examined). The overlying unit is a relatively thick sandy claystone (green), indicating the debris flow was deposited in the lake margin and the lake level remained consistent for a period of time.

**10-12cm (117.95 mbs):** directly touching lake clay unit (proximal).

**25-32cm (118.1 mbs):** not touching lake clay unit, but still stratigraphically close to it (proximal).

**79-83cm (118.64 mbs):** more stratigraphically separated from lake unit, but by less than a meter. Could potentially still be influenced by a long period of lake standing over the entire unit (Intermediate).

## 2A-50Y-2

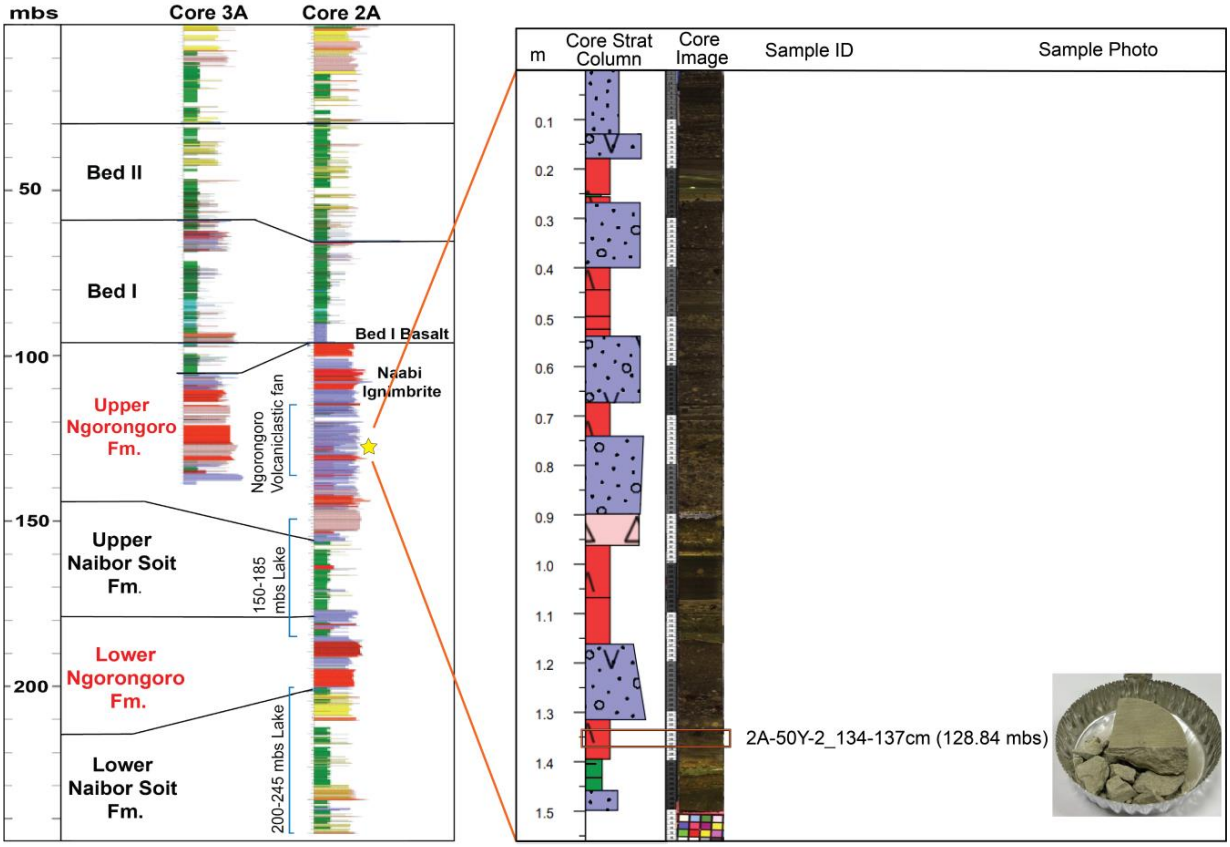


**Figure 25.** Core 2A-50Y-2. The sampled unit is a relatively thin unit of stacked airfall ash (red). Includes lapilli and pumice that dropped into layers of accumulating fine ash. This ash unit overlies a small unit of layered fine-grained lake claystone (green), which indicates deposition in a slightly deeper lake. Ash, lapilli, and pumice likely fell out over the lake and formed layers as they fell out of suspension.

**134-137cm (128.84 mbs):** touching lake, proximal.

**2A-51Y-1**

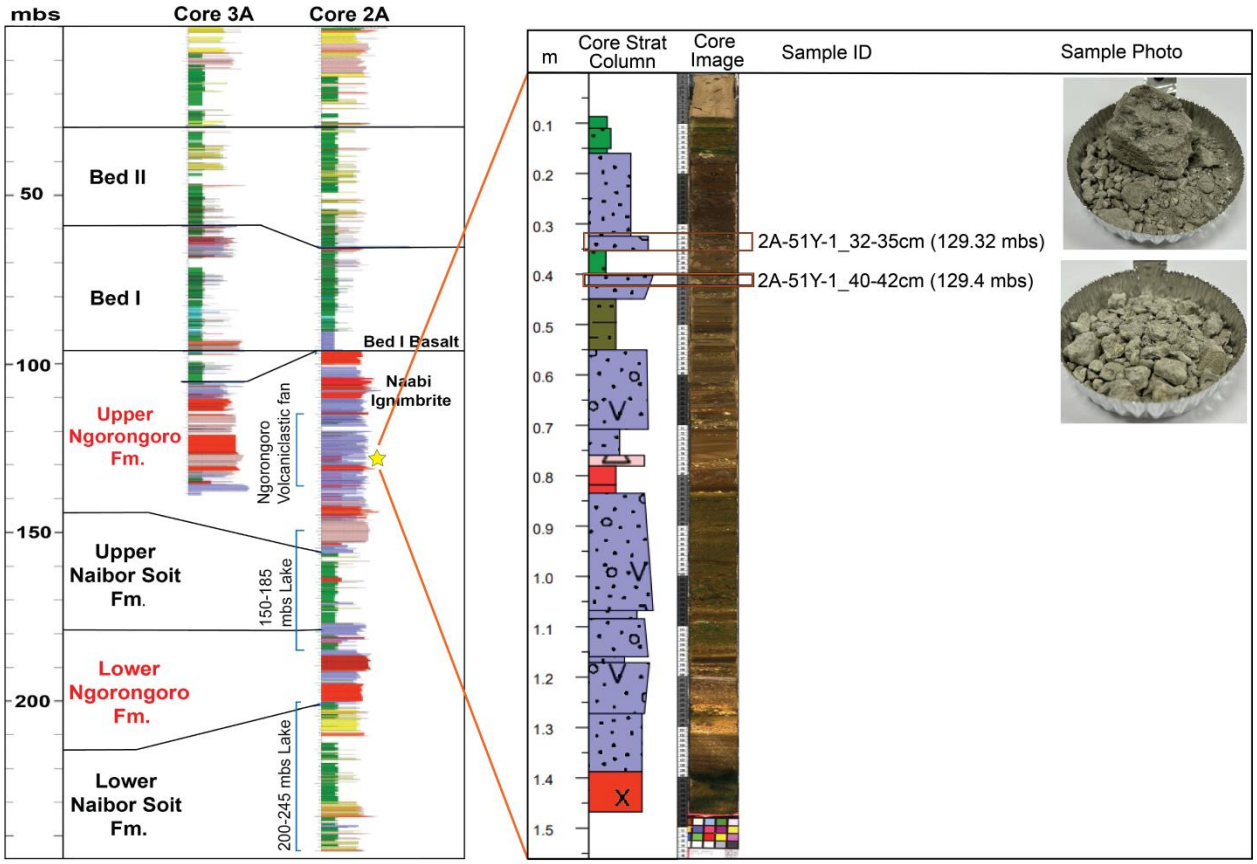


**Figure 26.** Core 2A-51Y-1. The sampled units are similar, both represent pumice wash/conglomerate in a volcaniclastic fan (purple). The sandy claystone unit (green) in-between both intervals indicates they were deposited in the lake margin, also indicated by pumice float in both samples.

**32-35cm (129.32 mbs):** touching lake, proximal.

**40-42cm (129.4 mbs):** touching lake, proximal.

**2A-54Y-1**

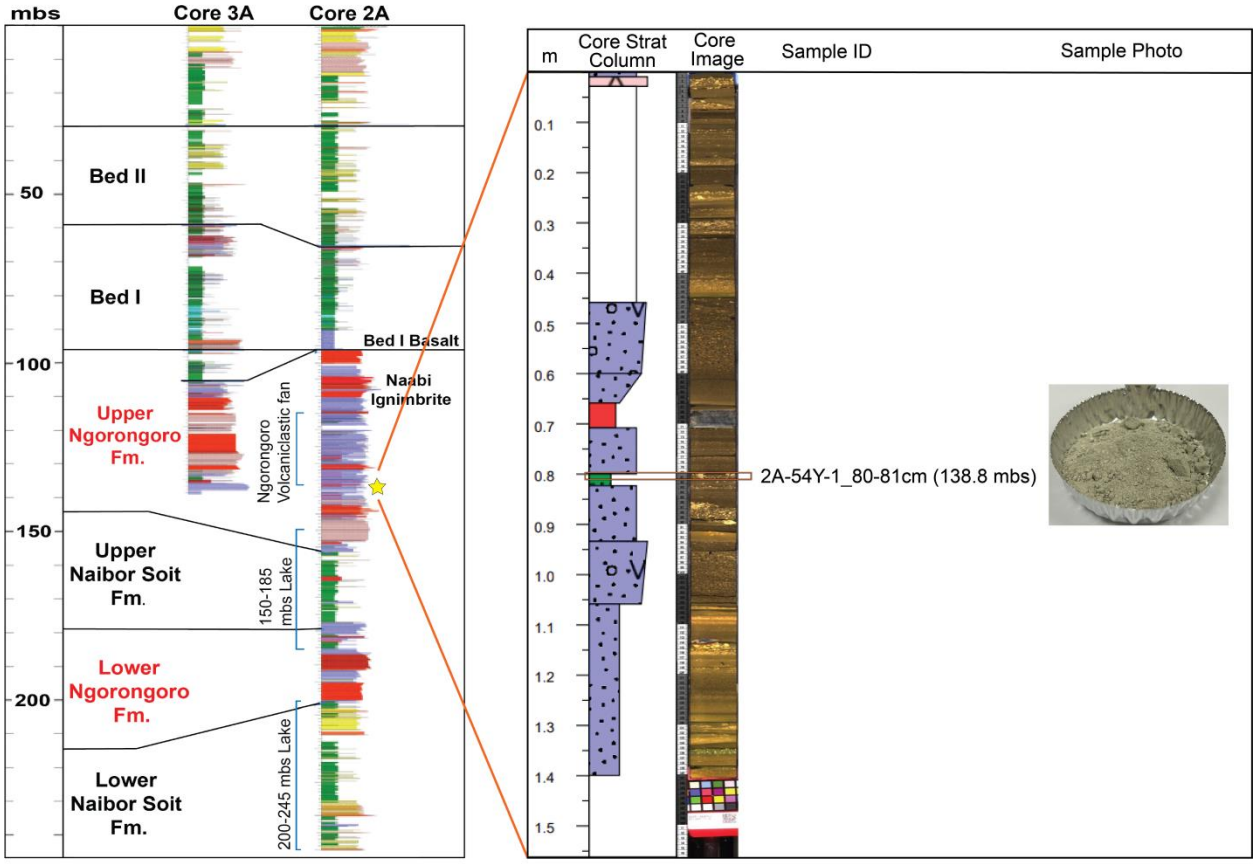


**Figure 27.** Core 2A-54Y-1. The sampled unit is a mudstone layer (green) with waterlogged pumices accumulating at the top. The claystone is sandy and sandwiched between two sandy volcaniclastic sheetwash units (purple), which indicates deposition in the lake margin.

**80-81cm (138.8 mbs):** in lake, proximal.

**2A-60Y-1**

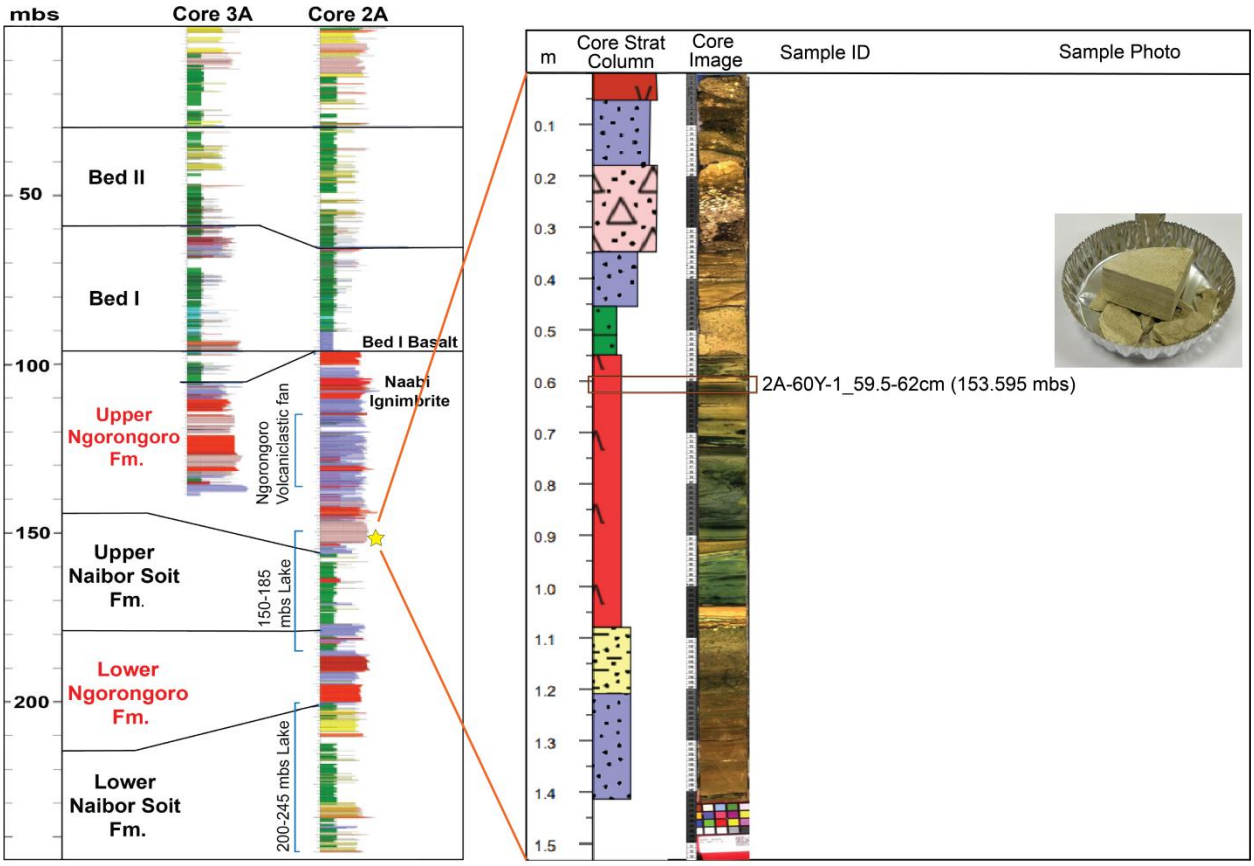


**Figure 28.** Core 2A-60Y-1. Sampled unit is a stacked airfall tuff (red). The overlying sandy claystone (green) unit indicates deposition in the lake margin. This is a bulk sample.

**59.5-62cm (153.595 mbs):** stratigraphically close to lake unit, proximal.

## 2A-63Y-2

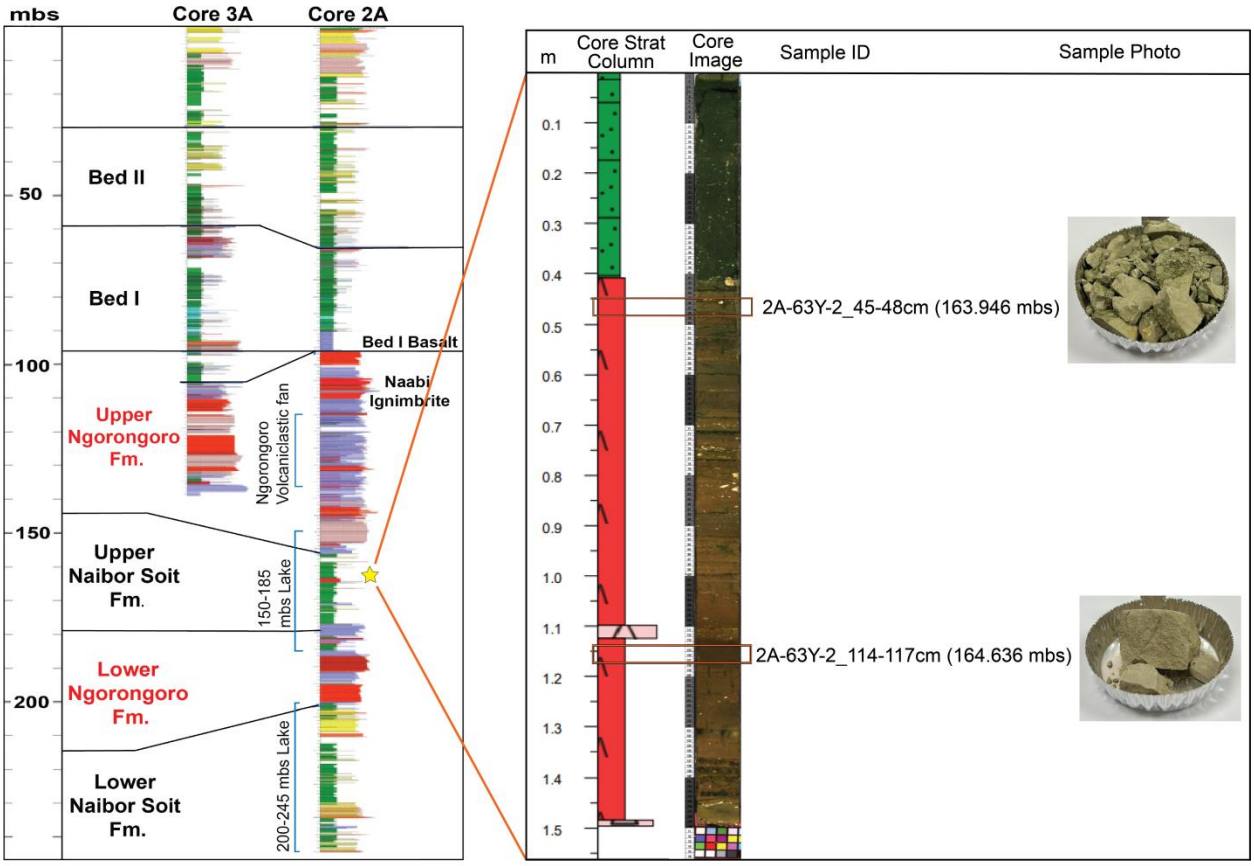


**Figure 29.** Core 2A-63Y-2. The sampled units are in the upper Naibor Soit Fm (between the two pulses of Ngorongoro fan progradation). The unit is comprised of a stacked series of airfall tuffs (red). The tuff was mostly graded, varying between a few mm to 5 cm thick. Some layers have lapilli concentrations at the base of the fall our units. Overlying unit is a thick sandy claystone (green), indicating deposition occurred along the lake margin.

**45-48cm (163.946 mbs):** touching lake unit, proximal.

**114-117cm (164.636 mbs):** somewhat stratigraphically separated from lake unit, but under a diamictite mudflow deposit (pink) and above a ‘water escape conduit', so intermediate.

## 2A-69Y-2

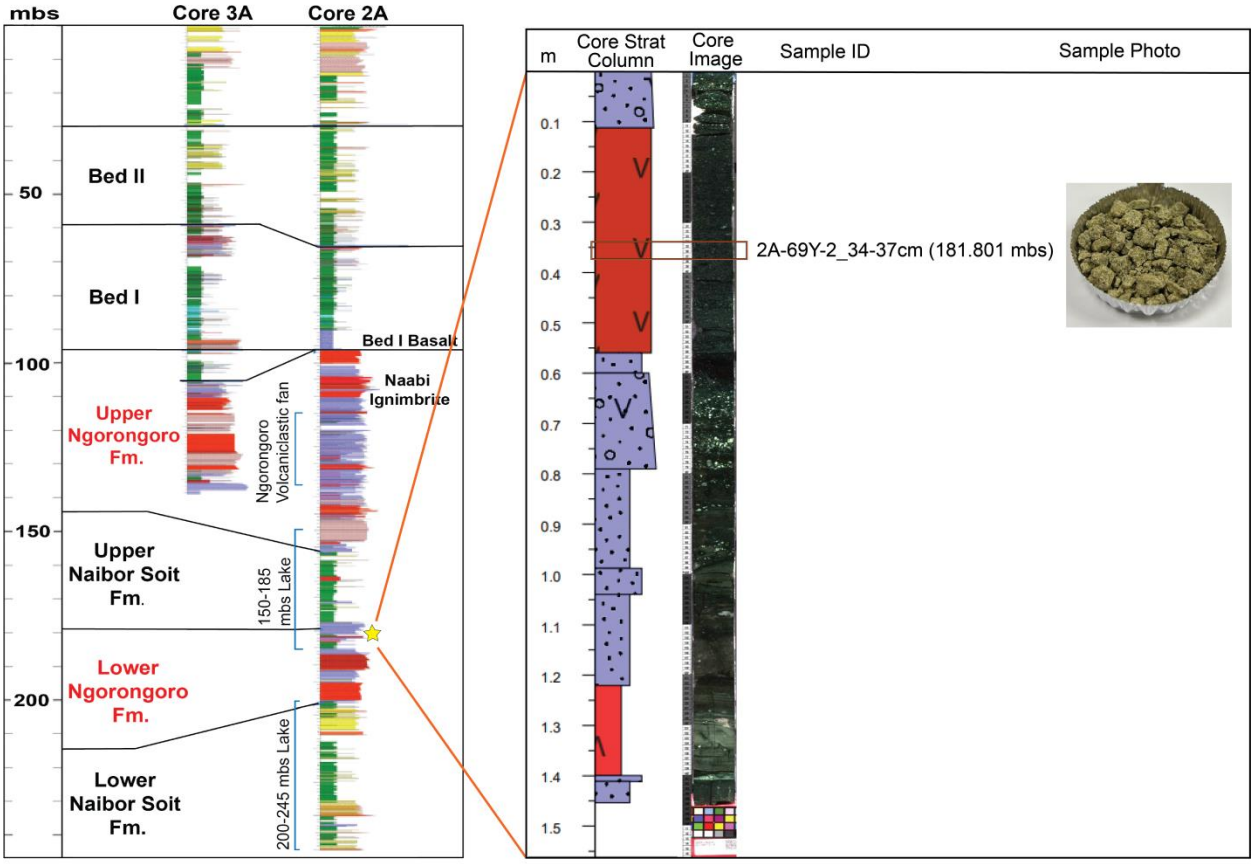


**Figure 30.** Core 2A-69Y-2. The sampled unit is under the upper Naibor Soit Fm, this is a lower Ngorongoro Fm sample. The unit is ash lapilli tuff (red). There are no lake claystones present in this portion of the core so it is difficult to determine depositional environment. However, the rock units below this unit are volcaniclastic (purple) sheetflows grading upwards into debris flows and the unit above is a volcaniclastic debris flow.

**34-37cm (181.801 mbs):** no lake clay units, but in the middle of a tuff unit likely deposited in lake margin, intermediate.

## 2A-70Y-1

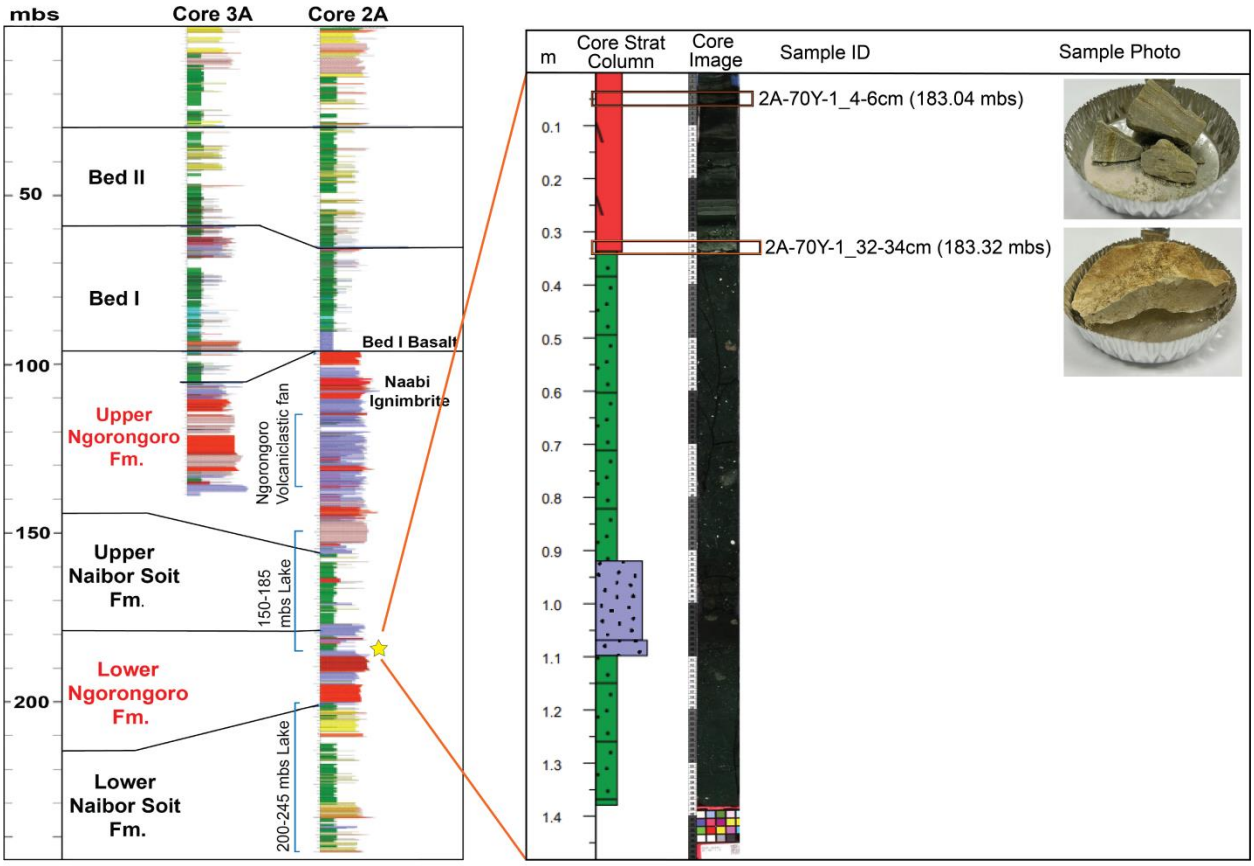


**Figure 31.** Core 2A-70Y-1. The sampled unit is a stacked fine ash airfall tuff (red). This unit directly overlies a sandy claystone (green), indicating deposition in the lake margin. Both are bulk samples.

**4-6cm (183.04 mbs):** slightly stratigraphically separated from thick lake unit, but still proximal.

**32-34cm (183.32 mbs):** touching lake unit, proximal.

## 2A-70Y-2

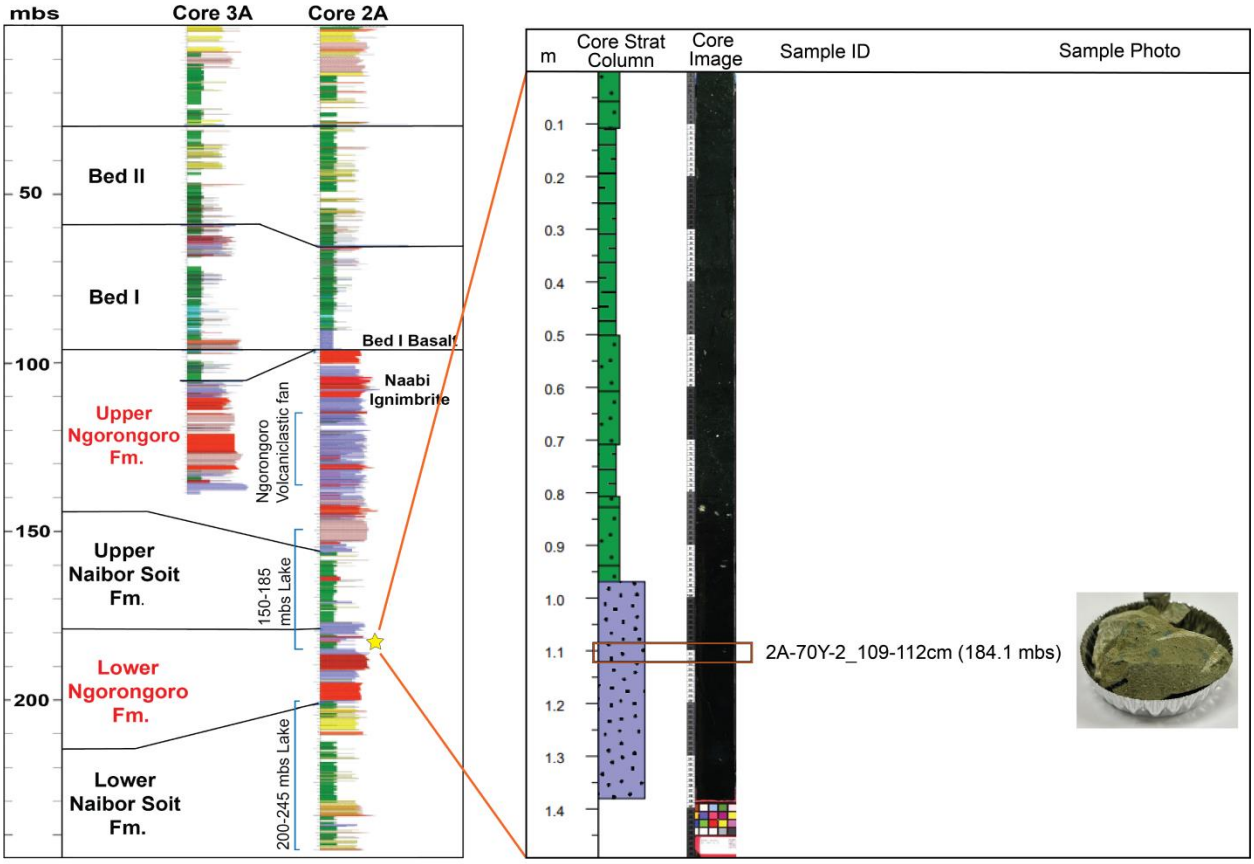


**Figure 32.** Core 2A-70Y-2. The sampled unit is a sandy debris flow (purple), carrying scattered volcanic clasts of porphyric and vesicular clasts <4.5cm. The thick sequence of lake clays (green) overlying the debris flow unit range from claystone to sandy claystone, indicating some fluctuation from lake margin to slightly deeper lake (transitional zone). This is a bulk sample.

**109-112cm (184.1 mbs):** close to lake interval, proximal.

**2A-72Y-1**

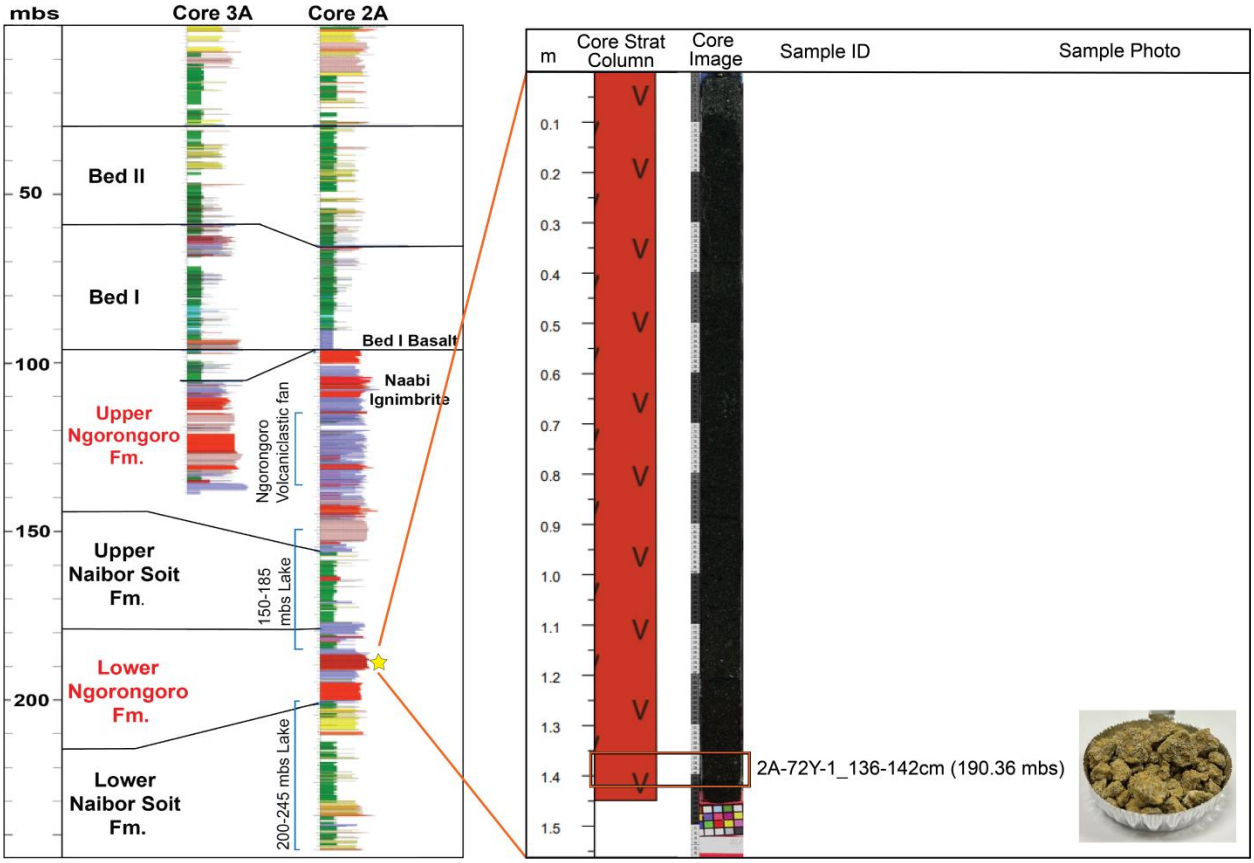


**Figure 33.** Core 2A-72Y-1. The sampled unit is a very thick ash lapilli tuff (red) from a pyroclastic flow. The sample interval contains prominent crystals. There are no lake units present in this core interval, but the color of this sample implies it has been zeolitized. Rather than depending on lake, alteration could have occurred with saline-alkaline groundwater or from meteoric water becoming trapped in pores. These scenarios seem likely since a volcanic deposit of this volume would likely fill in the lake margin and force the lake into a different area.

**136-142cm (190.36 mbs):** away from lake units, separated

## 2A-72Y-2

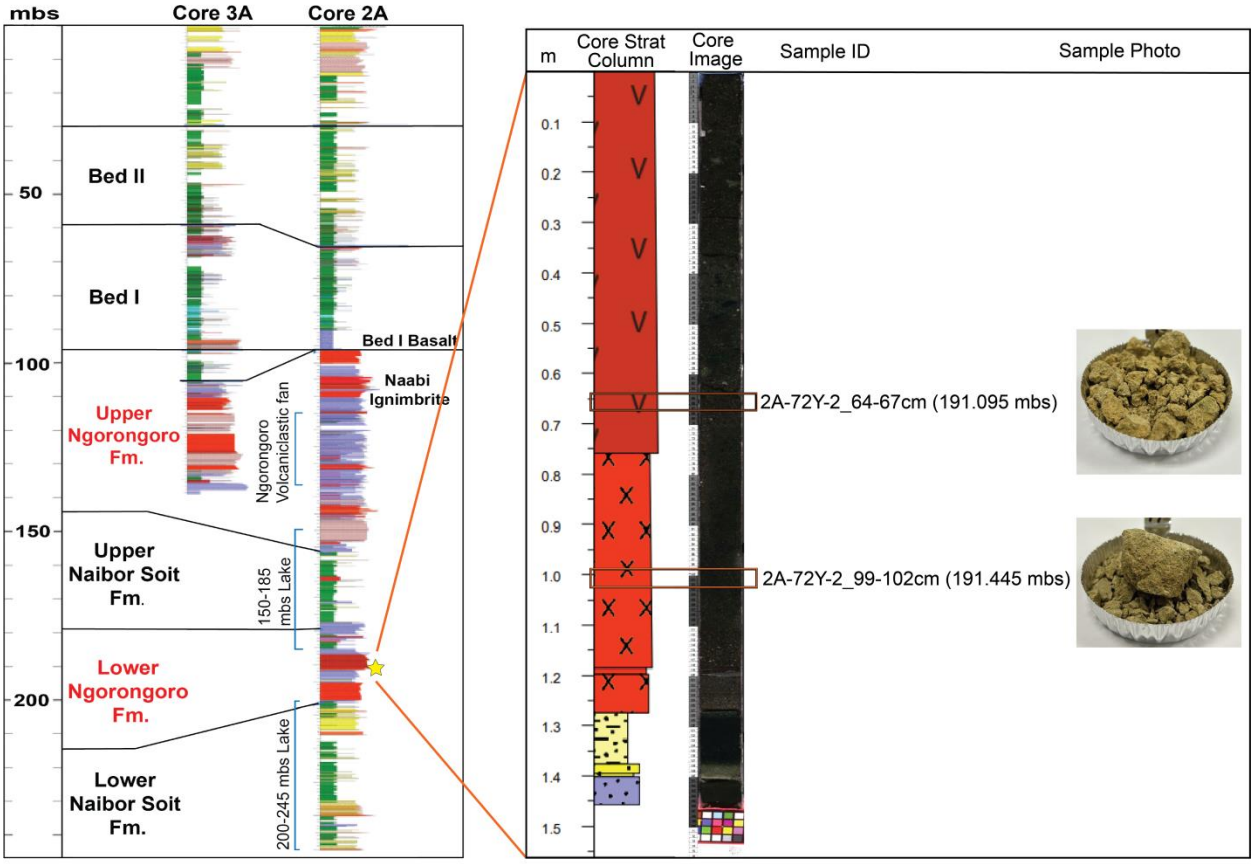


**Figure 34.** Core 2A-72Y-2. The first unit sampled (dark red) is the base of the pyroclastic flow unit sampled above. It is a lapilli ash tuff comprised of large clasts of wood fragments (up to 8mm), vesicular amygdaloidal volcanic lava clasts, and pumice concentrates.

The second unit sampled (light red) is a massive lapilli ash tuff containing feldspar crystals and lithic porphyritic lava fragments.

The other units in this core interval are detrital sand (yellows) and volcaniclastic sheetwash (purple). These units were likely along the lake margin.

**64-67cm (191.095 mbs):** far from lake, separated.

**99-102cm (191.445 mbs):** in the middle of a short tuff unit, no lake clays, but wet-related lithology nearby, so sample it intermediate.

## 2A-74Y-3

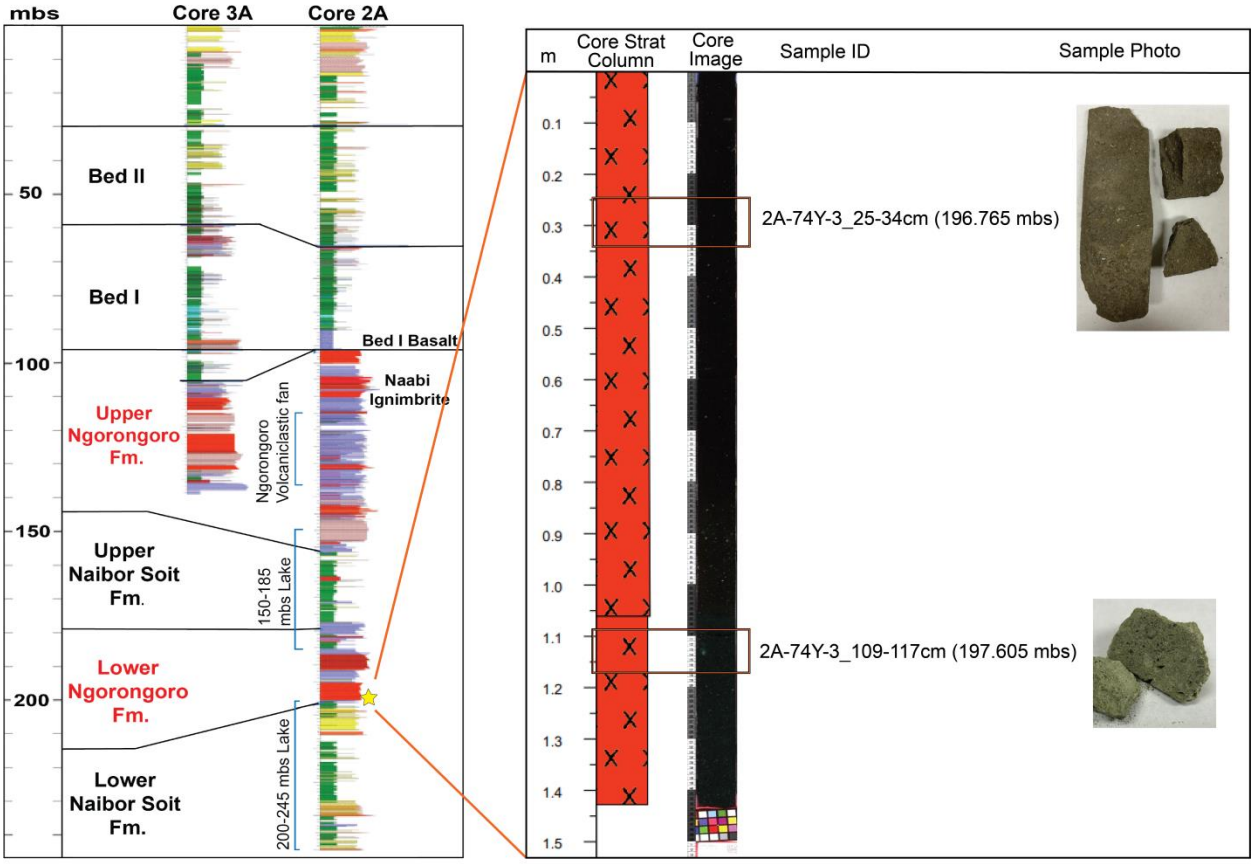


**Figure 35.** Core 2A-74Y-3. The sampled units are thick lapilli ash tuffs (red), the upper unit with coarse ash and the lower unit with thick lapilli (scattered clasts up to 15mm). Both units result from a pyroclastic flow. This interval is on top of the lower Naibor Soit Fm, but there are no lake claystone units in stratigraphic proximity to either sample. If there is alteration in these samples, it is likely a result of groundwater interaction.

**25-34cm (196.765 mbs):** away from lake units, separated.

**109-117cm (197.605 mbs):** away from lake units, separated.

**3A-41Y-1**

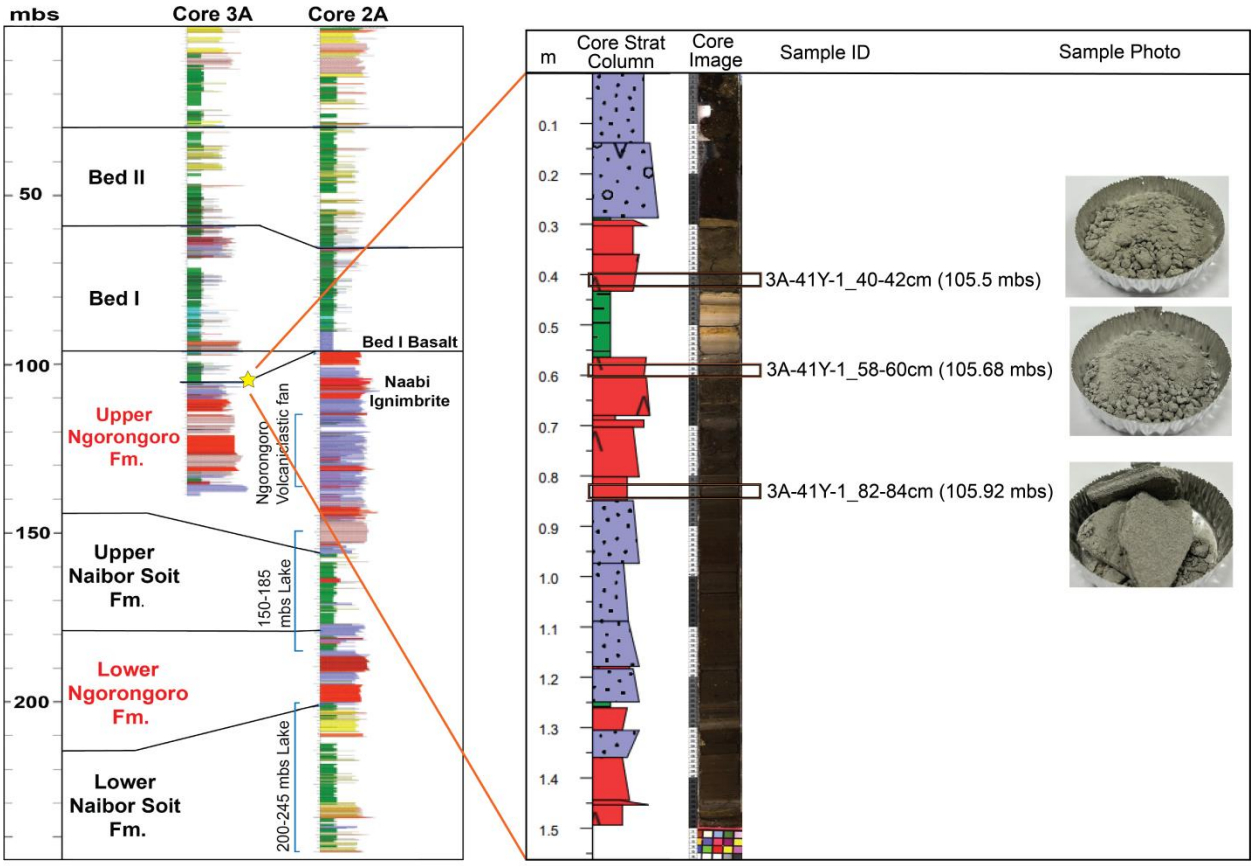


**Figure 36.** Core 3A-41Y-1. The first sampled unit (top red) is a coarse ash (red) exhibiting shard shapes and pumice grains. The bottom part is vesiculated. The underlying unit is a lake claystone (green), indicating deep lake conditions.

The second sampled unit (middle red) is a lapilli ash tuff comprising coarse ash. It has devitrified volcanic shards (in Y shapes). It lies under a lake claystone, indicating deeper conditions.

The third sampled unit (bottom red) is a fine ash comprised of a stack of surges exhibiting low angle cross lamination. This indicates deepening lake conditions, confirmed by the underlying unit (purple) is a sheetwash.

**40-42cm (105.5 mbs):** touching lake unit, proximal.

**58-60cm (105.68 mbs):** touching lake unit, proximal.

**82-84cm (105.92 mbs):** lake units are further stratigraphically but lake is still there, proximal.

## 3A-41Y-2

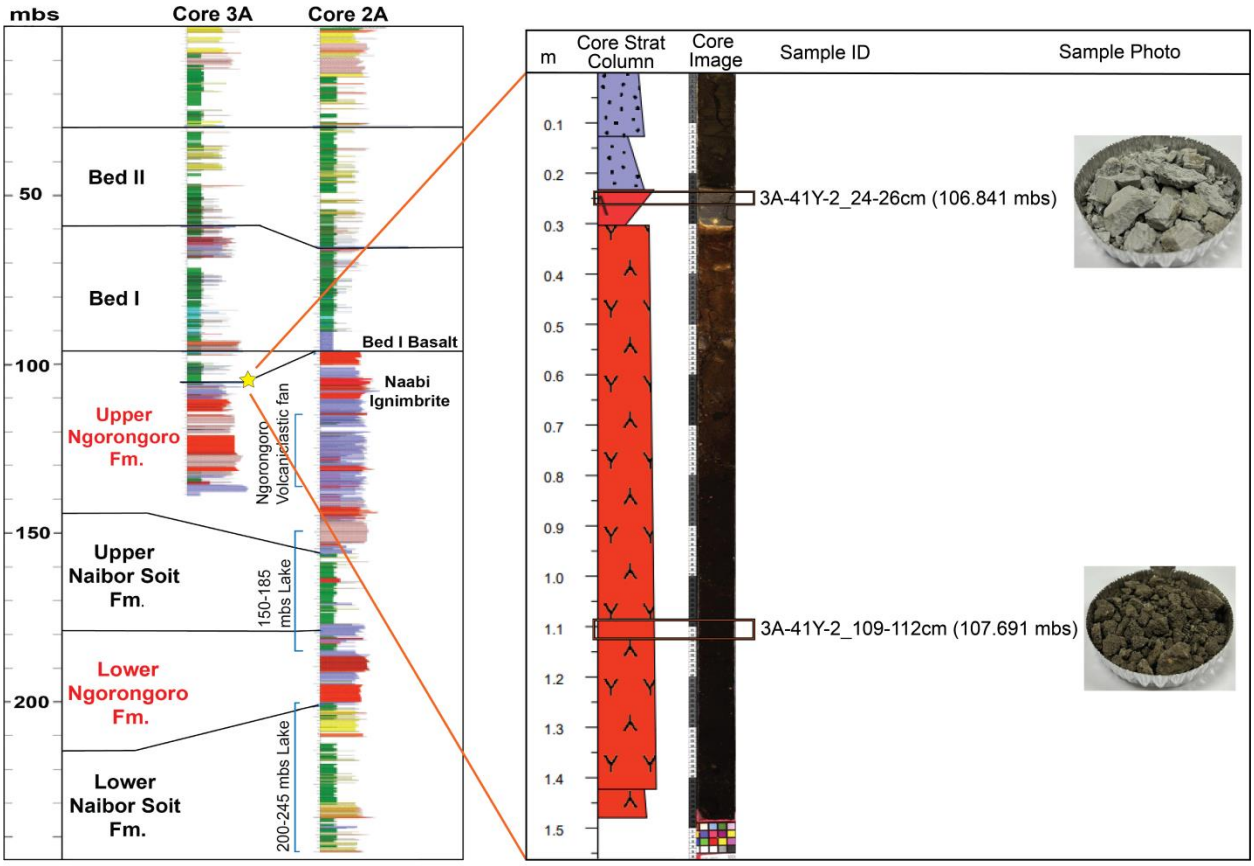


**Figure 37.** Core 3A-41Y-2. The first unit sampled is a water-laid fine ash tuff grading into a lapilli ash tuff. Pumice clasts are at the top (<4mm diameter) and winnowed out of the fall by floatation. There is a soil horizon starting before this unit was placed.

The second unit sampled is an ash lapilli tuff deposited by a pyroclastic flow unit. This unit has obsidian clasts and clasts of other lithologies throughout. There are no obvious lake intervals around this unit.

**24-26cm (106.841 mbs):** close to lake, proximal

**109-112cm (107.691 mbs):** far from lake, separated

**3A-45Y-2**

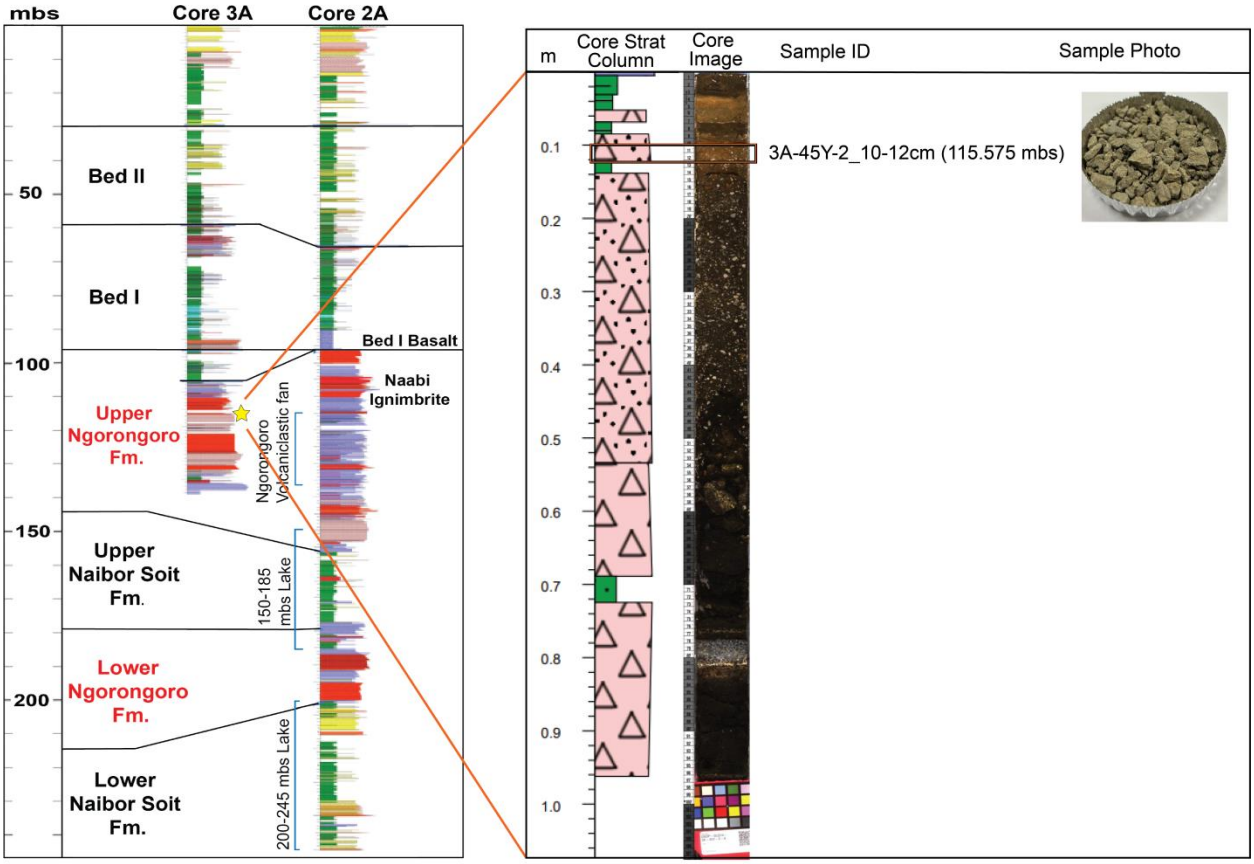


**Figure 38.** Core 3A-45Y-2. The sampled unit is a mudflow diamictite (pink) with round, weathered pumice and feldspar clasts. This unit is sandwiched between two lake claystone units (green).

**10-12cm (115.575 mbs):** touching clay intervals, proximal.

**3A-50Y-1**

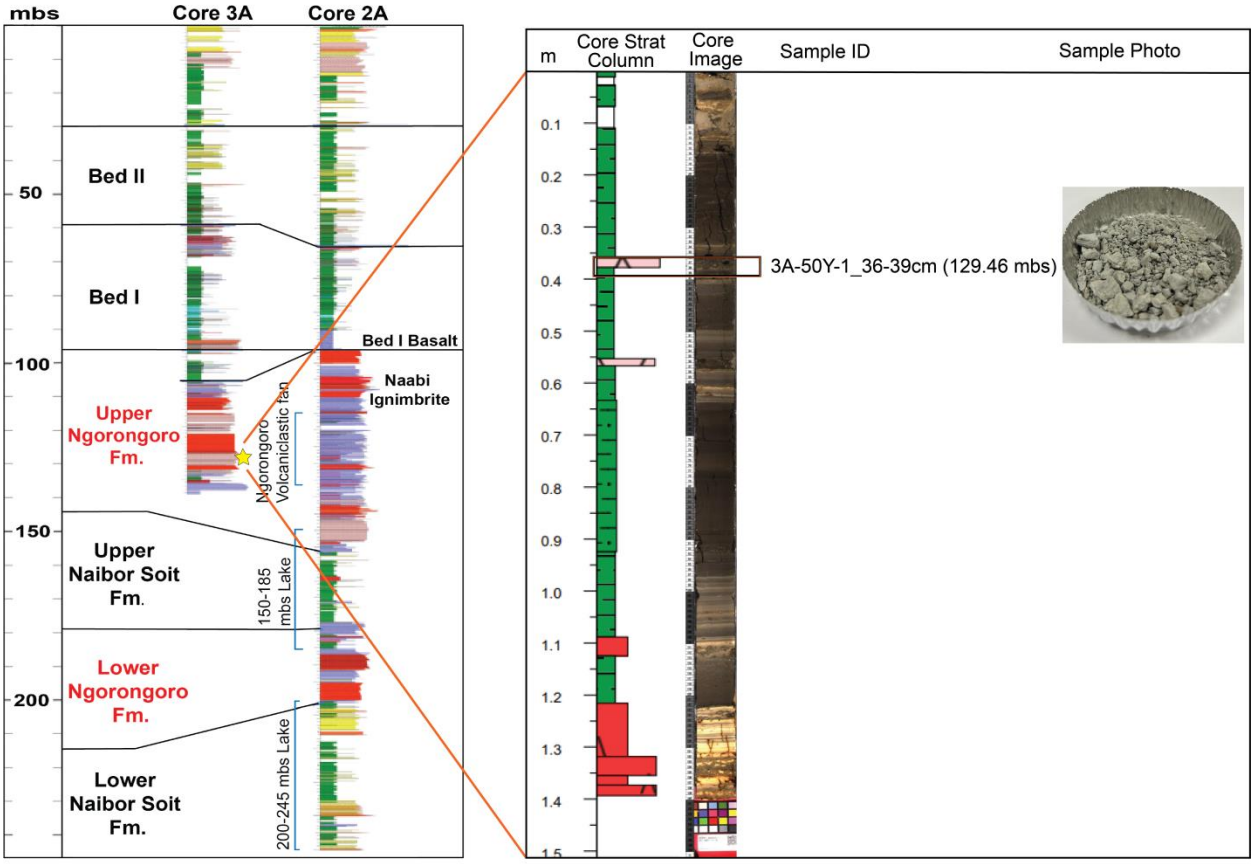


**Figure 39.** Core 3A-50Y-1. The sampled unit is a laminated clay with a concentration of waterlogged floating pumices (diamictite and clay interval). This unit (pink) is very thin and between two long claystone intervals (green).

**36-39cm (129.46 mbs):** touching clay, proximate.

**3A-50Y-2**

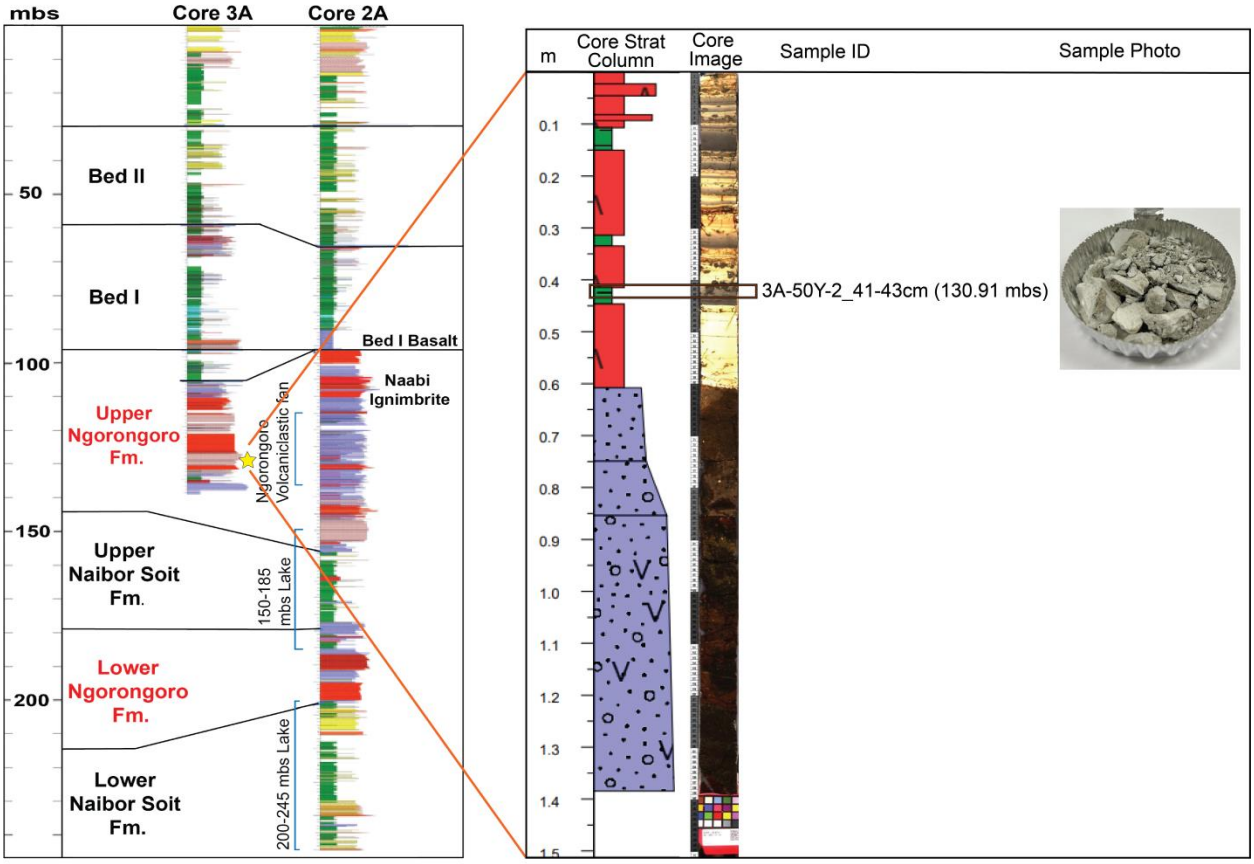


**Figure 40.** Core 3A-50Y-2. The sampled interval is a waxy claystone (green) with a concentration of waterlogged pumice. This was deposited in deeper water, indicating a rise in water level. The underlying volcaniclastic unit (purple) contains weathered trachyte, likely reflecting older volcanics.

**42-43cm (130.91 mbs):** in lake sediment, proximal.

## Appendix B: X-Ray Diffraction Patterns

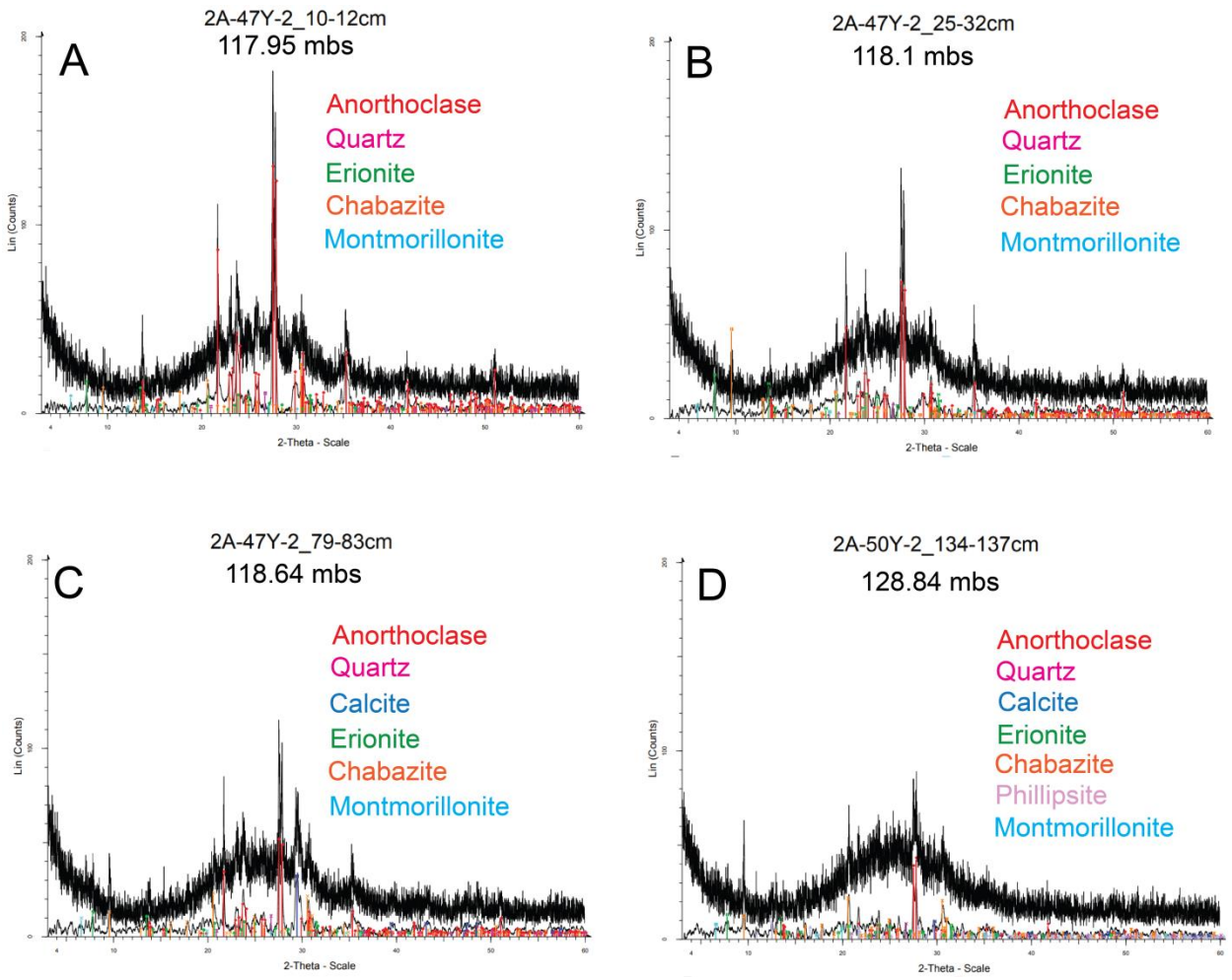


**Figure 41.** XRD plots from core 2A, displaying the major mineral assemblages. Plots show both the raw patterns (above) and smoothed, background-subtracted patterns below, used for pattern matching. Colored lines indicate Bruker EVA matches to ICDD PDF-2 patterns (McHenry et al., 2020). A) 117.95 mbs: anorthoclase, quartz, erionite, chabazite, and montmorillonite in a volcaniclastic debris flow of the Upper Ngorongoro Fm, proximal to a lake interval. B) 118.1 mbs: anorthoclase, quartz, erionite, chabazite, and montmorillonite in a volcaniclastic debris flow of the Upper Ngorongoro Fm, proximal to a lake interval. C) 118.64 mbs: anorthoclase, quartz, calcite, erionite, chabazite, and montmorillonite in a volcaniclastic debris flow of the Upper Ngorongoro Fm, intermediate to a lake interval. D) anorthoclase, quartz, calcite, erionite, chabazite, phillipsite, and montmorillonite in a stacked airfall ash with pumice of the Upper Ngorongoro Fm, proximal to a lake interval.

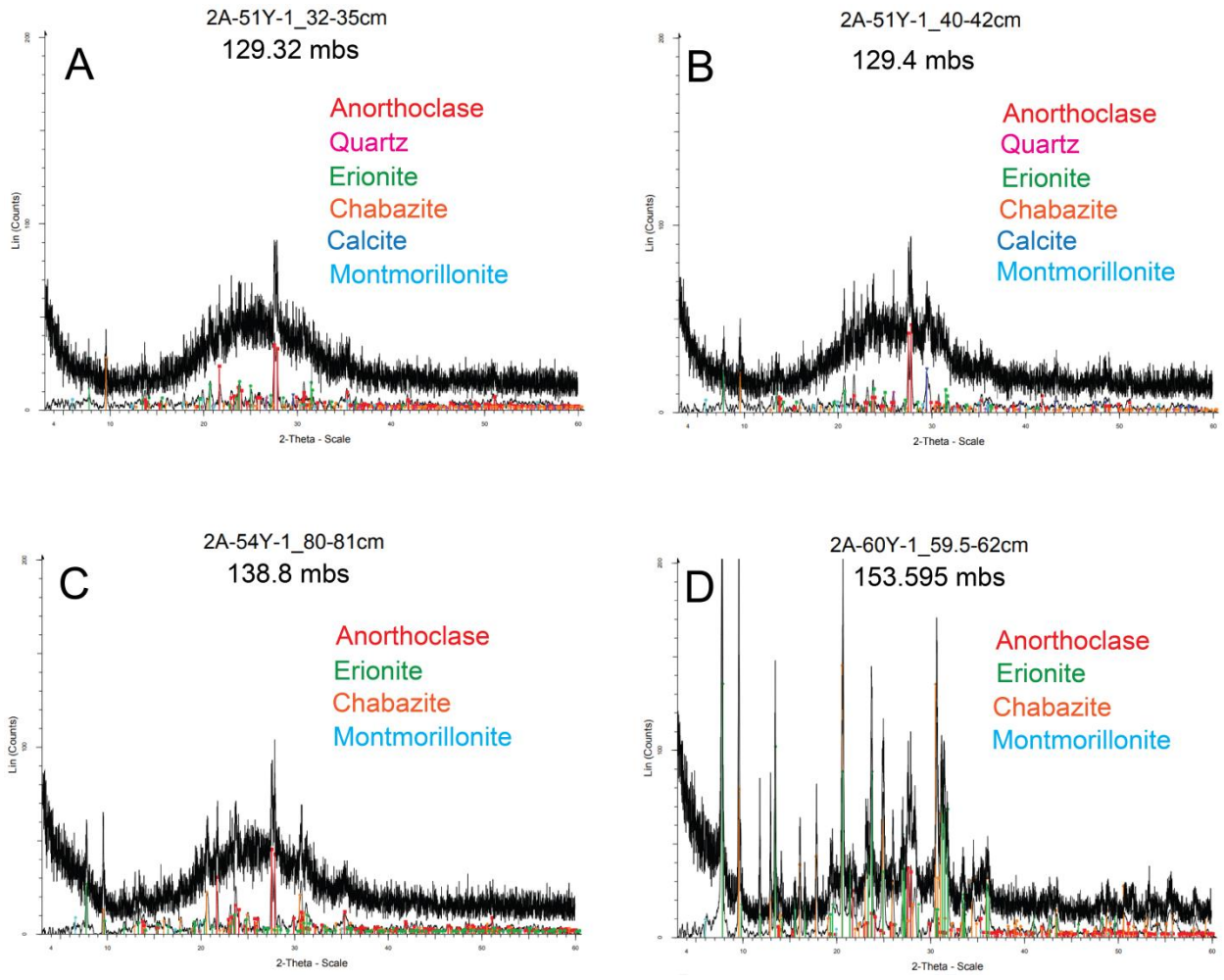


**Figure 42.** XRD plots from core 2A, displaying the major mineral assemblages. Plots show both the raw patterns (above) and smoothed, background-subtracted patterns below, used for pattern matching. Colored lines indicate Bruker EVA matches to ICDD PDF-2 patterns (McHenry et al., 2020). A) 129.32 mbs: anorthoclase, quartz, erionite, chabazite, calcite, and montmorillonite in pumice wash in a volcaniclastic fan deposit of the Upper Ngorongoro Fm, proximal to a lake interval. B) 129.4 mbs: anorthoclase, quartz, erionite, chabazite, calcite, and montmorillonite in pumice wash in a volcaniclastic fan deposit of the Upper Ngorongoro Fm, proximal to a lake interval. C)138.8 mbs: anorthoclase, erionite, chabazite, and montmorillonite in waterlogged pumice in a claystone of the Upper Ngorongoro Fm, proximal to a lake interval. D) 153.595 mbs: anorthoclase, erionite, chabazite, and montmorillonite in a stacked airfall tuff of the Upper Ngorongoro Fm, proximal to a lake interval.

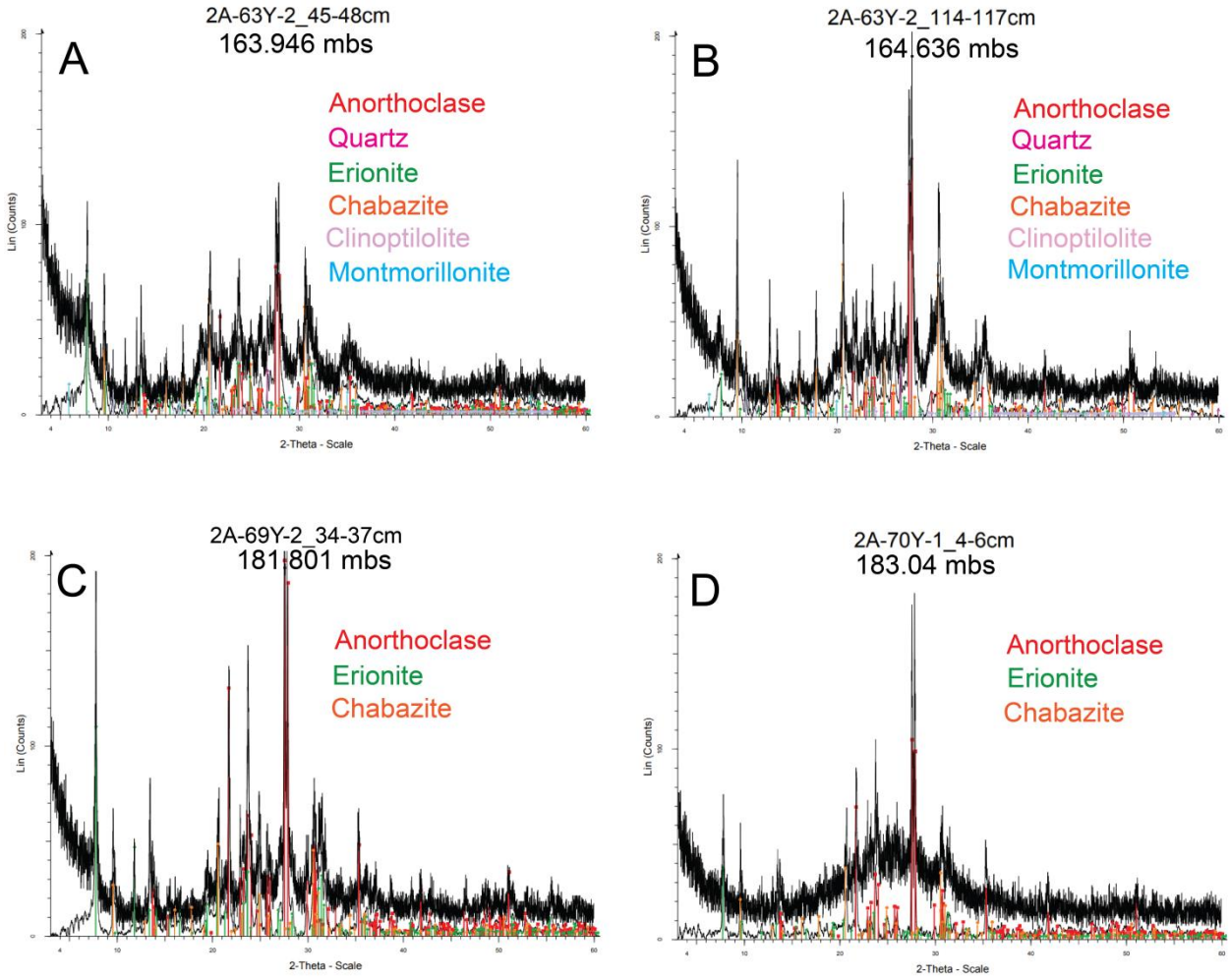


**Figure 43.** XRD plots from core 2A, displaying the major mineral assemblages. Plots show both the raw patterns (above) and smoothed, background-subtracted patterns below, used for pattern matching. Colored lines indicate Bruker EVA matches to ICDD PDF-2 patterns (McHenry et al., 2020). A) 163.946 mbs: anorthoclase, quartz, erionite, chabazite, clinoptilolite, and montmorillonite in a stacked airfall tuff, proximal to a lake interval. A) 163.946 mbs: anorthoclase, quartz, erionite, chabazite, clinoptilolite, and montmorillonite in a stacked airfall tuff of the Upper Naibor Soit Fm, proximal to a lake interval. B) 164.636 mbs: anorthoclase, quartz, erionite, chabazite, clinoptilolite, and montmorillonite in a stacked airfall tuff of the Upper Naibor Soit Fm, intermediately separated from a lake interval. C) 181.801 mbs: anorthoclase, erionite, and chabazite in an ash lapilli tuff of the Lower Ngorongoro Fm, intermediately separated from a lake interval. D) 183.04 mbs: anorthoclase, erionite, and chabazite in a stacked fine airfall tuff of the Lower Ngorongoro Fm, proximal to a lake interval.

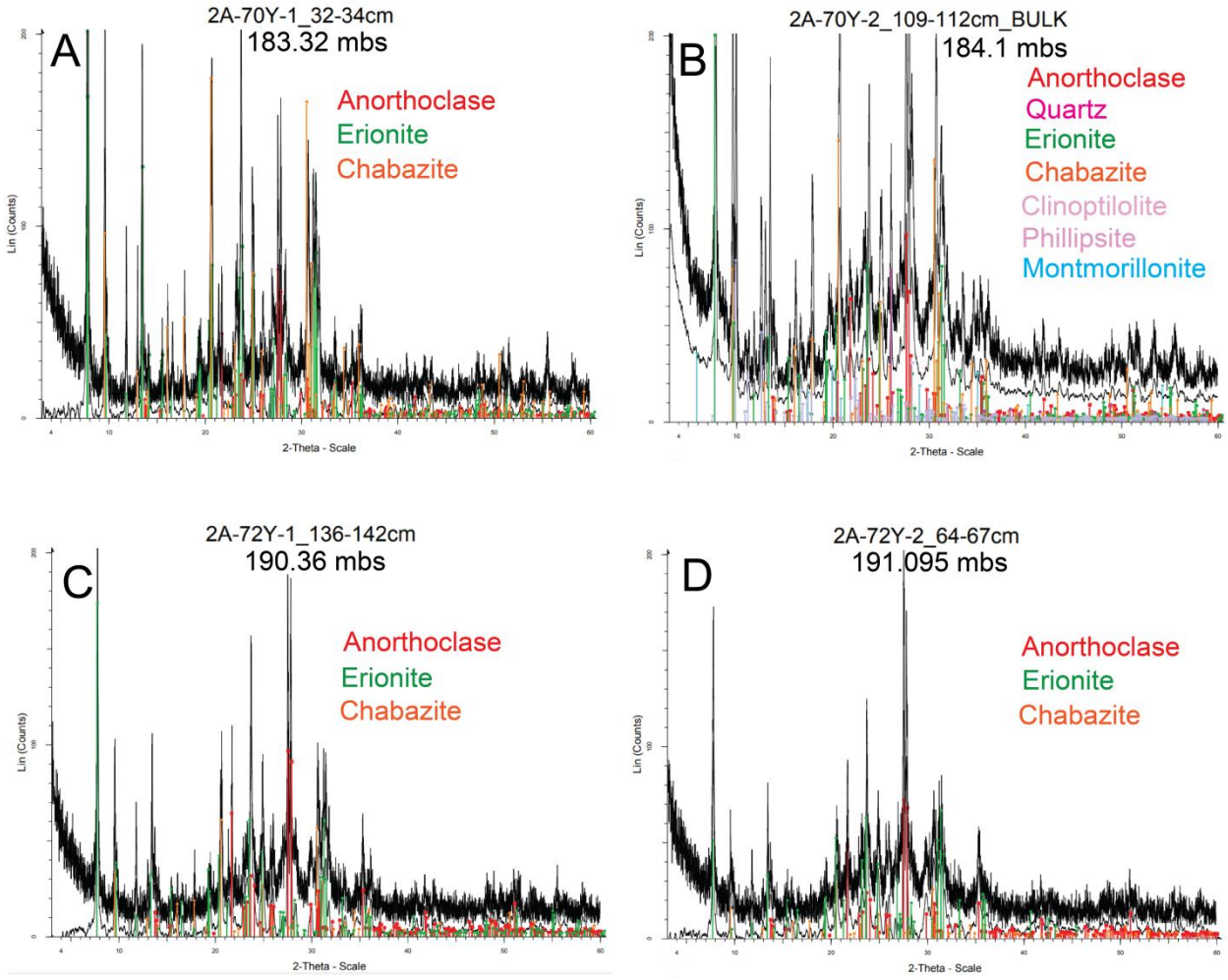


**Figure 44.** XRD plots from core 2A, displaying the major mineral assemblages. Plots show both the raw patterns (above) and smoothed, background-subtracted patterns below, used for pattern matching. Colored lines indicate Bruker EVA matches to ICDD PDF-2 patterns (McHenry et al., 2020). A) 183.32 mbs: anorthoclase, erionite, and chabazite in a stacked fine airfall tuff of the Lower Ngorongoro Fm, proximal to a lake interval. B) 184.1 mbs: anorthoclase, quartz, erionite, chabazite, clinoptilolite, phillipsite, and montmorillonite in a sandy debris flow of the Lower Ngorongoro Fm, proximal to a lake interval. C) 190.36 mbs: anorthoclase, erionite, and chabazite in a ash lapilli tuff of the Lower Ngorongoro Fm, stratigraphically separated from a lake interval. D) 191.095: anorthoclase, erionite, and chabazite in an ash lapilli tuff of the Lower Ngorongoro Fm, stratigraphically separated from a lake interval.

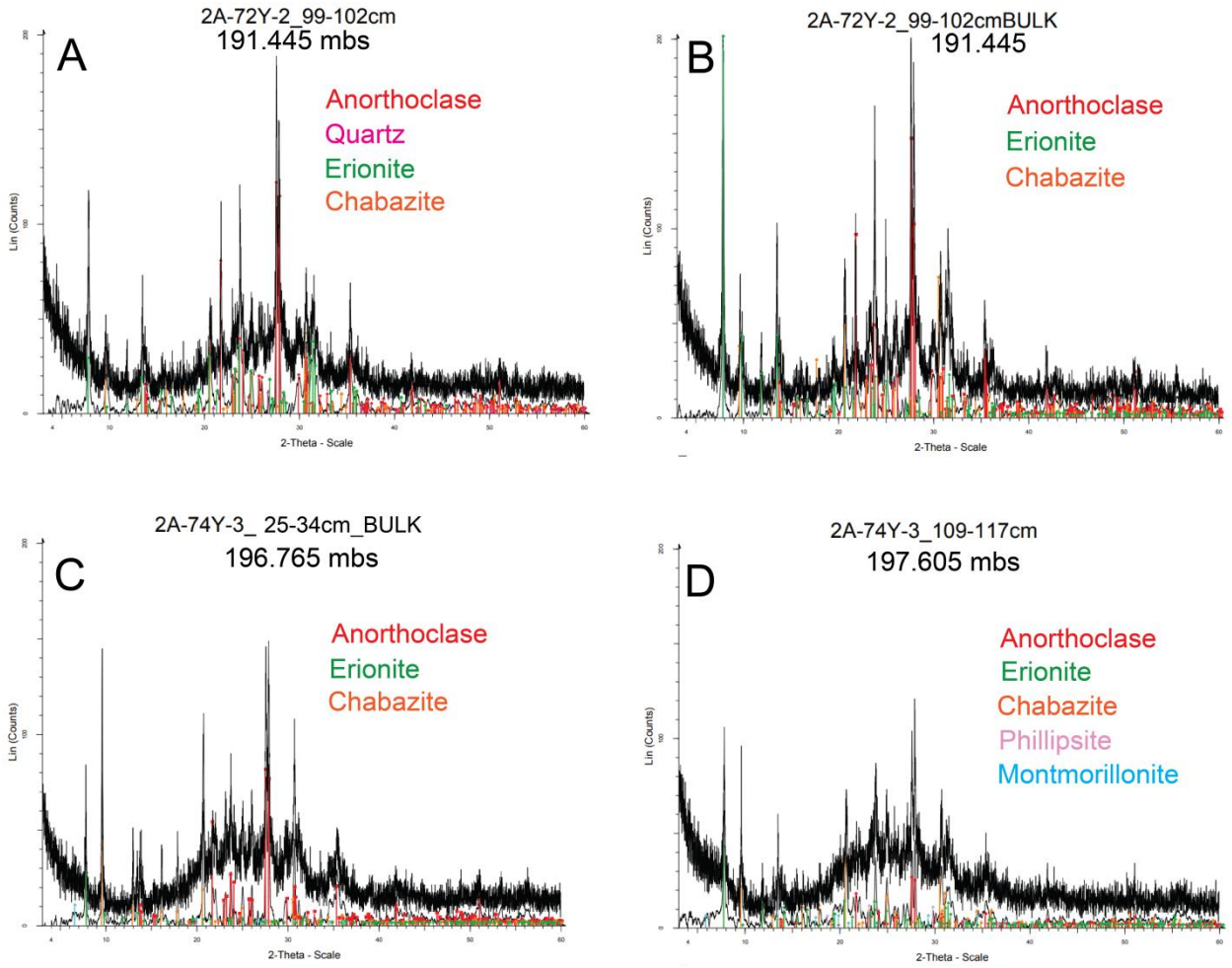


**Figure 45.** XRD plots from core 2A, displaying the major mineral assemblages. Plots show both the raw patterns (above) and smoothed, background-subtracted patterns below, used for pattern matching. Colored lines indicate Bruker EVA matches to ICDD PDF-2 patterns (McHenry et al., 2020). A) 191.445 mbs: anorthoclase, quartz, erionite, and chabazite in a lapilli ash tuff of the Lower Ngorongoro Fm, with intermediate separation from a lake interval. B) 191.445 mbs: anorthoclase, erionite, and chabazite in a lapilli ash tuff of the Lower Ngorongoro Fm, with intermediate separation from a lake interval. C) 196.765 mbs: anorthoclase, erionite, and chabazite in a lapilli ash tuff of the Ngorongoro Fm, stratigraphically separated from a lake interval. D) 197.605 mbs: anorthoclase, erionite, chabazite, phillipsite, and montmorillonite in a lapilli ash tuff of the Ngorongoro Fm, stratigraphically separated from a lake interval.

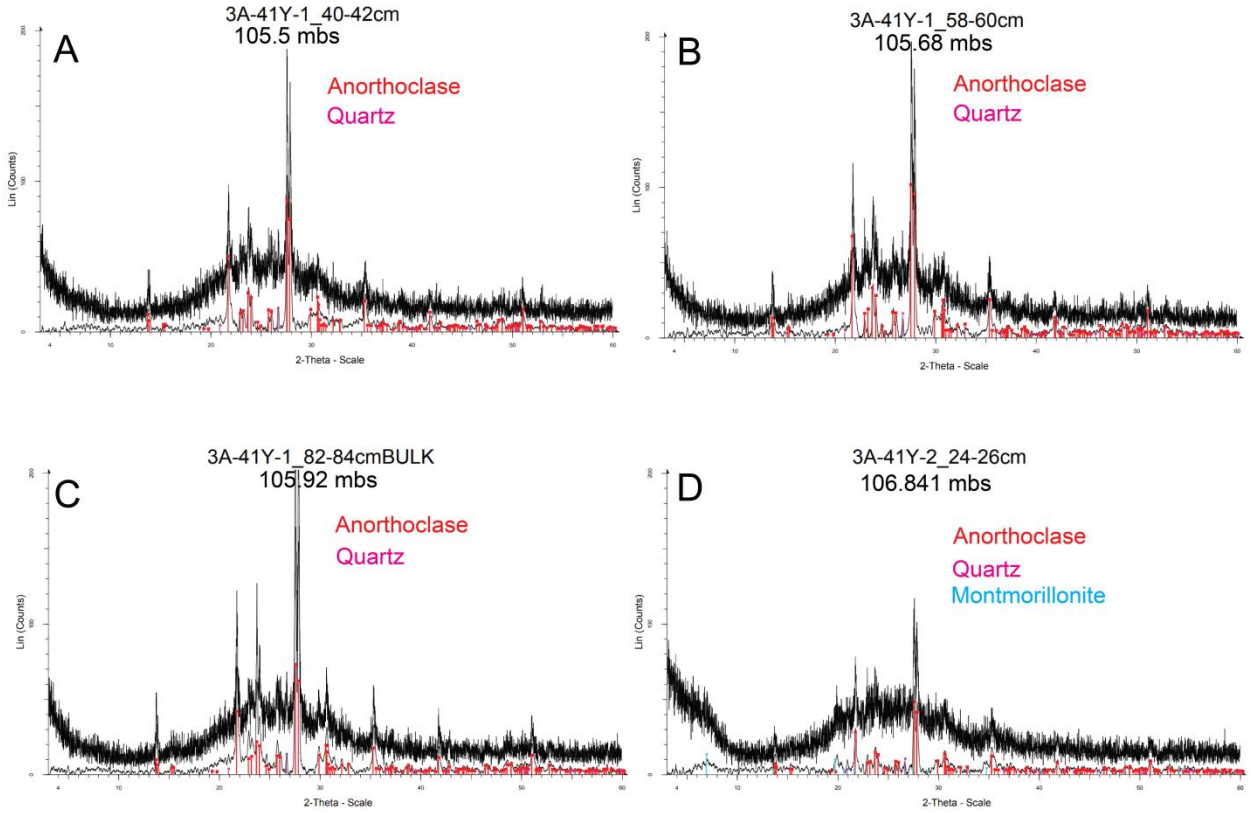


**Figure 46.** XRD plots from core 3A, displaying the major mineral assemblages. Plots show both the raw patterns (above) and smoothed, background-subtracted patterns below, used for pattern matching. Colored lines indicate Bruker EVA matches to ICDD PDF-2 patterns (McHenry et al., 2020). A) 105.5 mbs: anorthoclase and quartz in a coarse ash with pumice of the Upper Ngorongoro Fm, proximal to lake intervals. B) 105.68 mbs: anorthoclase and quartz in a lapilli ash tuff of the Upper Ngorongoro Fm, proximal to a lake interval. C) 105.92 mbs: anorthoclase and quartz in a fine ash of the Upper Ngorongoro Fm, proximal to a lake interval. D) 106.841 mbs: anorthoclase, quartz, and montmorillonite in a water-laid fine ash with pumice clasts of the Upper Ngorongoro Fm, proximal to a lake interval.

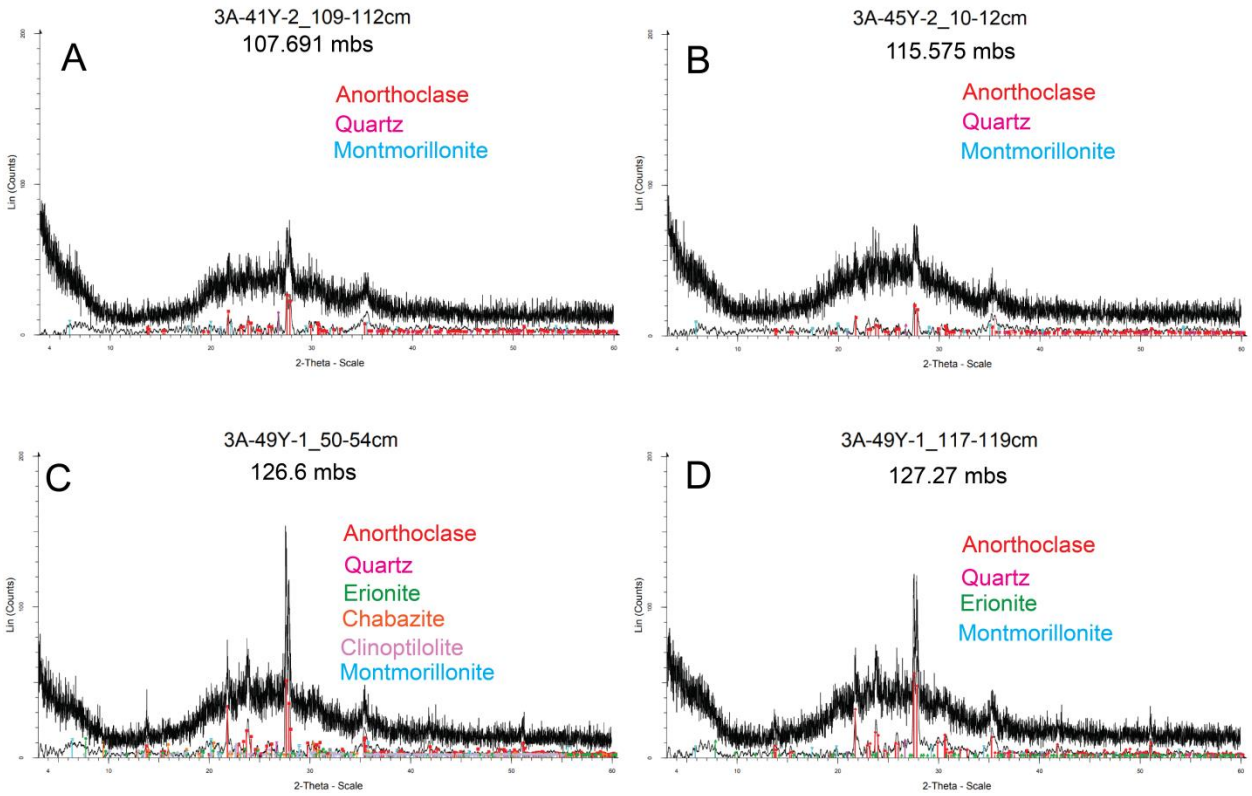


**Figure 47.** XRD plots from core 3A, displaying the major mineral assemblages. Plots show both the raw patterns (above) and smoothed, background-subtracted patterns below, used for pattern matching. Colored lines indicate Bruker EVA matches to ICDD PDF-2 patterns (McHenry et al., 2020).. A) 107.691 mbs: anorthoclase, quartz, and montmorillonite in an ash lapilli tuff of the Upper Ngorongoro Fm, stratigraphically separated from a lake interval. B) 115.575 mbs: anorthoclase, quartz, and montmorillonite in a mudflow diamictite with pumice of the Upper Ngorongoro Fm, proximal to a lake interval. C) 126.6 mbs: anorthoclase, quartz, erionite, chabazite, clinoptilolite, and montmorillonite in an ash lapilli tuff with pumice clasts of the Upper Ngorongoro Fm, with intermediate stratigraphic separation from a lake interval. D) 127.27 mbs: anorthoclase, quartz, erionite, and montmorillonite in an ash lapilli tuff with pumice clasts of the Upper Ngorongoro Fm, proximal to a lake interval.

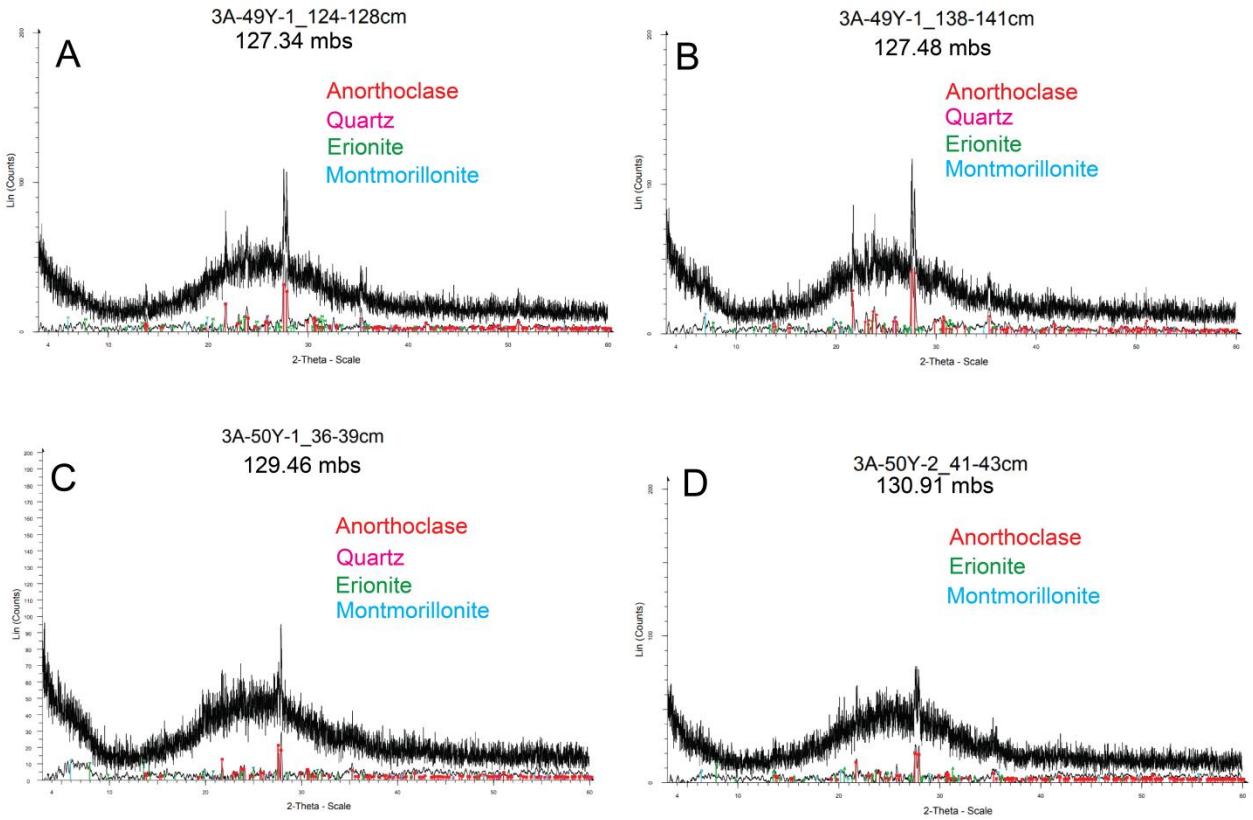


**Figure 48.** XRD plots from core 3A, displaying the major mineral assemblages. Plots show both the raw patterns (above) and smoothed, background-subtracted patterns below, used for pattern matching. Colored lines indicate Bruker EVA matches to ICDD PDF-2 patterns (McHenry et al., 2020). A) 127.34 mbs: anorthoclase, quartz, erionite, and montmorillonite in a water logged pumice in claystone of the Upper Ngorongoro Fm, proximal to a lake interval. B) 127.48 mbs: anorthoclase, quartz, erionite, and montmorillonite in a mudflow diamictite with pumice of the Upper Ngorongoro Fm, proximal to a lake interval. C) 129.46 mbs: anorthoclase, quartz, erionite, and montmorillonite in a laminated clay with waterlogged pumice of the Upper Ngorongoro Fm, proximal to a lake interval. D) 130.91 mbs: anorthoclase, erionite, and montmorillonite in a waxy claystone with waterlogged pumice of the Upper Ngorongoro Fm, proximal to a lake interval.

## Appendix C: Supplemental SEM Images

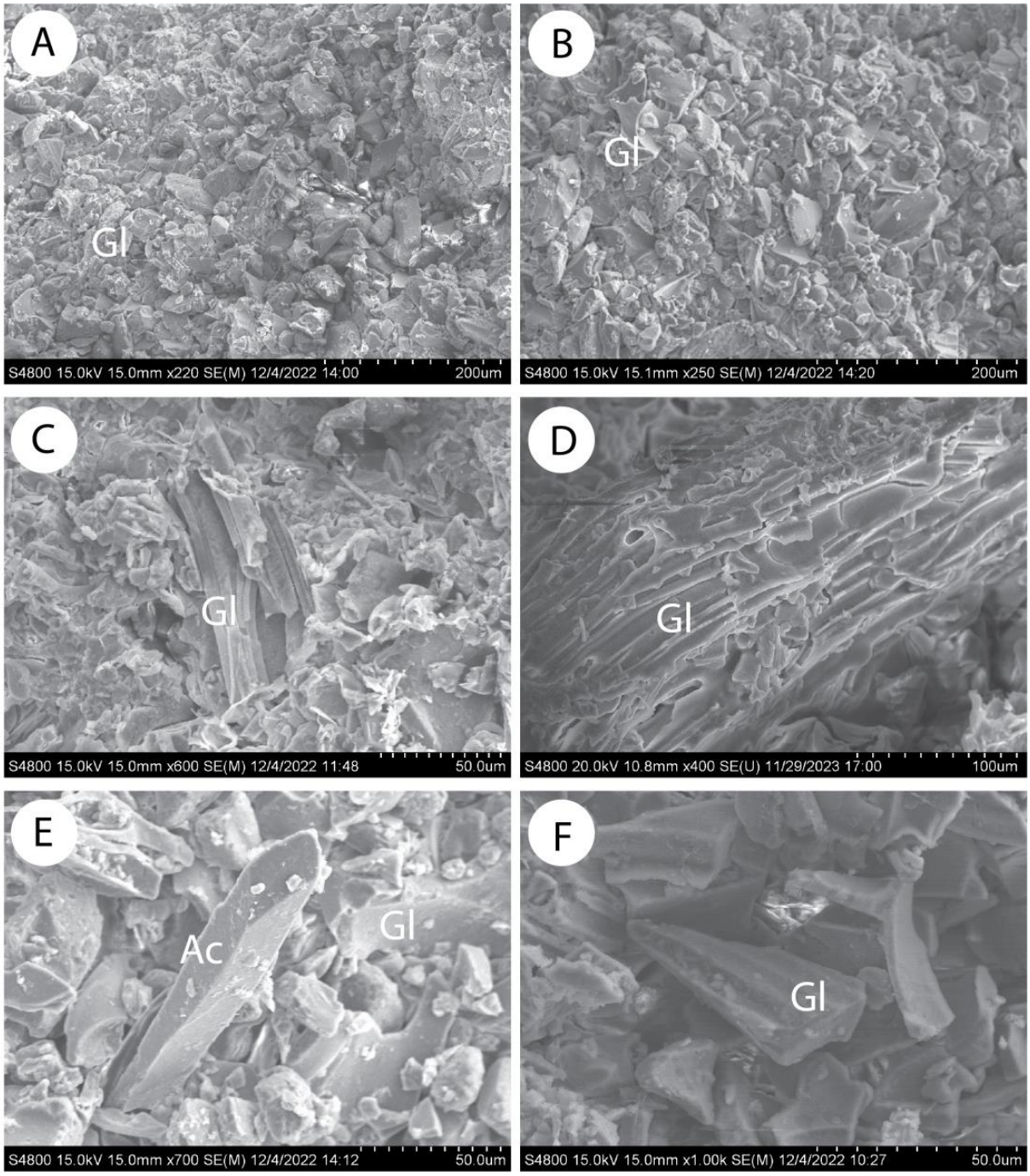


**Figure 49.** Additional SEM images showing features of 'fresh' samples. A) Morphology of relict glass shards. B) Morphology of relict glass shards. C) Glass 'tube' morphology. D) Elongated glass vesicle texture. E) Elongated prismatic anorthoclase crystal with glass shard background. F) Glass shard.

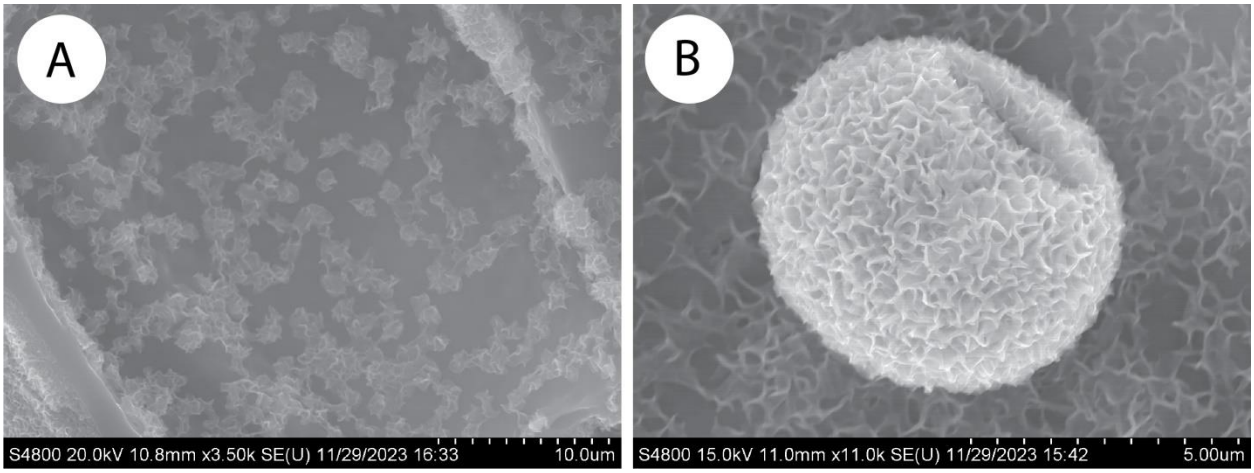


**Figure 50.** Additional SEM images showing different clay morphologies observed. A) Montmorillonite balls nucleating on glass surface. B) Montmorillonite ball nucleating. Displays characteristic wavy texture.

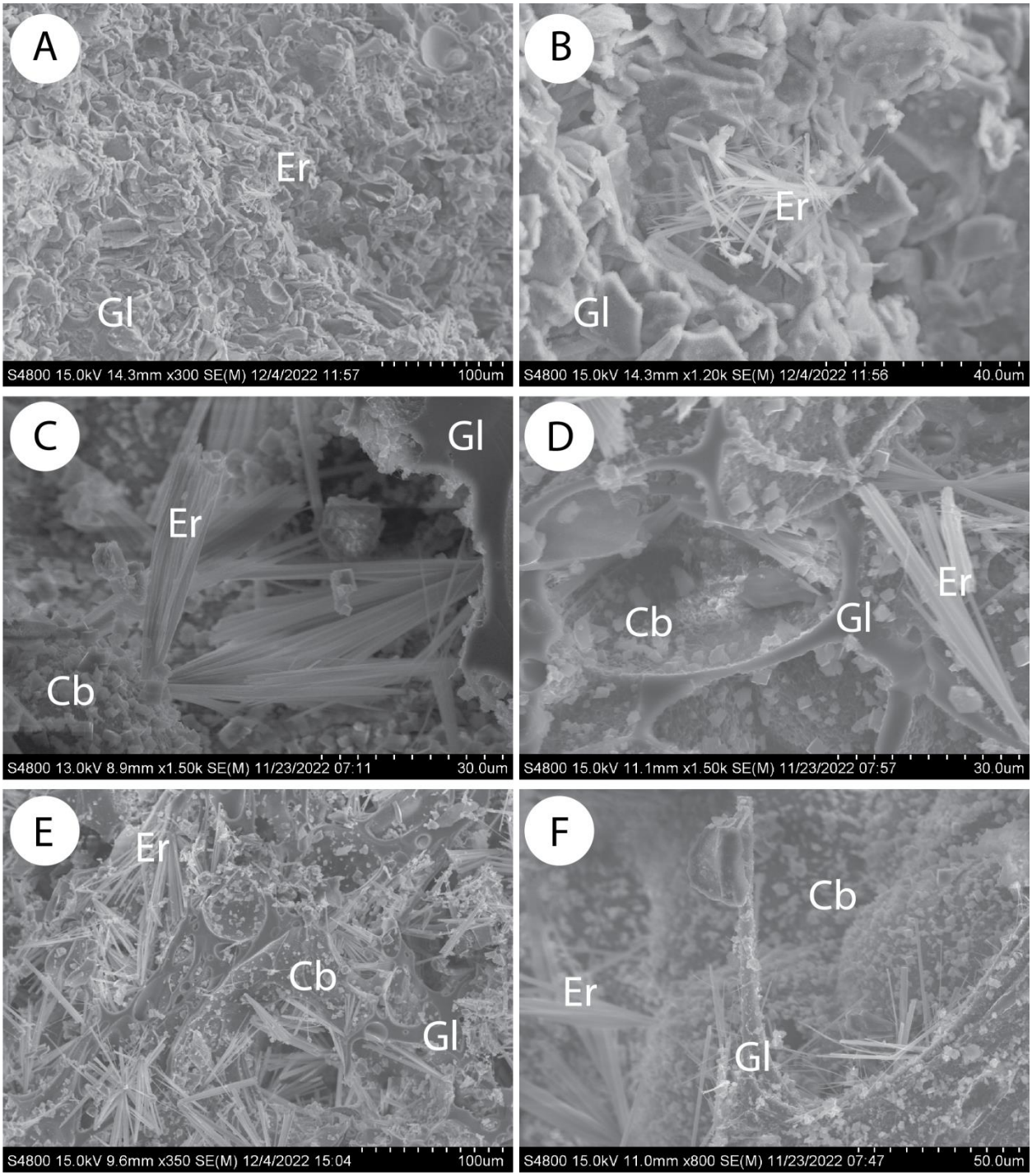


**Figure 51.** Additional SEM images showing authigenic zeolites. A) Mostly glass shards with a tiny erionite mass forming. B) A zoomed-in view of erionite seen in A. C) Fibrous erionite cluster growing out of glass. Fresh glass texture seen in upper right corner. Chabazite ‘cubes’ growing on glass and on erionite (bottom left). D) chabazite and erionite growing in glass vesicles. E. Erionite and chabazite growing in glass vesicles. F. Erionite and chabazite growing on glass surface.

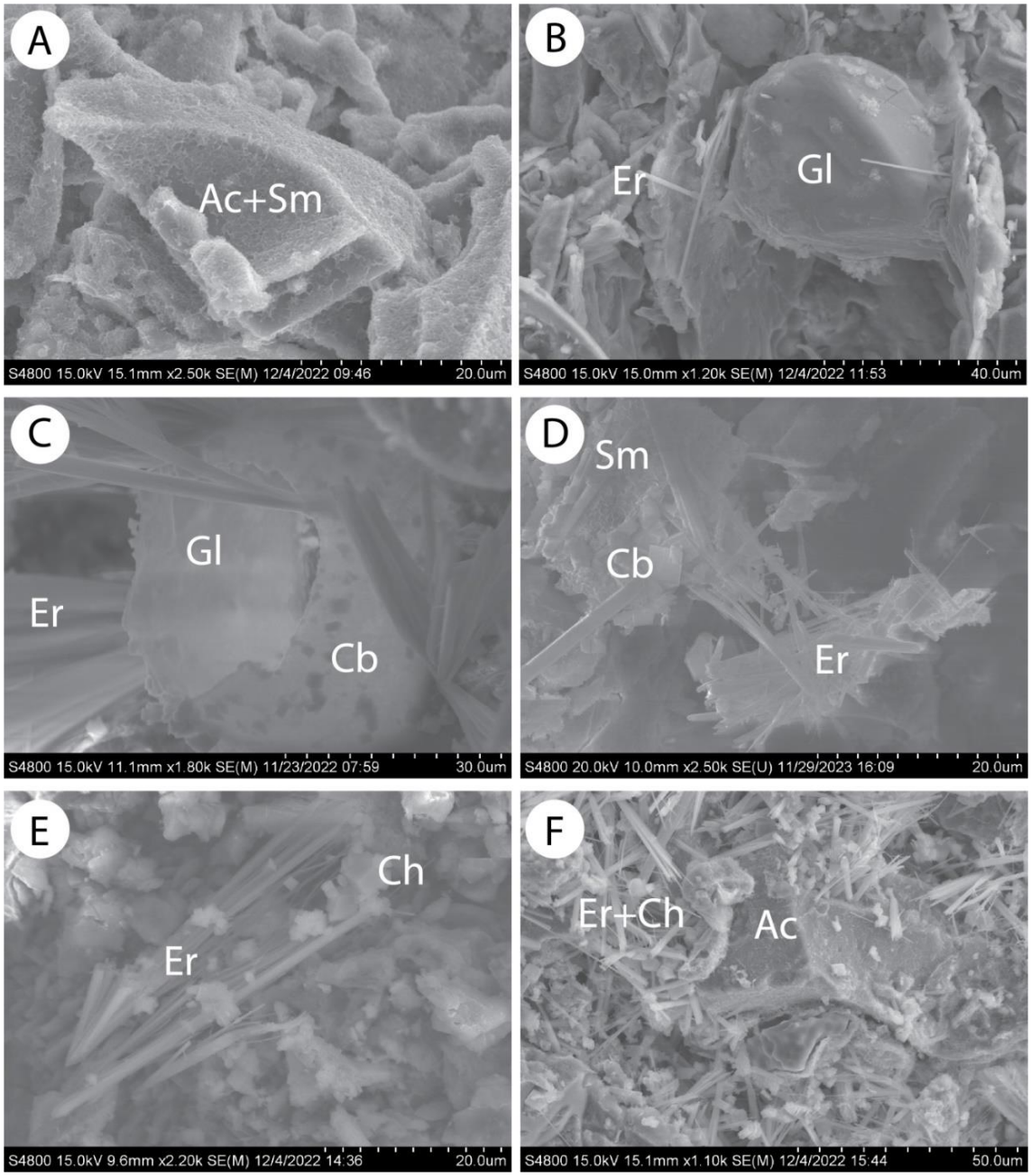


**Figure 52.** Additional SEM images showing the order of formation of authigenic minerals. A) montmorillonite coating on anorthoclase. B) small erionite blades growing from glass (no other phases present). C) chabazite and erionite growing on glass bubble simultaneously. Size of erionite blades suggest they formed sooner than smaller chabazite crystals. D) smectite appears to have grown on glass first, followed y erionite, then chabazite growing on top of both. E) chabazite growing on erionite. F) erionite and chabazite growing from anorthoclase.

## Appendix D: Supplemental EDS

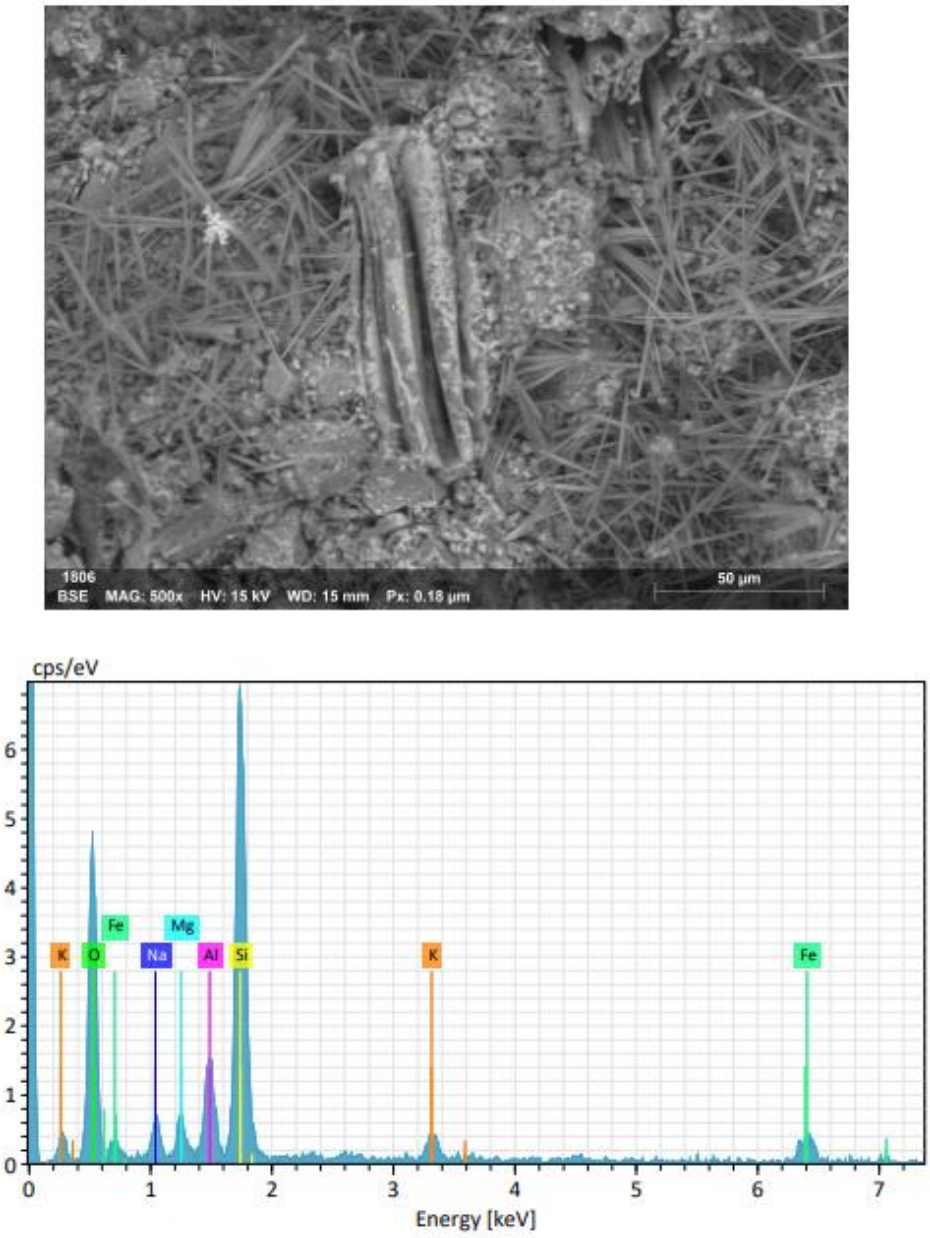


**Figure 53.** EDS analysis of sample 2A-47Y-2_10-12cm.

Dot analysis for object under yellow pointer. Elemental abundance (in order of intensity): Si, O, Al, Mg, Na, K, Fe. Likely a piece of volcanic glass.


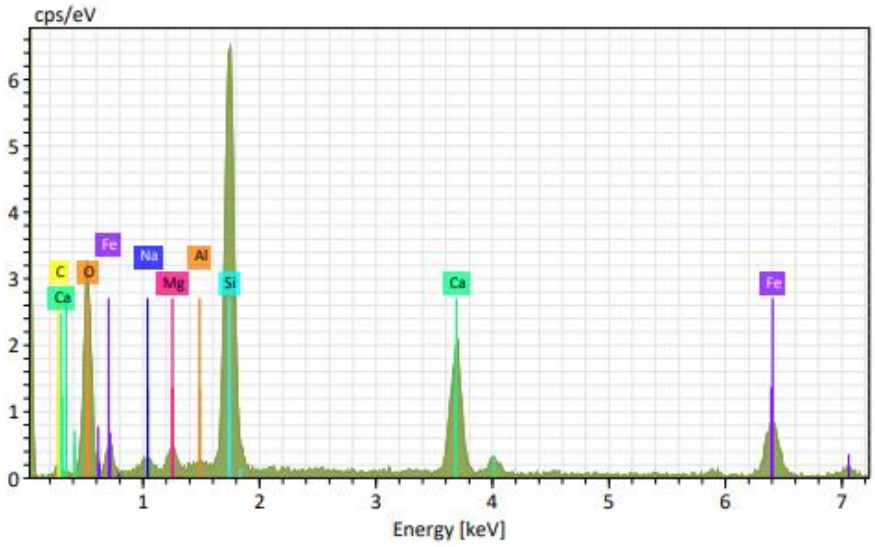


**Figure 54.** EDS Analysis of sample 2A-51Y-1_40-42cm.

Dot analysis for object under green pointer. Elemental abundance (in order of intensity): Si, O, Ca, Fe, Mg, Na, Al. Likely an augite (pyroxene) crystal.

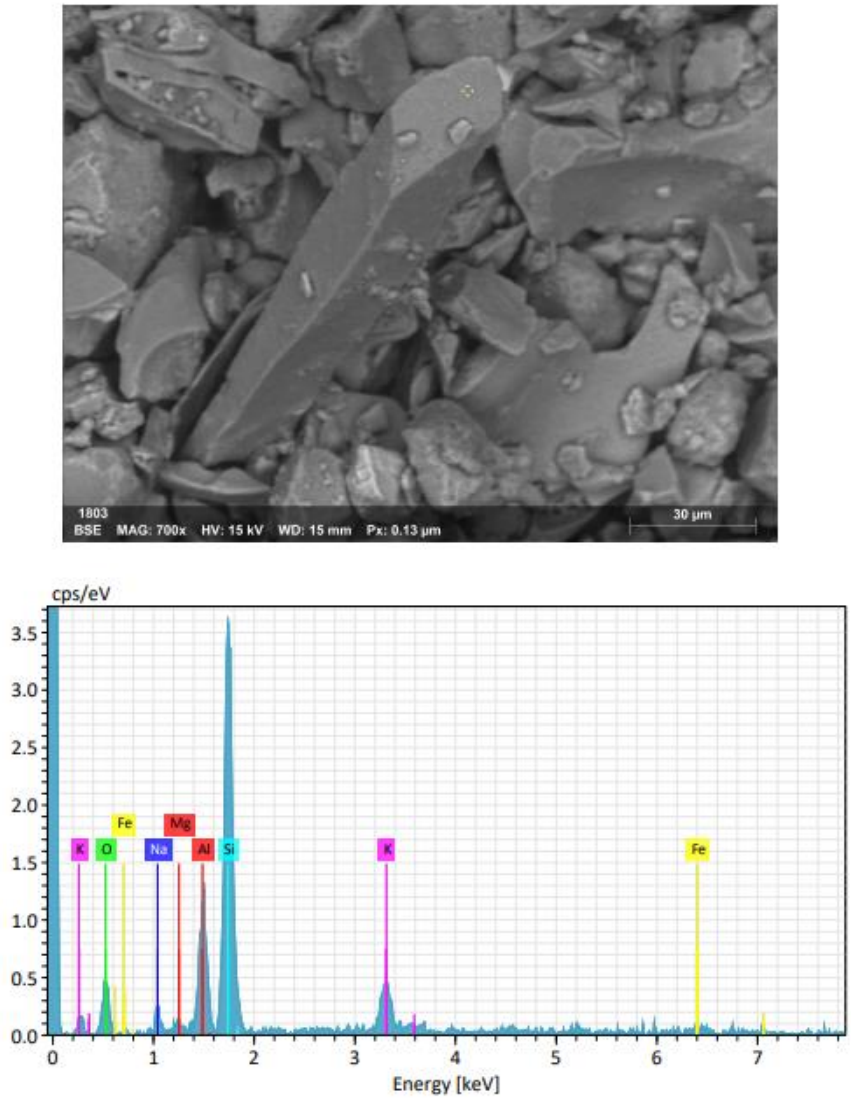


**Figure 55.** EDS analysis of sample 3A-41Y-1_58-60cm.

Dot analysis for object under yellow pointer. Elemental abundance (in order of intensity): Si, Al, O, K, Na, Mg, Fe. Likely a feldspar crystal.

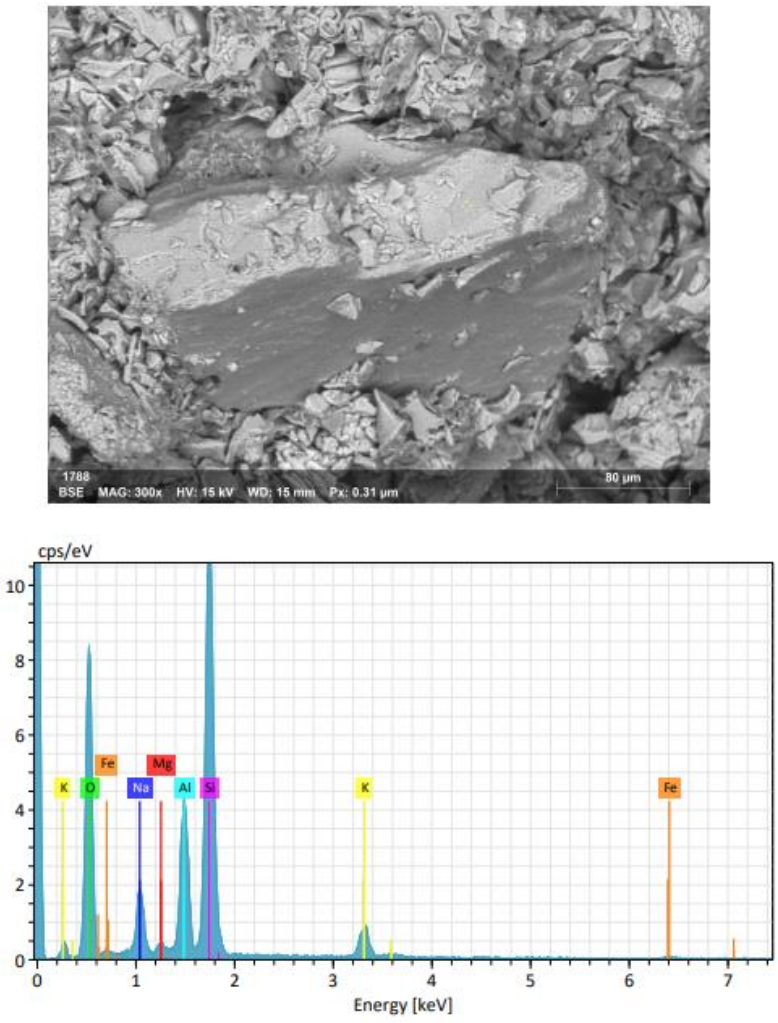


**Figure 56.** EDS analysis of sample 3A-49Y-1_138-141cm.

Dot analysis for object under yellow pointer. Elemental abundance (in order of intensity): Si, O, Al, Na, K, Mg, Fe. Likely a feldspar crystal.

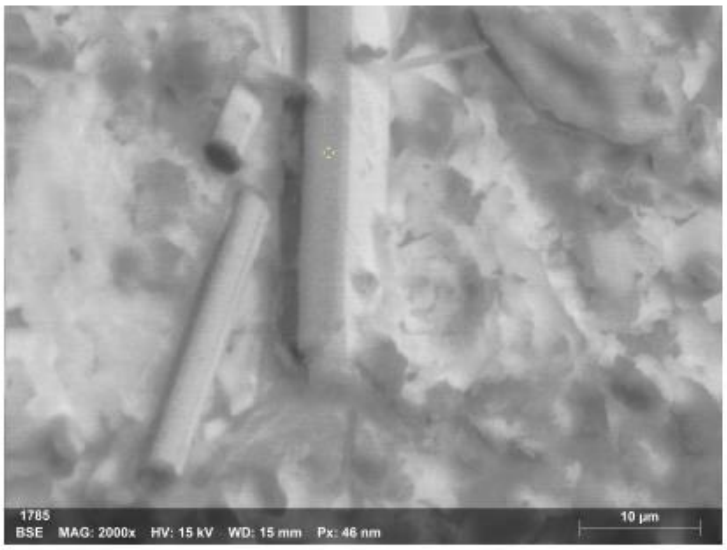


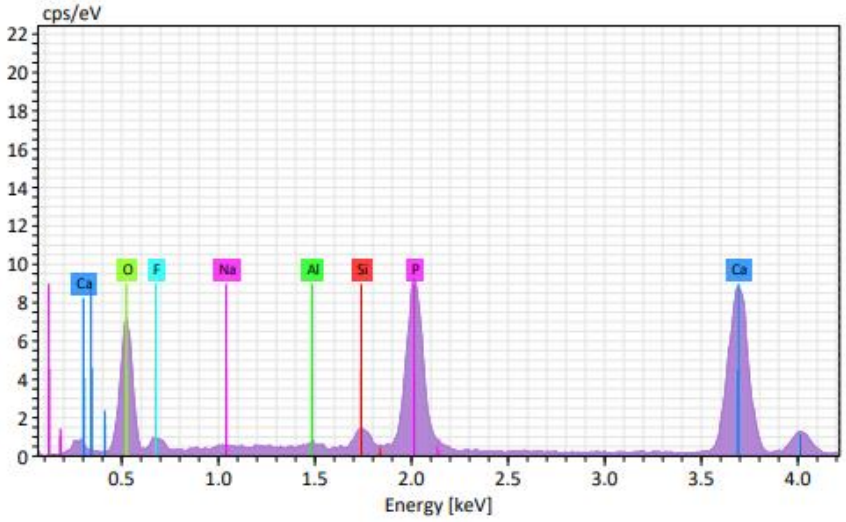


**Figure 57.** EDS analysis of sample 3A-50Y-1_36-39cm.

Dot analysis for object under yellow pointer. Elemental abundance (in order of intensity): P, Ca, Si, F, possibly trace Al and Na. Likely an Apatite crystal.

## Appendix E: X-Ray Fluorescence Data: Minor/Trace Elements

**Table 10**

Minor and trace elemental composition of core 2A samples.

| Sample | mbs | Ba | Sr | Cr | V | Zn | Zr | Y | Nb | Ce | Sum | LOI |
|---|---|---|---|---|---|---|---|---|---|---|---|---|
| 47Y-2_10-12cm | 117.95 | 772 | 109 | ND | 53 | 200 | 591 | 44 | 170 | 83 | 99.75 | 4.83 |
| 47Y-2_25-32cm | 118.10 | 135 | 135 | ND | 80 | 190 | 671 | 47 | 201 | 73 | 99.85 | 5.70 |
| 47Y-2_79-83cm | 118.64 | 381 | 258 | ND | ND | 200 | 718 | 51 | 202 | 68 | 99.63 | 7.47 |
| 50Y-2_134-137cm | 128.84 | 259 | 71 | ND | ND | 251 | 888 | 52 | 230 | 64 | 99.91 | 6.38 |
| 51Y-1_32-35cm | 129.32 | 291 | 105 | ND | ND | 214 | 939 | 54 | 242 | 67 | 99.31 | 5.84 |
| 51Y-1_40-42cm | 129.40 | 198 | 145 | ND | ND | 176 | 866 | 65 | 226 | 61 | 99.91 | 6.96 |
| 54Y-1_80-81cm | 138.80 | 372 | 145 | ND | ND | 184 | 806 | 53 | 209 | 78 | 99.37 | 6.33 |
| 60Y-1_59.5-62cm | 153.60 | 617 | 308 | ND | 216 | 243 | 665 | 36 | 185 | 92 | 99.16 | 7.89 |
| 63Y-2_45-48cm | 163.95 | 556 | 328 | ND | 80 | 157 | 504 | 41 | 200 | 76 | 98.86 | 6.59 |
| 63Y-2_114-117cm | 164.64 | 696 | 410 | 29 | 656 | 164 | 674 | 32 | 178 | 91 | 98.85 | 6.60 |
| 69Y-2_34-37cm | 181.80 | 1119 | 176 | ND | 81 | 132 | 358 | 32 | 166 | 98 | 99.36 | 5.49 |
| 70Y-1_4-6cm | 183.04 | 675 | 137 | ND | ND | 206 | 838 | 45 | 284 | 88 | 98.98 | 5.90 |
| 70Y-1_32-34cm | 183.32 | 515 | 151 | ND | ND | 98 | 802 | ND | 230 | 57 | 99.29 | 7.45 |
| 72Y-1_136-142cm | 184.10 | 753 | 189 | ND | ND | 130 | 491 | 31 | 163 | 77 | 97.95 | 6.03 |
| 72Y-2_64-67cm | 190.36 | 813 | 277 | ND | ND | 169 | 534 | 39 | 176 | 84 | 98.27 | 6.19 |
| 72Y-2_99-102cm | 191.10 | 827 | 278 | ND | ND | 168 | 597 | 36 | 172 | 89 | 98.11 | 6.13 |
| 74Y-3_25-34cm | 196.77 | 589 | 70 | ND | ND | 177 | 563 | 40 | 172 | 82 | 98.70 | 4.37 |
| 74Y-3_109-117cm | 197.61 | 415 | 92 | ND | ND | 188 | 541 | 34 | 158 | 60 | 98.56 | 4.93 |

**Table 11**

Minor and trace elemental composition of core 3A samples.

| Sample | mbs | Ba | Sr | Cr | V | Zn | Zr | Y | Nb | Ce | Sum | LOI |
|---|---|---|---|---|---|---|---|---|---|---|---|---|
| 41Y-1_40-42cm | 105.50 | 800 | 84 | ND | ND | 191 | 740 | 50 | 177 | 88 | 98.85 | 4.59 |
| 41Y-1_58-60cm | 105.68 | 920 | 96 | ND | ND | 181 | 700 | 50 | 167 | 91 | 98.68 | 4.16 |
| 41Y-1_82-84cm | 105.92 | 1047 | 97 | ND | ND | 182 | 655 | 45 | 158 | 99 | 98.29 | 3.82 |
| 41Y-2_24-26cm | 106.84 | 610 | 124 | ND | 166 | 229 | 730 | 48 | 164 | 81 | 98.70 | 5.80 |
| 41Y-2_109-112cm | 107.70 | 990 | 293 | ND | 66 | 157 | 441 | 46 | 120 | 95 | 98.02 | 4.63 |
| 45Y-2_10-12cm | 115.58 | 453 | 99 | ND | ND | 258 | 826 | 52 | 220 | 76 | 97.76 | 6.49 |
| 49Y-1_50-54cm | 126.60 | 340 | 107 | ND | ND | 206 | 905 | 53 | 240 | 70 | 98.07 | 5.28 |
| 49Y-1_117-119cm | 127.27 | 296 | 101 | ND | ND | 224 | 971 | 56 | 255 | 66 | 97.95 | 5.27 |
| 49Y-1_124-128cm | 127.34 | 134 | 47 | ND | ND | 242 | 1151 | 63 | 299 | 70 | 97.86 | 5.44 |
| 49Y-1_138-141cm | 127.48 | 171 | 60 | ND | ND | 221 | 1049 | 60 | 277 | 61 | 99.05 | 6.30 |
| 50Y-1_36-39cm | 129.46 | 1434 | 82 | ND | ND | 170 | 846 | 51 | 228 | 130 | 98.47 | 6.18 |
| 50Y-2_41-43cm | 130.91 | 599 | 62 | ND | ND | 181 | 822 | 61 | 238 | 91 | 98.04 | 5.70 |

## Appendix F: Isocon Diagrams

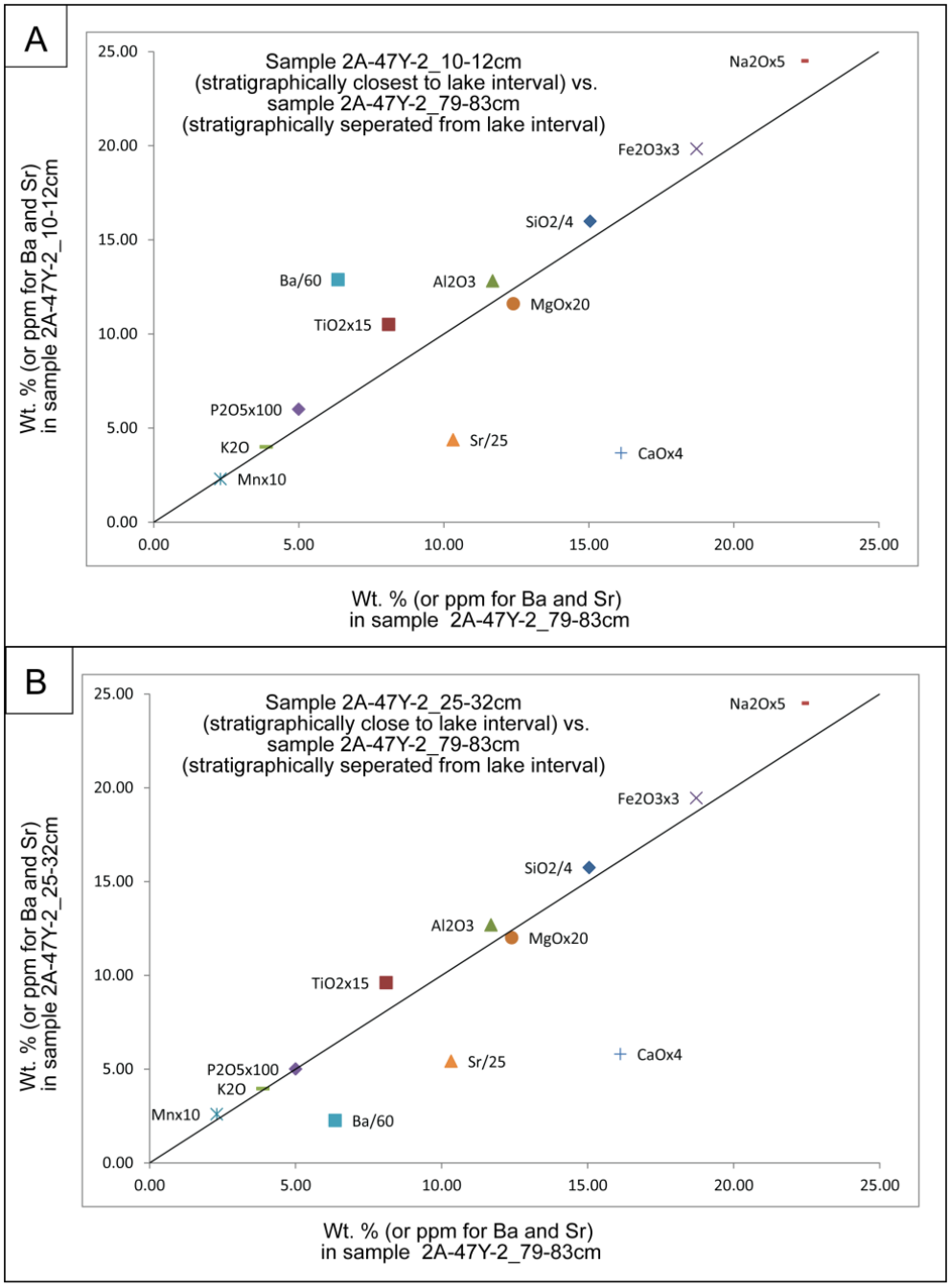


**Figure 58.** Isocon diagrams for samples from core 2A-47Y-2, plotting all major elements (and minor elements Ba2+ and Sr2+). A: A sample that is stratigraphically closest to a lake interval (2A-47Y-2_10-12cm) plotted against a samples that is stratigraphically separated from the same lake interval (2A-47Y-2_79-83cm). B: A sample that is stratigraphically closest to a lake interval (2A-47Y-2_25-32cm) plotted against a samples that is stratigraphically separated from the same lake interval (2A-47Y-2_79-83cm).

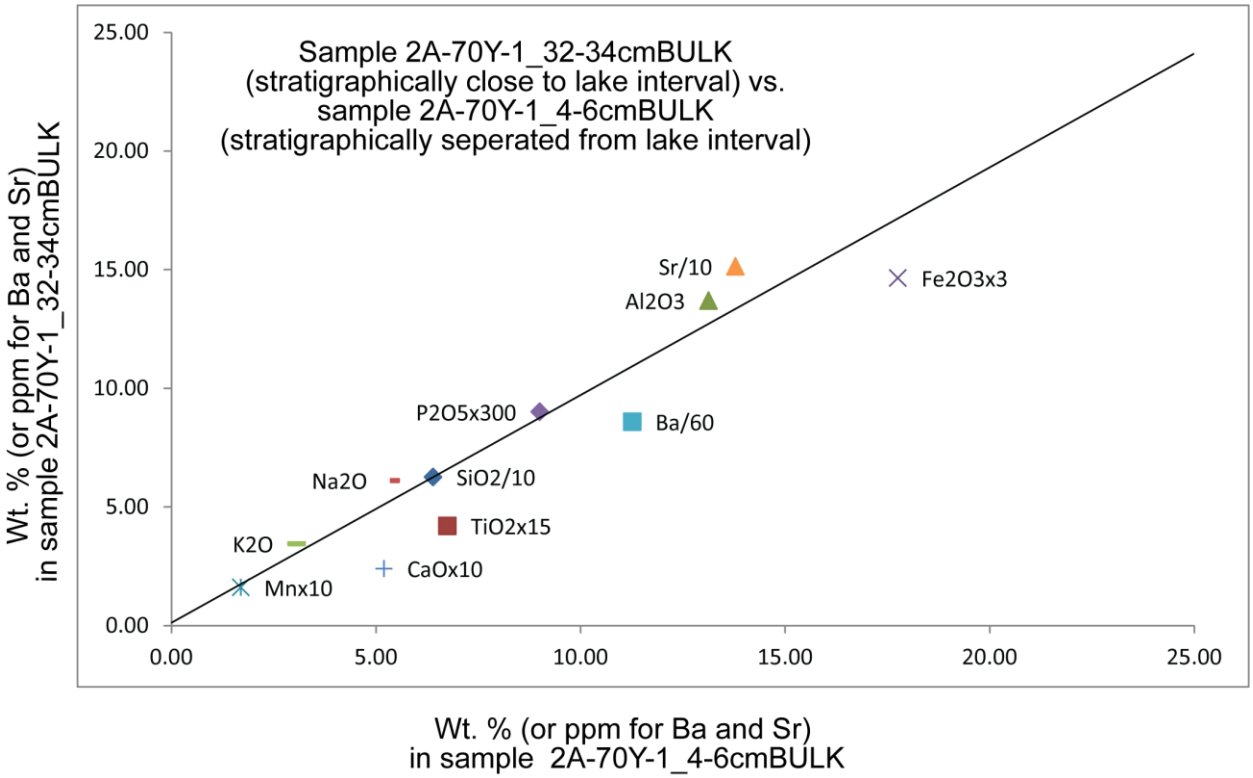


**Figure 59.** Isocon diagram for samples from core 2A-70Y-1, plotting all major elements (and minor elements Ba2+ and Sr2+). A sample that is stratigraphically closest to a lake interval (2A-70Y-1_32-34cm) is plotted against a samples that is stratigraphically separated from the same lake interval (2A-70Y-1_4-6cm). Most elements plot fairly close to the isocon line, indicating little to no change between the samples.

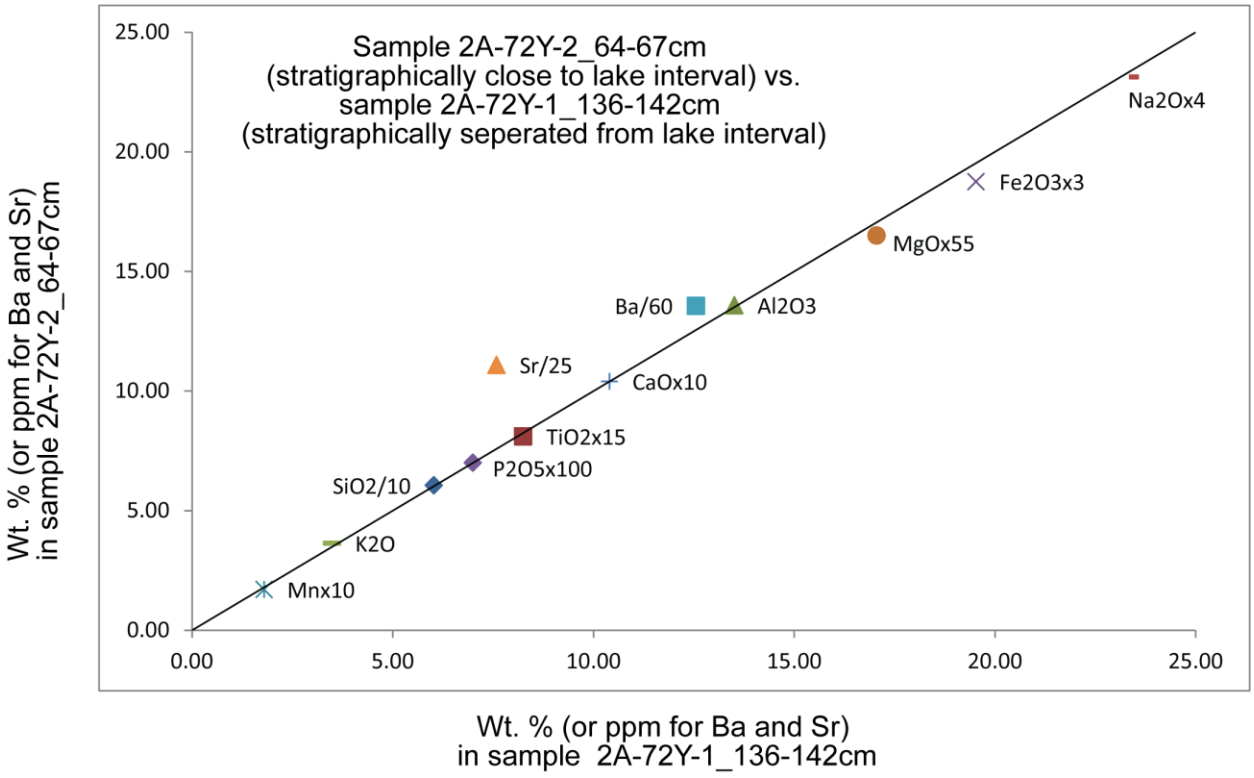


**Figure 60.** Isocon diagram for samples from core 2A-72Y-1, plotting all major elements (and minor elements Ba2+ and Sr2+). A sample that is stratigraphically closest to a lake interval (2A-72Y-2_64-67cm) is plotted against a samples that is stratigraphically separated from the same lake interval (2A-72Y-2_136-142cm). All elements plot fairly close to the isocon line, indicating little to no change between the samples.

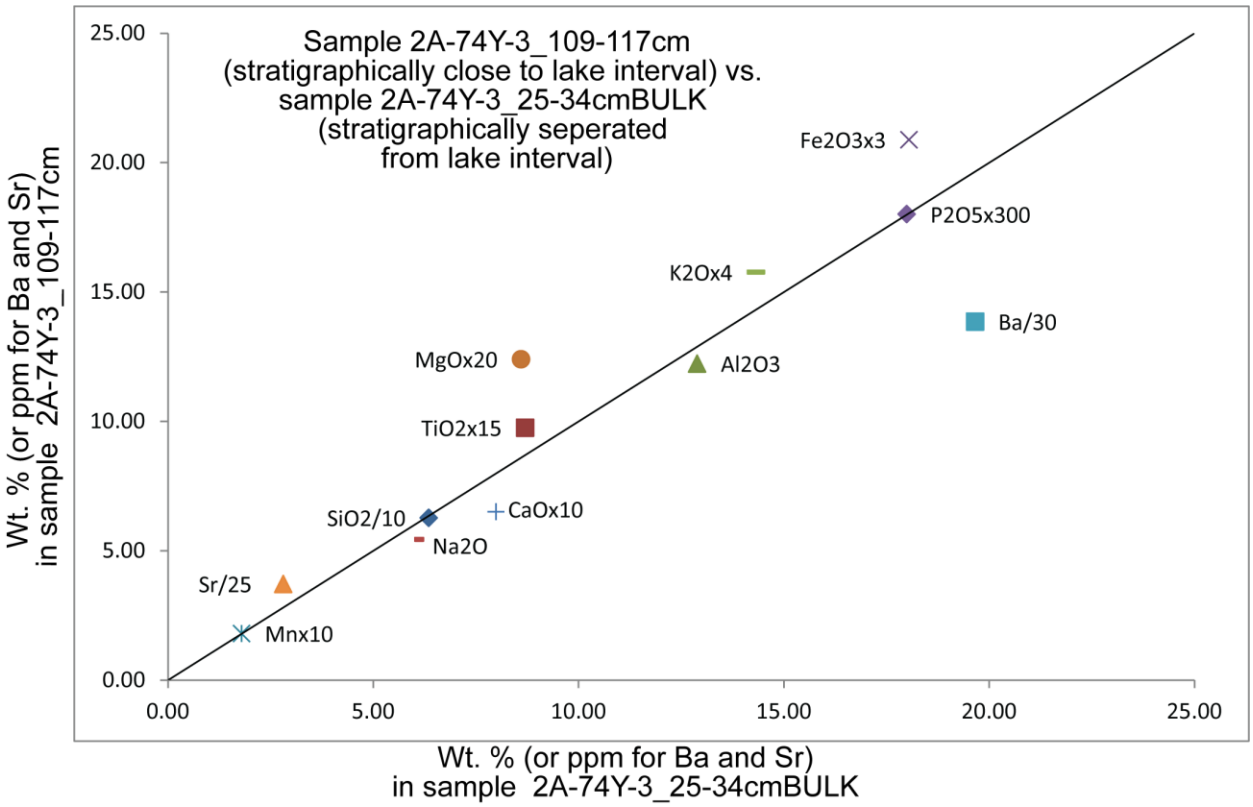


**Figure 61.** Isocon diagram for samples from core 2A-74Y-3, plotting all major elements (and minor elements Ba2+ and Sr2+). A sample that is stratigraphically closest to a lake interval (2A-74Y-3_109-117cm) is plotted against a samples that is stratigraphically separated from the same lake interval (2A-74Y-3_25-34cm). Most major elements plot fairly close to the isocon line, indicating little to no change between the samples.

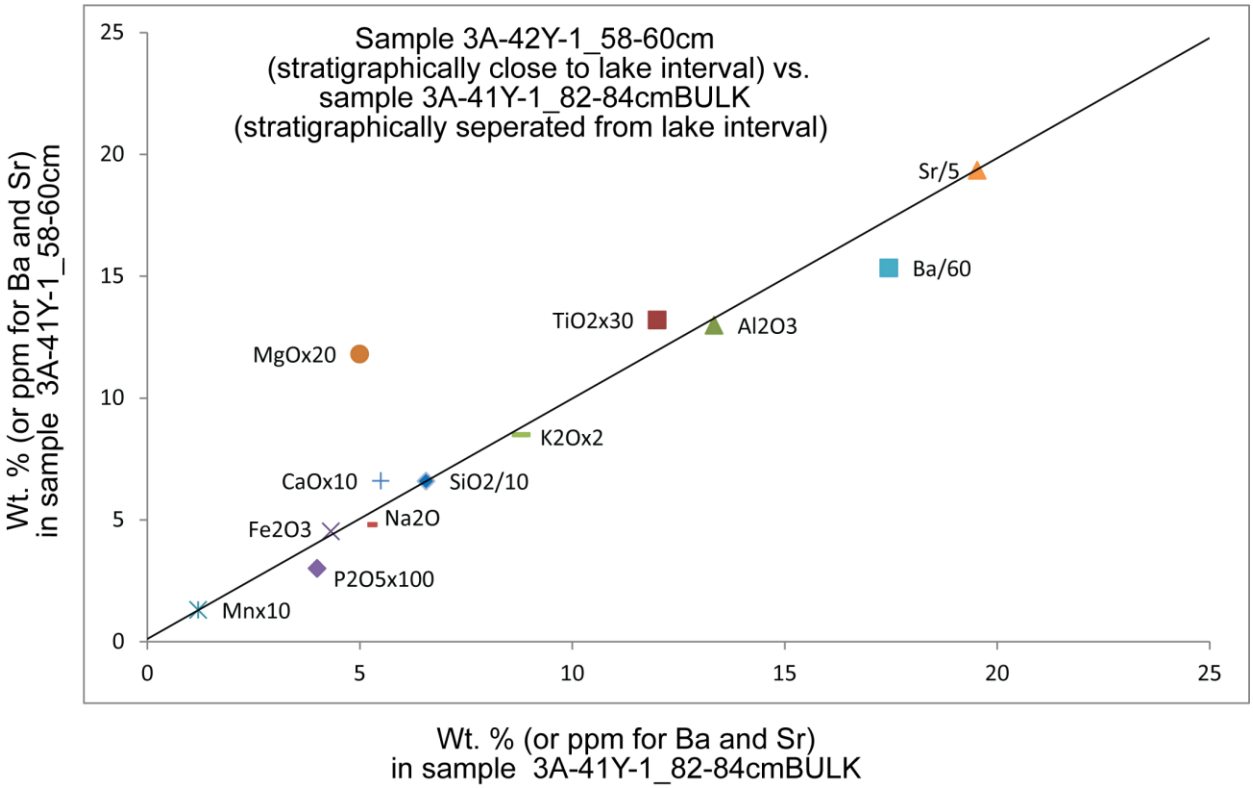


**Figure 62.** Isocon diagram for samples from core 3A-41Y-1, plotting all major elements (and minor elements Ba2+ and Sr2+). A sample that is stratigraphically closest to a lake interval (3A-42Y-1_58-60cm) is plotted against a samples that is stratigraphically separated from the same lake interval (3A-42Y-1_82-84cm). Most major elements plot fairly close to the isocon line, indicating little to no change between the samples.